

ABSTRACT

Title of Dissertation: HEALTH ESTIMATION AND REMAINING
USEFUL LIFE PREDICTION OF
ELECTRONIC CIRCUIT WITH A
PARAMETRIC FAULT

Arvind Sai Sarathi Vasam, Doctor of Philosophy,
2016

Dissertation directed by: Professor Michael G. Pecht,
Department of Mechanical Engineering

Degradation of electronic components is typically accompanied by a deviation in their electrical parameters from their initial values. Such parametric drifts in turn will cause degradation in performance of the circuit they are part of, eventually leading to function failure due to parametric faults. The existing approaches for predicting failures resulting from electronic component parametric faults emphasize identifying monotonically deviating parameters and modeling their progression over time. However, in practical applications where the components are integrated into a complex electronic circuit assembly, product or system, it is generally not feasible to monitor component-level parameters. To address this problem, a prognostics method that exploits features extracted from responses of circuit-comprising components exhibiting parametric faults is developed in this dissertation.

The developed prognostic method constitutes a circuit health estimation step followed by a degradation modeling and remaining useful life (RUL) prediction step. First, the circuit health estimation method was developed using a kernel-based machine learning technique that exploits features that are extracted from responses of circuit-comprising components exhibiting parametric faults, instead of the component-level parameters. The performance of kernel learning technique depends on the automatic adaptation of hyperparameters (i.e., regularization and kernel parameters) to the learning features. Thus, to achieve high accuracy in health estimation the developed method also includes an optimization method that employs a penalized likelihood function along with a stochastic filtering technique for automatic adaptation of hyperparameters.

Second, the prediction of circuit's RUL is realized by a model-based filtering method that relies on a first principles-based model and a stochastic filtering technique. The first principles-based model describes the degradation in circuit health with progression of parametric fault in a circuit component. The stochastic filtering technique on the other hand is used to first solve a joint 'circuit health state—parametric fault' estimation problem, followed by prediction problem in which the estimated 'circuit health state—parametric fault' is propagated forward in time to predict RUL. Evaluations of the data from simulation experiments on a benchmark Sallen–Key filter circuit and a DC–DC converter system demonstrate the ability of the developed prognostic method to estimate circuit health and predict RUL without having to monitor the individual component parameters.

HEALTH ESTIMATION AND REMAINING USEFUL LIFE PREDICTION
OF ELECTRONIC CIRCUIT WITH A PARAMETRIC FAULT

by

Arvind Sai Sarathi Vasani

Dissertation submitted to the Faculty of the Graduate School of the
University of Maryland, College Park, in partial fulfillment
of the requirements for the degree of
Doctor of Philosophy
2016

Advisory Committee:
Professor Michael G. Pecht, Chair
Professor Abhijit Dasgupta
Professor Peter Sandborn
Professor Patrick McCluskey
Professor Rama Chellappa

© Copyright by
Arvind Sai Sarathi Vasani
2016

Dedication

To my son Ishaan for all the happiness he has been giving me.

To my wife, Lakshmi, and parents, Sai Sarathi Vasan & Meera, for their
unconditional love and support throughout my life.

Acknowledgements

I express my sincere gratitude to my advisor Prof. Michael Pecht for providing guidance and ideas not only for this dissertation but also for all projects that I carried during the course of my graduate study. He is a role model and a tremendous mentor who is ready to discuss academic or real world problem at any time and place, whether it is CALCE's 8am morning meeting or 8pm racquetball session break time.

I would like to also express my gratitude to Prof. Rama Chellappa, Prof. Patrick McCluskey, and Prof. Abhijit Dasgupta for being a part of my thesis committee and reviewing my research. I would like to express my thanks especially to Prof. Peter Sandborn for not only being a part of my thesis committee but also for his time and effort in guiding me while submitting NSF proposals on behalf of CALCE.

I would also like to thank Prof. Bing Long of Harbin Institute of Technology, who introduced me to this dissertation topic during his visit to CALCE in 2011-2012 and stressed the lack of prognostics effort for electronic circuits. Furthermore, he had also spent time to review some of the conference and journal articles that I have written in relation to this thesis. My sincere thanks to Prof. Long for his time and effort.

During my time at CALCE research center, many people helped me to grow as a researcher. Most important among them are Dr. Diganta Das, Dr. Michael Azarian, Mr. Mark Zimmerman, and Mrs. Cheryl Wurzbacher. Without having Dr. Das and Dr. Azarian play the devil's advocate and constantly questioning my work, this dissertation would not have come to be. Thanks to Mark and Cheryl who have made my papers read well with their English edits.

My life as a graduate student would not have been possible without the constant support from my family. Words cannot express my gratitude for all of the sacrifices that they all have made on my behalf. My father, K. Sai Sarathi Vasani, and mother, Meera Sai Sarathi Vasani, has dedicated most of their life to raise me and provide the best opportunities for me. My parents instilled in me mental strength, determination, patience, and the drive to always be better. I realized that, all these qualities that my parents instilled in me were critical when pursuing a PhD.

Beyond all, my wife Lakshmi Krishnan who lives true by the words 'better half'.

She would work along side me, doing her own research, when I was pulling off all-nighters to meet my work related deadlines. In 2012, she introduced me to the Machine Learning course offered by Coursera, which ended-up being critical for me in finishing my second contribution of this dissertation. While I went through tough times in research, she provided the much-needed motivation that helped me complete my thesis. When I went through tough times in family life, she took much of the heat so that I could focus on my thesis when in fact she herself was completing here PhD. I am really lucky to have Lakshmi in my life and there is no way I can repay the debt I owe her.

The last 7 years have been a very demanding phase of my life with stress filled days. My friends were always there to lighten the mood, which helped me deal with stress. I would like to thank Sandeep, Sameer, Senthil, Rahul, Raghul, Ragav, Ganesh, Sriram, Vydhi, Elviz, Anto, Sony, and Dinesh from the bottom of my heart.

Table of Contents

Dedication.....	ii
Acknowledgements	iii
Table of Contents	v
List of Tables.....	vii
List of Figures.....	viii
List of Abbreviations	xi
Chapter 1: Introduction.....	1
Chapter 2: Literature Review	5
<u>2.1 Component-Centric Approach</u>	5
<u>2.2 Circuit-Centric Approach</u>	6
<u>2.3 Gaps in Existing Literature</u>	9
<u>2.4 Dissertation Objectives</u>	11
Chapter 3: Electronic Circuit Health Estimation Through Kernel Learning.....	12
<u>3.1 Kernel-Based Learning</u>	12
<u>3.2 Health Estimation Method</u>	14
<u>3.1.1 Likelihood-based Function for Model Selection</u>	18
<u>3.1.2 Optimization Approach for Model Selection</u>	20
<u>3.3. Implementation Results</u>	24
<u>3.3.1 Band-Pass Filter Circuit</u>	26
<u>3.3.2 DC-DC Buck Converter System</u>	39
Chapter 4: RUL Prediction using Model-based Filtering.....	49
<u>4.1 Prognostics Problem Formulation</u>	50
<u>4.2 Circuit Degradation Modeling</u>	52
<u>4.3 Model-based Prognostic Methodology</u>	56
<u>4.4 Implementation Results</u>	61
<u>4.4.1 Low-Pass Filter Circuit</u>	61
<u>4.4.2 Voltage Feedback Circuit</u>	65
<u>4.4.3 Source of RUL Prediction Error</u>	69
<u>4.4.4 Effect of first principles-based modeling of θ_t</u>	71

Chapter 5: Conclusions and Future Work	74
Chapter 6: Dissertation Contributions	77
Appendix A: Comparison of Particle Filter with Other Optimization Methods	78
Bibliography	83

List of Tables

Table 1: Performance Results of Developed Health Estimation Method on Sallen-Key BPF.....	34
Table 2: Performance Results of Developed Health Estimation Method on DC-DC Converter System.....	47
Table 3: Comparison of CE, PSO, and Grid search methods for optimal selection of hyperparameters in SVM on various benchmark classification datasets [50].....	75

List of Figures

Figure 1:	Example plots for parametric drifts exhibited by electronic components	2
Figure 2:	Typical steps involved in a prognostic approach	3
Figure 3:	Examples where linear separability between healthy and failure classes ensures $d_{hh} < d_{hf}$ either in (a) Euclidean Space or (b) Principal Component Space	10
Figure 4:	Illustration of the principle underlying kernel-based learning methods.	13
Figure 5:	Overview if the proposed circuit health estimation method	19
Figure 6:	Particle filtering approach for optimization of hyperparameters	24
Figure 7:	Schematic of a Sallen-Key band pass filter centered at 25kHz.	27
Figure 8:	Magnitude and phase of Sallen-Key BPF's transfer function with and without faults	27
Figure 9:	Example of a sweep (test) signal	28
Figure 10(a):	Illustration of wavelet decomposition using filter banks	30
Figure 10(b):	Frequency range coverings for the detail and approximate coefficients for three levels of decomposition	30
Figure 11:	Plot of training error rate with respect to iteration number	32
Figure 12:	(a) Progression of parametric fault in C_1 of Sallen-Key BPF. (b) Health estimates using the developed kernel (blue) and MD-based (green) method for fault in C_1 .	35
Figure 13:	(a) Progression of parametric fault in C_2 of Sallen-Key BPF. (b) Health estimates using the developed kernel (blue) and MD-based (green) method for fault in C_2 .	36
Figure 14:	(a) Progression of parametric fault in R_2 of Sallen-Key BPF. (b) Health estimates using the developed kernel (blue) and MD-based (green) method for fault in R_2 .	37
Figure 15:	(a) Progression of parametric fault in R_3 of Sallen-Key BPF. (b) Health estimates using the developed kernel (blue) and MD-based (green) method for fault in R_3 .	38
Figure 16:	DC-DC buck converter system design abstraction levels	40
Figure 17:	Schematic of a LC low pass filter circuit in a DC-DC converter system.	41
Figure 18:	LPF circuit health estimated using the kernel method	42

	(blue) in comparison to the actual health HI_t^A for the progression of parametric fault in C – Run 1.	
Figure 19:	LPF circuit health estimated using the kernel method (blue) in comparison to the actual health HI_t^A for the progression of parametric fault in C – Run 2.	42
Figure 20:	LPF circuit health estimated using the kernel method (blue) in comparison to the actual health HI_t^A for the progression of parametric fault in C – Run 3.	43
Figure 21:	LPF circuit health estimated using the kernel method (blue) in comparison to the actual health HI_t^A for the progression of parametric fault in C – Run 4	43
Figure 22:	Schematic of voltage divider feedback circuit in a DC-DC converter system.	44
Figure 23:	Voltage divider feedback circuit health estimated using the kernel method (blue) in comparison to the actual health HI_t^A for the progression of parametric fault in R_1 .	45
Figure 24:	Voltage divider feedback circuit health estimated using the kernel method (blue) in comparison to the actual health HI_t^A for the progression of parametric fault in R_3 .	46
Figure 25:	Prognostic illustration.	52
Figure 26:	Simple one-component circuit for degradation modeling illustration.	53
Figure 27:	Illustration of the steps involved in simple particle filter	59
Figure 28:	Observed and estimated degradation in health of low pass filter circuit due to progression of fault in electrolytic capacitor.	63
Figure 29:	Estimated deviation in capacitance of liquid electrolytic capacitor.	64
Figure 30:	<i>RUL</i> estimation result for low pass filter circuit using model-based filtering method.	64
Figure 31:	Observed and estimated degradation in voltage feedback circuit health due to progression of fault in R_1 .	66
Figure 32:	Estimated deviation in resistor R_1 of voltage feedback circuit.	66
Figure 33:	<i>RUL</i> estimation result in voltage feedback circuit due to progression of fault in R_1 using model-based filtering method.	67
Figure 34:	Observed and estimated degradation in voltage feedback circuit health due to progression of fault in R_3 .	67
Figure 35:	Estimated deviation in resistor R_3 of voltage feedback	68

	circuit.	
Figure 36:	<i>RUL</i> estimation result in voltage feedback circuit due to progression of fault in R_3 using model-based filtering method.	68
Figure 37:	Estimated voltage feedback circuit health due to simulated progression of fault in component R_3 .	69
Figure 38:	Estimated deviation in resistance R_3 of voltage feedback circuit with simulated component degradation.	70
Figure 39:	<i>RUL</i> estimation result in voltage feedback circuit due to simulated progression of fault in R_3 using model-based filtering method.	71
Figure 40:	<i>RUL</i> prediction results for voltage divider feedback circuit with (a) random walk model for θ_t and (b) first principles-based model for θ_t .	72
Figure 41:	Predicted <i>RUL</i> distribution for voltage divider feedback circuit with random walk model (red) and first principles-based model (blue) for θ_t at (a)-(c) 100hours and (b)-(d) 50hours before failure.	73
Figure 42:	Average performance of particle filter and CE optimization methods on 20-D Powell singular function [49].	78
Figure 43:	Average performance of MRAS, CE, and SA optimization methods on 20-D Powell singular function [50].	79
Figure 44:	Comparison of filtering-based optimization with PSO on benchmark problems: (a) Trigonometric, (b) Powel's singular, and (c) Rosenbrock function.	81
Figure 45:	Comparison of filtering-based optimization with and without gradient information on Trigonometric function.	82

List of Abbreviations

ALT – Accelerated Life Test

BPF – Band Pass Filter

CUT – Circuit Under Test

ED – Euclidean Distance

EOL – End of Life

IGBT – Insulated Gate Bipolar Transistor

HI – Health Indicator

LPF – Low Pass Filter

LS-SVM – Least Squares Support Vector Machine

MD – Mahalanobis Distance

PDF – Probability Density Function

RUL – Remaining Useful Life

SVM – Support Vector Machine

Chapter 1: Introduction

Electronics are increasingly used in mission, safety, and infrastructure-critical systems. Unexpected failures in such electronic systems during field operation can have severe implications [1]. Failures could be prevented and unexpected system downtime could be eliminated if an appropriate prognostic method is incorporated to determine the advent of failure and mitigate system risk [2].

Electronic system failures can result from any part of the electronics, including faults in the circuit board (e.g. traces), electronic components, or connectors. Many discrete electronic components such as capacitors, resistors, transistors, and more exhibit parametric faults as they age i.e., exhibit fractional deviation in component parameters (such as resistance, capacitance, and more) from their initial values and beyond their acceptable tolerance range [3]. The intensity of the fault, meaning the magnitude in parametric drift from initial value, increases as the fault progresses. For example, the capacitance of a liquid electrolytic capacitor decreases with constant exposure to elevated temperature [4]. The resistance between collector and emitter of an insulated gate bipolar transistor (IGBT) increases due to die-attach degradation resulting from thermo-mechanical stresses induced by power cycling [5]. Figure 1 shows parametric drifts exhibited by electrolytic capacitor [4], IGBT [5], embedded capacitor [6], and resistor [7] under accelerated stress tests.

Parametric faults in circuit components affect the performance of the circuit they are part of and eventually compromise the electronic system functions [3]. For example, photovoltaic power inverters often are plagued by parametric faults in electrolytic capacitors and IGBTs, which result in loss of power generation that are

valued in millions of dollars [8][9]. A parametric fault in capacitors and inductors within railway track circuit leads to significant disruption of rail service and could pose safety risks [10]. Thus predicting electronic circuit failures resulting from the progression of parametric faults in components will aid in improving the operational reliability and availability of electronic systems.

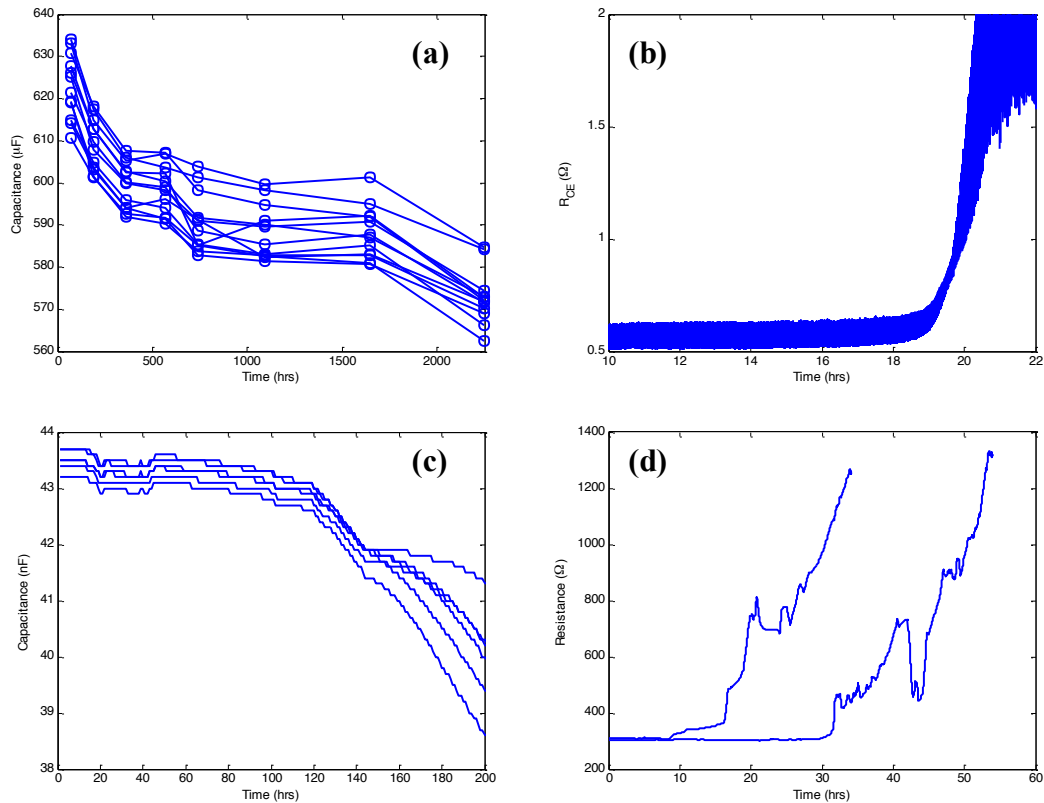


Figure 1. Example plots for parametric drifts exhibited by electronic components. (a) Degradation of electrolytic capacitors under isothermal aging is accompanied by decrease in capacitance parameter. (b) Increase in resistance between the collector and emitter (R_{CE}) terminals of an insulated gate bipolar transistor due to die attach degradation. (c) Decrease in capacitance with degradation of embedded capacitors under combined temperature and voltage aging. (d) Increase in resistance with solder joint degradation of surface mount resistors under thermal cycling conditions.

Development of a prognostic method generally involves the development of a (1) health estimation method, (2) degradation model, and (3) failure prediction method

(see Figure 2). In the health estimation step, the degradation in circuit health (or performance) is quantified and expressed as a health indicator (**HI**). The health indicator could be an estimate of the accumulated damage or a drift in circuit performance. In the degradation-modeling step, a first principles-based or an empirical model is developed to estimate the progression of **HI** based on the current health and operating conditions. In the failure prediction step, the end of life (**EOL**) is predicted (from which remaining useful life (**RUL**) is estimated) by integrating the degradation model with knowledge about future operating conditions, current and past estimates of **HI** using an appropriate regression technique.

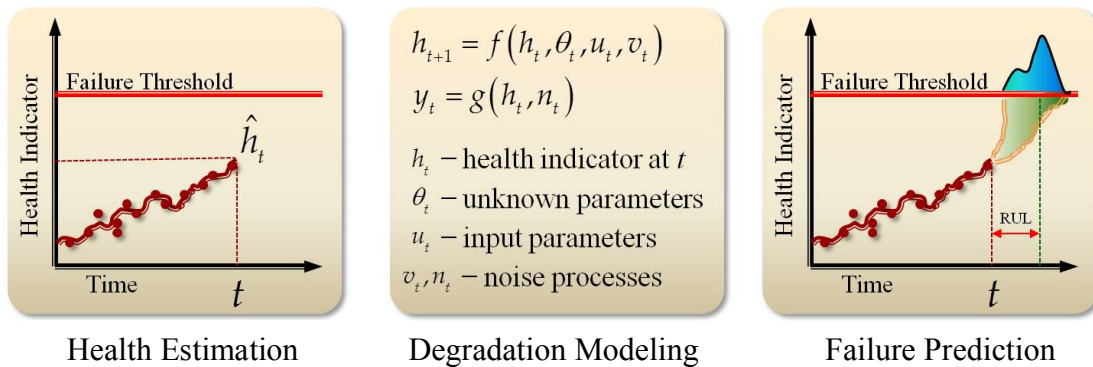


Figure 2. Typical steps involved in a prognostic approach.

The scope of this dissertation is focused on the estimation and degradation modeling of the circuit health in the presence parametric faults in circuit components. Here, an electronic circuit is defined as a collection of discrete components that are connected in a closed- or open-loop format to carry out a predetermined function. A parametric fault is defined as the deviation in circuit component parameters from their initial values and beyond their acceptable tolerance range [3]. The existing literature pertaining to health estimation and *RUL* prediction of parametric fault is reviewed in

Chapter 2: Literature Review. Additionally, the research gaps in the existing literature and the objectives of this dissertation are also provided in Chapter 2.

Chapter 2: Literature Review

Many methods have been developed to estimate health and predict failures of mechanical systems [11]-[14]. However, health estimation and failure prediction in electronics is made challenging by the presence of component tolerances, interdependency of electronic components, and the complex nature of fault mechanisms. The existing literature is classified and reviewed based on the approach employed for health estimation and failure prediction. The two approaches being the component-centric and circuit-centric approaches.

2.1 Component-Centric Approach

Most of the current methods for the prognosis of failures resulting from component parametric faults implements a component-centric approach that have relied on the in-situ measurements of component-level parameters exhibiting monotonicity and trending them using an appropriate regression technique. For example, Celaya et al. [14] and Kulkarni et al. [15] developed a first principles-based model that uses capacitance (C) and equivalent series resistance (ESR) measurement to predict electrolytic capacitor failures. Patil et al. [5] and Celaya et al. [16] employed statistical filtering technique along with an empirical model to predict insulated gate bipolar transistor (IGBT) failures using resistance between collector-emitter, R_{CE} parameter. Kwon et al. [17][18] used particle filtering to predict the time-to-failure of solder joints subjected to a mechanical stress condition based on RF impedance monitoring. A study by Alam et al. [6] focused on a distance-based data-driven approach to track the degradation of embedded capacitors using past and current measurements of the capacitance, dissipation factor, and insulation resistance

parameters. These methods approach prognostics from a component-centric perspective. However, in practical applications it may not be viable to measure the parameters of individual components of a circuit to predict failures. In particular, the number of components one needs to monitor can make it economically prohibitive. Additionally, parameters like resistance, capacitance, or inductance have to be measured when the component is not part of circuit. Once the component of interest is part of a circuit, the contributions from the rest of the circuit components affect the measurement of individual component parameters. It is for all of these reasons that the work in this dissertation takes a circuit-centric approach in contrast to a component-centric approach to predict failures resulting from parametric faults.

2.2 Circuit-Centric Approach

The principle underlying a circuit-centric approach is that the presence of a parametric fault in circuit components will change the circuit characteristics and as the parametric fault increases in magnitude, the circuit performance degrades, eventually leading to a functional failure. Thus, a health estimation or failure prediction method that exploits features specific to the electronic circuitries will alleviate the need to monitor the individual circuit components.

The concept behind circuit-centric approach is not new. However, most of the existing research that employs a circuit-centric approach has aimed at detecting and isolating the component exhibiting parametric fault [19]-[24] using a machine learning technique. A few studies [25]-[28] have developed methods to quantify degradation in the health of a circuit and predict circuit failures due to parametric deviations in circuit components. These studies employ a distance-based method to

estimate the circuit health from the extracted circuit features and uses an empirical-model along with particle filter or relevance vector machine (RVM) to estimate the trend in circuit health degradation and predict *RUL*. For example, in Vasan et al. [25], the circuit health (also referred to as health indicator, *HI*) was estimated using a Mahalanobis distance (MD)-based feature transformation:

$$HI = \frac{\prod_{i=1}^r (MD_i)^{-n_i}}{\sum_{i=1}^r (MD_i)^{-n_i}} \quad (1)$$

where r represents the total number of feature sets extracted (e.g., time-domain, wavelet-based, or statistical features) with each feature set containing n_i elements, and MD_i represents the MD value for the i^{th} feature set. The idea behind Eq. (1) is that MD amplifies parametric deviations outside the tolerance range compared to the allowable parametric deviations within the tolerance range. *RUL* prediction in [25] was realized by coupling a sum of double-Gaussian process model (see Eq.(2)) with particle filter:

$$HI_t = a_t^{(1)} \left[- \left(\frac{t-b_t^{(1)}}{c_t^{(1)}} \right)^2 \right] + a_t^{(2)} \left[- \left(\frac{t-b_t^{(2)}}{c_t^{(2)}} \right)^2 \right] \quad (2)$$

where HI_t is the circuit health at time t is the time index; and $a_t^{(1)}, b_t^{(1)}, c_t^{(1)}, a_t^{(2)}, b_t^{(2)}$ and $c_t^{(2)}$ are the model parameters.

Following [25], Li et al. [26] provided an estimate for analog filter circuit health (*HI*) using a Euclidean distance (ED) measure:

$$HI = \frac{1}{n} \sum_{i=1}^n \bar{f}_i; \text{ with } \bar{f}_i = \frac{f_i - f_{min}}{f_{max} - f_{min}} \quad (3)$$

where f_i denotes the deviation in i^{th} feature, f_{min} denotes the minimum deviation distance, f_{max} denotes the maximum deviation distance, and n the total number of features. However, the HI calculated using Eq. (2) does not take into account the correlation between extracted features. Thus, if two features are correlated, the HI calculated using Eq. (2) might exhibit a rapid increase leading to a false alarm, even before the circuit has functionally failed. Furthermore, RUL prediction in [26] was carried out in a fashion similar to the approach employed in [25] with the only difference being the use of sum of double-exponential process model, as in Eq. (4), in place of a Gaussian process model:

$$HI_t = a_t[\exp(t.b_t)] + c_t[\exp(t.d_t)] \quad (4)$$

where HI_t is the circuit health at time t is the time index; and $a_t, b_t, c_t,$ and d_t are the model parameters.

Zhang et al. [27] and Zhou et al. [28] calculated the HI as the $\cos(*)$ and $\sin^{-1}(*)$ of the distance between the test features and the features extracted from circuit response under no-fault condition, but failed to take into account the effect of component tolerances. Prior experience has shown that the presence of component tolerances induces noise (in addition to measurement noise) in the features extracted and as a result affects the accuracy of a diagnostic and prognostic technique. Zhou et al. [28] employed the same model and regression technique as Li et al. [26] for RUL prediction. Zhang *et al.* [27] on the other hand used a RVM's inherent model instead of a regression fit to realize RUL prediction, which requires and assumes the RUL random variable is Gaussian distributed.

The work of Kumar et al. [29] and Sutrisno [30], although not directly applied to circuits, can be adopted for circuit health estimation. The *HI* estimation method developed by Kumar et al. [29] was based on the fractional contributions by the MD measures over a time window of extracted features and was applied to detect anomalies. When an anomaly occurs, the number of higher MD values in a time window would increase, resulting in greater fractional contribution from the histogram bin's with higher MD values and eventual increase in *HI*. Sutrisno [29] proposed a *k*-nearest neighbor (*k*-NN)-based *HI* method, where the health is estimated as the ED measure between data to the centroid of the nearest neighbors from offline constructed healthy and failure classes.

2.3 Gaps in Existing Literature

The above-mentioned MD and ED measure-based health estimation methods [25]-[30] rely on the assumption that the distance between samples of the healthy classes is smaller when compared to the distance between samples from the healthy class to that from the failure class in the principal component space (PCS) or Euclidean space (ES) respectively. This condition requires that the healthy and failure classes be linearly separable in the extracted feature space (see Figure 3) i.e., classification between healthy and failure classes can be realized using a decision function of the following form:

$$h_w(x) = g(w^T x) \quad (5)$$

such that, $w^T x > k$ (or $< k$); $x \in H$

and, $w^T x < k$ (or $> k$); $x \in F$.

where, w is a weighting vector, H and F denotes the healthy and failure classes, and k is a constant. However, prior work [22]-[25] has demonstrated that circuit responses under no-fault and faulty conditions require nonlinear methods such as kernel-learning techniques for fault diagnosis and are seldom linearly classifiable in the extracted feature space.

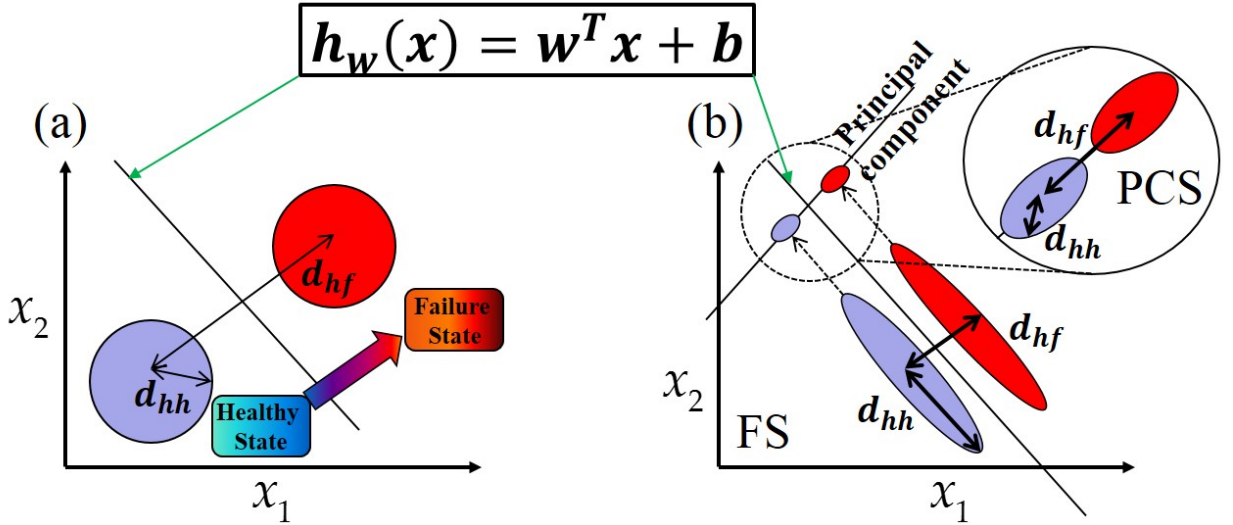


Figure 3. Examples where linear separability between healthy and failure classes ensures $d_{hh} < d_{hf}$ either in (a) Euclidean Space or (b) Principal Component Space.

Menon et al. [31] compared various covariance estimation method with MD to classify parametric faulty from healthy features of Sallen-Key Band Pass Filter. The best fault classification accuracy achieved with MD method was $\sim 78\%$. However, Vasan et al. [25] demonstrated that for the same benchmark circuit with same training and testing data, a trained least square-support vector machine (LS-SVM, a kernel-based classifier) can achieve classification accuracy $\sim 99\%$. This proves that, a non-linear method is required to classify a healthy circuit from a circuit with parametric fault. Since health estimation methods extend the idea of fault classification, it is

expected that a health estimation method based on non-linear technique such as kernel-based learning is likely to provide health estimates with higher efficiency.

Furthermore, the degradation models used in the above-mentioned studies for failure prediction [25]-[28] are entirely empirical and does not describe the actual progression of parametric fault in the circuit components. It has been demonstrated earlier [32] that, a first principles-based model that uses domain knowledge to capture the physics-behind degradation leads to a reliable prognostics outcome. This was also demonstrated by Kulkarni et al. [25], who used a first principles-based model instead of an empirical model, as used by Celaya et al. [14], to improve accuracy in electrolytic capacitor failure prediction. Thus there is a need for a first principles-based degradation model that describes the progression of parametric fault in the circuit component to generate reliable *RUL* estimates for circuits with parametric faults.

2.4 Dissertation Objectives

The first objective of this dissertation is to develop a kernel-based learning technique to estimate the health degradation of an electronic circuit due to parametric deviation in the circuit components. The health estimate should closely reflect intensity of the fault, meaning the magnitude in parametric drift from nominal value, as closely as possible.

The second objective of this dissertation is to develop a first principles-based model to track degradation in circuit health due to the progression of parametric fault. This model will be used in conjunction with a stochastic filtering technique to predict *EOL* of a circuit generate *RUL* estimates.

Chapter 3: Electronic Circuit Health Estimation Through Kernel Learning

This chapter presents the developed circuit-centric approach to circuit health estimation, which was posed and solved as a soft classification problem (first established by Wahba [33]) in the kernel Hilbert spaces using a parameterized kernel function. Thus, the circuit-centric approach uses a kernel-based machine learning technique to exploit features extracted from responses of circuit-comprising components exhibiting parametric faults, instead of component-level parameters to generate health estimates. Hence, this chapter begins by providing a brief background on kernel-based learning and hyperparameter selection in the context of kernels in Section 3.1. The health estimation problem is formulated as a kernel-based learning problem for which an efficient solution is developed in Section 3.2. Section 3.3 presents the performance results of the health estimation method on a Sallen–Key band pass circuit and the circuits of a DC–DC buck converter system.

3.1 Kernel-Based Learning

The principle underlying kernel-based approaches (illustrated in Figure 4) that capture nonlinear relationships in the learning dataset (i.e., fault dictionary built for a circuit), is to map the data from a feature space to a higher-dimensional space and fit linear models in the projected space [34][35]. This task of projecting to a higher-dimensional space is realized through computations in the form of inner products via kernel functions [36]. Given new test data, a decision on the test data is made by projecting the test data to the higher-dimensional space and then calculating the

similarity measures between the test data, \mathbf{x}_t , and all other training data, $\{\mathbf{x}_i\}_{i=1}^n$, (both healthy and failure).

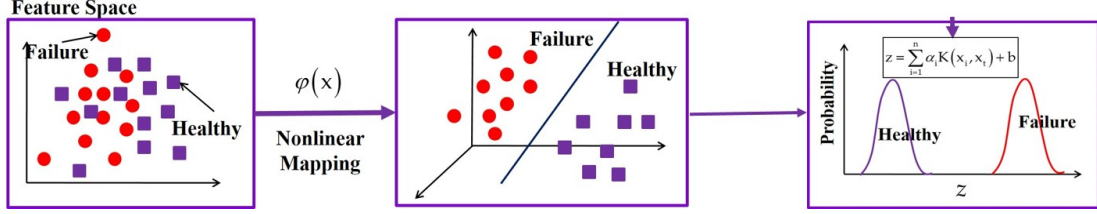


Figure 4. Illustration of the principle underlying kernel-based learning methods.

The function, $K(x_i, x_t): \mathbb{R}^{n_d} \times \mathbb{R}^{n_d} \rightarrow \mathbb{R}$, determines the similarity measure between the test, x_t , and training feature, x_i , of length n_d and often a parameterized family of kernel functions is considered. For example, the automatic relevance determinant Gaussian kernel function

$$K(x_i, x_t) = \exp\left(-\sum_{j=1}^{n_d} \frac{\|x_{i,j} - x_{t,j}\|^2}{\sigma_j}\right) \quad (6)$$

is parameterized by $\boldsymbol{\sigma} = [\sigma_1 \ \sigma_2 \ \dots \ \sigma_{n_d}]$, where $\boldsymbol{\sigma}$ is generally referred to as the kernel parameters. Furthermore, in the presence of component tolerances, the learning dataset is noisy and as a result one has to also include a regularization parameter, γ , to control the complexity of the decision function.

The representation of the intermediate metric, z , which aids in decision making (i.e., in classification the decision function is $\text{sign}(z)$; for regression, z is the output; and for health estimation, $HI = g(z)$) of the test data x_t , takes the following form [37]-[39]:

$$z = \sum_{i=1}^n \alpha_i K(x_i, x_t) + b \quad (7)$$

where $[\alpha_1 \ \alpha_2 \ \dots \ \alpha_n \ b]$ are the model parameters, and n represents the total training features available for learning. The estimation of model parameters has been

extensively dealt with in the literature [37]-[39]. However, the estimation of model parameters depends on the choice of regularization parameter, γ , and kernel parameters, σ , which are collectively referred to as the hyperparameters, \mathbf{h} . The automatic selection of hyperparameter values by the learning algorithm for a given training dataset is referred to as the model selection problem.

The model selection problem can be solved by optimizing an error measure, such as ν -fold cross-validation error, on a grid of hyperparameter values [33][40]. However, a grid search approach does not cover the entire hyperparameter space and is computationally expensive (depending on the length n_d of feature vector x). Gradient descent-based methods have also been reported in the literature for model selection [41]-[43]. However, it is well understood that the gradient descent is optimal only when the validation measure is convex (or concave). Otherwise, the gradient descent-based methods are affected by the local minima problem. Alternatively, evolutionary direct search methods that allow for different solutions to interact with the purpose to allocate more resources in the regions of the search space have been successfully applied to estimate hyperparameters [44]-[47]. However, in higher-dimensional search spaces, it is desirable to base the search on directional information as provided by the gradient descent. Hence, this study combined the advantage of gradient descent with an evolutionary search by drawing inspiration from Zhou et al. [48] to solve the model selection problem in the context of circuit health estimation.

3.2 Heath Estimation Method

The developed circuit health estimation method involves both learning and testing phase. During the learning phase, a fault dictionary is constructed, on which the

kernel-based learning algorithm is trained. In the testing mode the circuit health is estimated by extracting and comparing features with those stored in the constructed fault dictionary using a trained kernel algorithm.

In order to construct a fault dictionary, the critical components of the circuit under test (CUT) are identified, using failure modes, mechanisms, and effects analysis (FMMEA) [51] or historical data or test results. Then we determine how the critical components will exhibit parametric faults and then perform fault-seeded simulations. For each critical component identified and for each failure mode through which the critical component can exhibit fault, a fault-seeded simulation must be performed. Thus, if there are four critical components and each component can exhibit faults in two different modes, such as in Sallen-Key filter, there are eight (4x2) fault-seeded conditions and one no-fault condition. Overall, a Sallen-Key filter circuit has nine fault conditions.

A critical component is a discrete element, such as an electrolytic capacitor or IGBT, which has a high risk of exhibiting parametric deviations (see Figure 1) and eventually prevents the circuit from performing its intended functions. For example, assume a low-pass filter designed to allow signals with frequencies less than 2 kHz. If the low-pass filter's critical components exhibit parametric faults and cause the circuit to allow 3 kHz signals, then the circuit is considered to have failed.

For electronic circuits, the behavioral characteristics are assumed to be embedded in either or both the time and frequency responses. Hence, the circuit must be excited by a test signal to extract features. For example, the characteristics of a filter circuit are contained in its frequency response. In order to extract features from the

frequency response, the filter circuit has to be excited by an impulse signal or a sweep signal, based on whether the filter circuit is linear or nonlinear.

Once the critical component and its fault modes (i.e., how the component exhibits parametric deviation) are identified, the CUT is then replicated in a simulation environment (e.g., PSPICE) for its hypothesized fault conditions and excited by a test signal to extract features. Here, a fault condition refers to a situation where one of the CUT's critical components has deviated beyond a predefined failure range, which is larger than the actual tolerance range, such that the CUT fails to carry out its intended function. Fault-seeded testing can also be performed instead of running simulations, however, depending on the circuit complexity and the number of critical components this task may be time-consuming. Applying a signal processing technique such as wavelet transform on the CUT responses typically performs the feature extraction task. Feature extraction for CUT diagnostics is extensively addressed in the literature [20]-[22], [25], [52]-[55] and can be employed as needed for circuit health estimation. Features extracted under various fault conditions are stored in a fault dictionary.

Let the features available during training be denoted by $S = \{x_i, y_i\}_{i=1}^n$, where n denotes the number of training samples, x_i is the i th feature vector of length n_d that is extracted from the circuit response to test stimulus and belongs to feature space X , and $y_i \in Y$ is the label for which $y_i = +1$ denotes the feature vector x_i is extracted when the circuit was healthy, and $y_i = -1$ denotes the feature vector x_i is extracted when the circuit failed, (i.e., the parametric deviation in one of the circuit components has caused the circuit characteristics to go out of bounds). The goal of the circuit

health estimation problem is to estimate a metric $HI \in [0,1]$ for a test input x_t given S .

In kernel methods a feature vector (x) is projected to a higher-dimensional space where the healthy and failure classes are linearly separable. An intermediate metric (z) is calculated to identify where the test point is projected to in the higher-dimensional space using Eq. 6. For a given choice of hyperparameters, the model parameters in Eq. 7 can be optimally estimated. For example, in least squares-support vector machine (LS-SVM) or regularization network, the model parameters can be estimated by solving a system of linear equations [38][39]:

$$\begin{bmatrix} \mathbf{\Omega} + \frac{1}{\gamma} \mathbf{I} & \mathbf{1} \\ \mathbf{1}^T & 0 \end{bmatrix} \begin{bmatrix} \boldsymbol{\alpha} \\ b \end{bmatrix} = \begin{bmatrix} \mathbf{Y} \\ 0 \end{bmatrix} \quad (8)$$

where $\boldsymbol{\alpha} = [\alpha_1 \ \alpha_2 \ \dots \ \alpha_n]^T$, $\mathbf{Y} = [y_1 \ y_2 \ \dots \ y_n]^T$, $\mathbf{1} = [1,1,1 \dots 1]_{n \times 1}^T$, \mathbf{I} is an identity matrix of size $n \times n$, and $\mathbf{\Omega} = [\Omega_{ij}] = [K(x_i, x_j)]$.

In order to estimate the circuit health HI_t , at time t , the metric is treated as the healthy class conditional probability i.e., the probability that x_t is extracted when the CUT is healthy and no critical component exhibit parametric fault. Platt [56] demonstrated that the conditional probability of the positive label given the prediction from Eq. 7 could be represented by a logistic regression function. Thus, using Platt's [56] posterior class probability function, the circuit health HI_t can be estimated from z_t using the following form:

$$\widehat{HI}_t = P(y_t = +1/x_t) = g(z_t) = \frac{1}{1 + \exp(Az_t + B)} = p_t \quad (9)$$

where \mathbf{A} and \mathbf{B} are parameters are estimated by using Newton's backtracking method over the training dataset \mathbf{S} [57]. As can be seen from Eq. 9, \mathbf{HI} depends on \mathbf{z} , and it

has been established in Sec. 3.1 that \mathbf{z} depends on the hyperparameters \mathbf{h} . Thus, the proper selection of \mathbf{h} for a given \mathbf{S} is necessary to achieve the best possible accuracy in health estimation. An overview of the developed circuit health estimation method is schematically represented in Figure 5.

3.1.1 Likelihood-based Function for Model Selection

The model selection problem is often solved by constructing an objective function with a probabilistic interpretation of a term that takes form $F + \lambda R$, where F depends on the empirical loss, R is the regularization term, and λ is the regularization parameter. Glasmachers and Igel [41] argued that this function is better off represented as a negative logarithm of a posterior probability than choosing priors on hyperparameters. Based on this argument, an objective function has been developed that extends Platt's [56] posterior class probability function to a negative log-likelihood function.

Let p denote the health estimate for a CUT from which a feature vector (x) is extracted. Then, the likelihood function $\mathcal{L}(\cdot)$ for a feature vector (x_i) is p_i if $y_i = +1$ (circuit is healthy) and $(1 - p_i)$ if $y_i = -1$ (circuit failed). This can be mathematically expressed as follows:

$$\mathcal{L}(x_i, y_i) = p_i^{\left(\frac{y_i+1}{2}\right)} (1 - p_i)^{\left(\frac{1-y_i}{2}\right)}. \quad (10)$$

However, in Eq. (10), p_i is a function of z_i , i.e., $p_i = g(z_i)$ and z_i in turn depends on the model parameters α and b (see Eq. 7), which in turn depend on the hyperparameters γ and σ (see Eq. 8). Thus, the likelihood function is essentially a function of the hyperparameters. The objective function is typically defined over

cross-validation datasets that are extracted from the training dataset. Thus, the cost function is the negative log-likelihood function over a cross-validation set $\tilde{S} = \{x_l, y_l\}_{l=1}^L$:

$$\mathcal{L}_{\tilde{S}}(\gamma, \sigma) = - \sum_{l=1}^L \left(\left(\frac{y_l+1}{2} \right) \log(p_l) + \left(\frac{1-y_l}{2} \right) \log(1 - p_l) \right) \quad (11)$$

where $p_l = \frac{1}{1+\exp(Az_l+B)}$ and $z_l = \sum_{i=1}^n \alpha_i K(x_i, x_l) + b$.

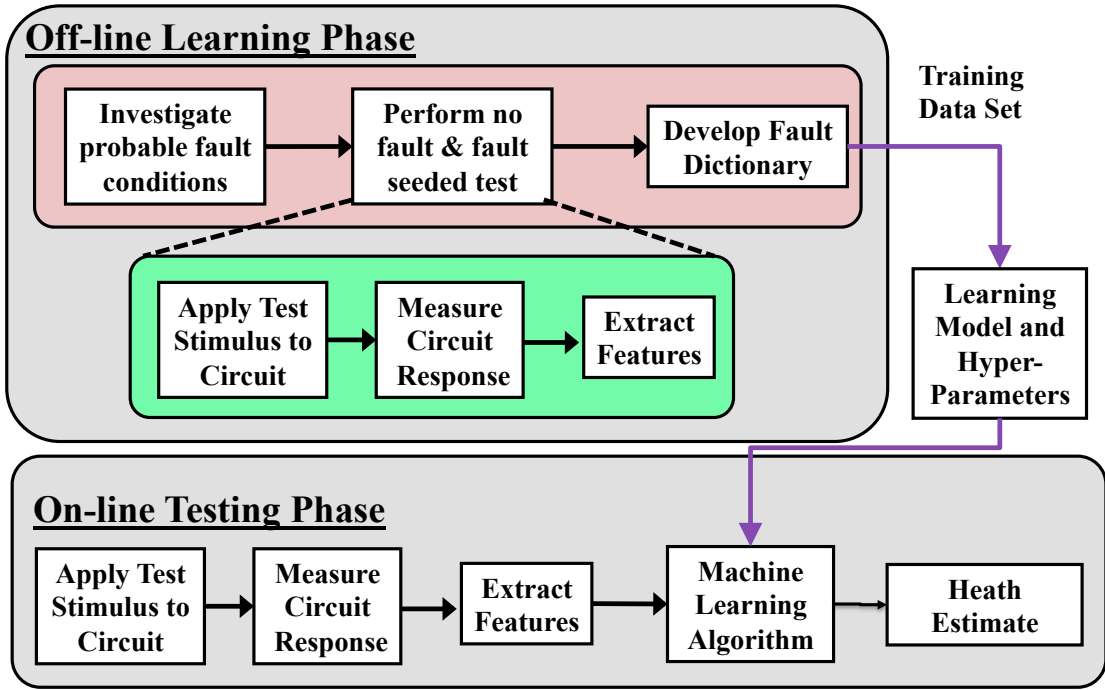


Figure 5. Overview of the proposed circuit health estimation method.

For model selection, this study focuses on minimizing the k-fold cross-validation log-likelihood

$$\bar{\mathcal{L}} = \sum_{k=1}^K \mathcal{L}_{\tilde{S}_k}(\gamma, \sigma) \quad (12)$$

where $S = \tilde{S}_1 \cup \tilde{S}_1 \cup \dots \tilde{S}_K$ is a partition of the training dataset into K disjoint subsets and $\mathcal{L}_{\tilde{S}_k}(\gamma, \sigma)$ denotes the objective function given the holdout set S_k .

3.1.2 Optimization Approach for Model Selection

To identify the hyperparameter values that will reduce the generalization error (Eq. 12), the optimization problem can be mathematically expressed as follows:

$$h^* = \arg \min_{h \in \mathcal{H}} \mathcal{L}_S(h) \quad (13)$$

where $\mathcal{L}_S(h)$ denotes the likelihood function $\bar{\mathcal{L}}$ in Eq. 12 over the cross-validation set \mathcal{S} , and \mathcal{H} denotes the solution space for hyperparameters. It is assumed that $\mathcal{L}_S(h)$ has a unique global optimal solution h^* .

Many global optimization algorithms such as particle swarm optimization (PSO) [58] or simulated annealing (SA) [59] could be applied to solve this problem. Global optimization algorithms share the similarity of iteratively repeating the following two steps: (1) the candidate solutions are generated from an intermediate distribution over the solution space, and (2) the intermediate distribution is updated using the candidate solutions. The difference between various global optimization methods depends on how the aforementioned two steps are performed. An approach for global optimization with a faster convergence rate was developed by Zhou *et al.* [48] by reformulating the global optimization problem as a stochastic filtering problem. Zhou [49] demonstrated in her thesis that a filtering-based global optimization approach outperforms cross entropy (CE) and SA optimization methods. Boubezoul and Paris [50] in-turn demonstrated that the classification accuracy obtained using CE method for selecting the hyperparameters of a SVM classifier is better than the classification accuracy obtained with PSO or grid search optimization methods. Additional simulation studies were carried out in Appendix A to demonstrate superiority of Zhou's [49] filtering-based global optimization approach over PSO. The stochastic

filtering-based global optimization approach allows for directional information to be included during the search process and thus was incorporated into this work to solve the model selection problem.

The goal of stochastic filtering is to estimate the unobserved state in a dynamic system through a sequence of noisy observations of the state. The unobserved state corresponds to the optimal solution to be estimated; the noisy observations in filtering bring randomization into the optimization algorithm; and the conditional distribution of the unobserved state is a distribution over the solution space, which approaches a delta function concentrated on the optimal solution as the system evolves. Hence, the task of searching for the optimal solutions is carried out through the procedure of estimating the conditional density sequentially. Some sort of approximation is required to implement a stochastic filtering method. Particle filter is a widely used sequential Monte Carlo technique that does not apply a constraint on the state's distribution and does not need Gaussian assumption on the process noise. Hence, a particle filter is employed for performing global optimization to solve the model selection problem.

The optimization problem is transformed into a filtering problem by constructing an appropriate state-space model. Let the state space model be:

$$h_k = h_{k-1} - \varepsilon \nabla \mathcal{L}(h_{k-1}); \quad k = 1, 2, \dots \quad (14)$$

$$e_k = \mathcal{L}(h_k) - v_k \quad (15)$$

where h_k is the unobserved state to be estimated (i.e., the new set of hyperparameters) and e_k is the observation with noise v_k (which brings randomization into the optimization algorithm).

In Eq. 14, $\nabla\mathcal{L}(h_k)$ denotes the gradient of the likelihood function $\mathcal{L}_S(h)$ with respect to the hyperparameters h_k . Since $\mathcal{L}(h_k)$ is log-likelihood function, it is differentiable with respect to the hyperparameters whenever the kernel function is differentiable. $\nabla\mathcal{L}(h_k)$ can be found by solving the following system of linear equations if the automatic relevance determinant Gaussian kernel function is chosen:

$$\frac{\partial\mathcal{L}_S}{\partial\gamma} = \sum_{l=1}^L \frac{\partial\mathcal{L}_S}{\partial p_l} \left[\frac{-A \exp[A\boldsymbol{\psi}^T(x_l)\boldsymbol{\beta}]}{p_l^2} \right] \boldsymbol{\psi}^T(x_l)\dot{\boldsymbol{\beta}} \quad (16)$$

$$\frac{\partial\mathcal{L}_S}{\partial\sigma_i} = \sum_{l=1}^L \frac{\partial\mathcal{L}_S}{\partial p_l} \left[\frac{-A \exp[A\boldsymbol{\psi}^T(x_l)\boldsymbol{\beta}]}{p_l^2} \right] \{\boldsymbol{\psi}^T(x_l)\dot{\boldsymbol{\beta}} + \dot{\boldsymbol{\psi}}^T(x_l)\boldsymbol{\beta}\} \quad (17)$$

where $p_l = (1 + \exp(A\boldsymbol{\psi}^T(x_l)\boldsymbol{\beta} + B))^{-1}$,

$\boldsymbol{\psi}^T(x_l) = [k(x_1, x_l) \quad k(x_2, x_l) \quad \cdots \quad k(x_n, x_l) \quad 1]$, and

$\boldsymbol{\beta} = [\alpha_1 \quad \alpha_2 \quad \cdots \quad \alpha_n \quad b]^T$. In Eq. 16 and Eq. 17, $\dot{\boldsymbol{\beta}}$ is obtained by solving

$$\text{for } \dot{\boldsymbol{\beta}} = -\mathbf{P}^{-1}\dot{\mathbf{P}}\boldsymbol{\beta}, \text{ where } \mathbf{P} = \begin{bmatrix} \boldsymbol{\Omega} + \frac{1}{\gamma}\mathbf{I} & \mathbf{1} \\ \mathbf{1}^T & 0 \end{bmatrix}.$$

Figure 6 illustrates the use of particle filter for optimization in model selection, and the algorithm is summarized below, where the hyperparameter is assumed to be one-dimensional for illustration purposes. Initially, a distribution b is assumed over the solution space for hyperparameters \mathcal{H} as shown in Figure 6(a). This distribution represents the probability of having a global optimum at different regions of the solution space. Random sampling of the hyperparameter space is done in an independent and identically distributed (i.i.d) fashion, and the corresponding generalization error $\bar{\mathcal{L}}$ (see Eq. 12) for each choice of hyperparameter h_k^j is obtained. Next, the hyperparameter vectors are updated as shown in Figure 6(b) based on their

gradients $\nabla\mathcal{L}(h_k^N)$. In the next step, the hyperparameter vectors with least generalization error (i.e., elite performing particles) are selected as $(1 - \rho)$ -quantile of all generalization error as shown in Figure 6(c). Then, the distribution b is updated as shown in Figure 6(d) based on the elite performing particle locations on the solution space. Since the distribution b is represented by particles and their associated weights, various shapes for b can be realized without having to establish a parametric model. The above-mentioned steps are repeated until the distribution b is close to a delta function, indicating that the global optimum is identified.

Algorithm 1. Particle filtering algorithm for hyperparameter optimization.

Input: Training features from fault dictionary

$$S = \{x_i, y_i\}_{i=1}^n$$

Output: Estimated optimal hyperparameter vector: $h \in \mathcal{H}$

1. **Initialization step:** Specify $\rho \in (0,1]$ and an initial probability density function

(pdf) b_0 that is defined on \mathcal{H} . Sample $\{h_1^j\}_{j=1}^N$ i.i.d. from b_0 . Set $k = 1$.

2. **Observation construction step:** Let e_k be the sample $(1 - \rho)$ -quantile of

$\{\mathcal{L}(h_1^j)\}_{j=1}^N$. If $k > 1$ and $e_k < e_{k-1}$, then set $e_k = e_{k-1}$.

3. **State update step:** Update the particle locations in the hyperparameter space as per the system dynamic model

$$h_k = h_{k-1} - \varepsilon \nabla \mathcal{L}(h_{k-1}); \quad k = 1, 2, \dots$$

4. **Bayes' updating step:** $b_k(h_k) = \sum_{j=1}^N w_k^j \delta(h_k - h_k^j)$ where weights are calculated according to

$$w_k^j \propto \varphi(\mathcal{L}(h_1^j) - e_k)$$

and normalized.

5. Resampling step: Construct a continuous approximation from $b_k(h_k)$ and then perform i.i.d sampling to get $\{h_{k+1}^j\}_{j=1}^N$.

Stopping criterion: If the standard deviation of $b_k(h_k) < \omega$, then stop. Else, $k \leftarrow k + 1$ and go to step observation construction step.

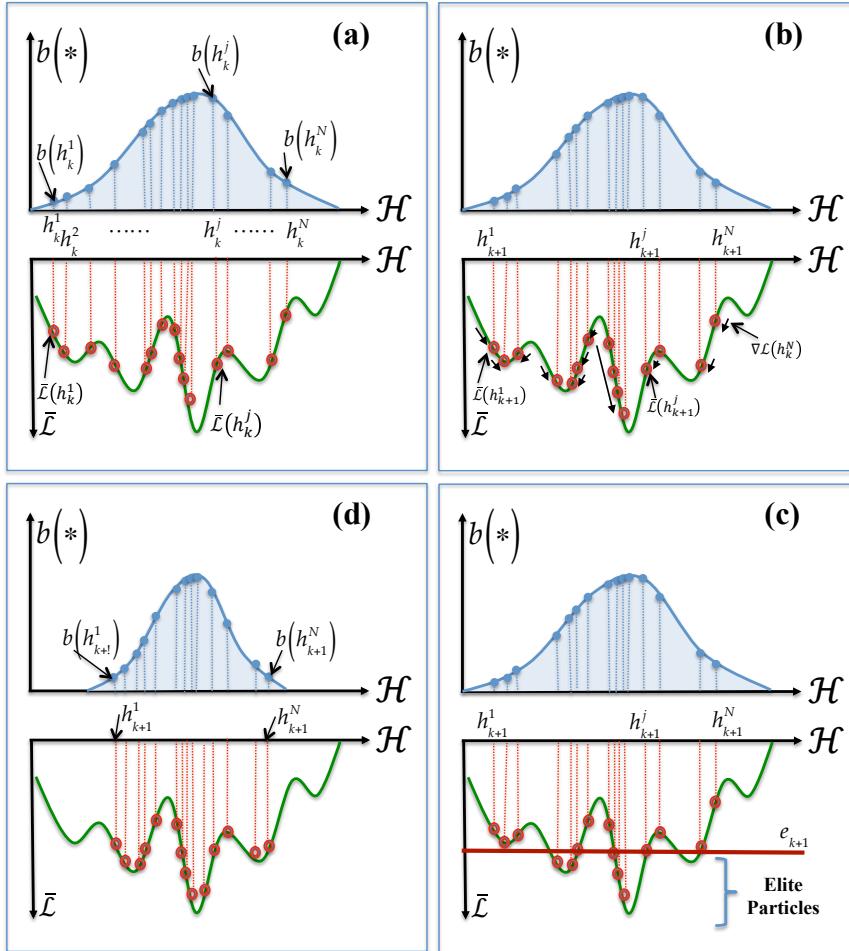


Figure 6. Particle filtering approach for optimization of hyperparameters.

3.3. Implementation Results

This section demonstrates the developed circuit health estimation approach using a model-adapted kernel method to estimate the health of a benchmark Sallen–Key band

pass filter (BPF) circuit and a DC–DC converter system. The following demonstration focuses on circuit health estimation in the presence of a single-fault condition wherein one of the CUT’s critical components is degrading.

During the off-line learning phase, simulations-before-tests were conducted in a PSPICE environment to understand the behavior of the CUT under healthy and failure conditions. Hence, faults of varying intensity were seeded into the critical components. A circuit was considered to be healthy when all the components varied within their tolerance range, i.e., $(1 - T)X_n < X < (1 + T)X_n$, where T is the tolerance range, X is the actual value of the component, and X_n is the nominal value of the component. If any of the components varied beyond their tolerance, i.e., $X < (1 - T)X_n$ and $X > (1 + T)X_n$, then the circuit was termed to have a parametric fault. Parametric fault need not mean the circuit had failed. The circuit was considered to have failed only when the parametric deviation in a circuit component beyond its tolerance range has led to the circuit failing to perform its intended functions. The features were extracted from the circuit’s response to a test stimulus under these hypothesized fault conditions and were stored in a fault dictionary for use during on-line health estimation.

The parametric degradation data of resistors and capacitors from accelerated life tests (ALTs) conducted in previous CALCE studies [4][6][7] were used to validate the developed health estimation approach. Resistor degradation trends were obtained from the temperature cycling test (–15 to 125 °C with 10-min dwell) on 2512 ceramic chip resistors (300 Ω) [7]. On the other hand, capacitor degradation trends for the Sallen–Key filter circuit were obtained from temperature and voltage aging tests

(125 °C and 285 V) on 0.44nF embedded capacitors [6]. For the low-pass filter circuit in the DC–DC converter system, capacitor degradation trends were obtained from isothermal aging tests at 105 °C on electrolytic capacitors [4].

3.3.1 Band-Pass Filter Circuit

A schematic of the Sallen–Key BPF with 25kHz center-frequency is shown in Figure 7. C_1 , C_2 , R_2 , and R_3 are the critical components of this CUT and the condition for failure of this CUT is assumed to be 20% shift in center-frequency, and/or the gain at the center-frequency increases by twice or reduces by half the nominal gain value. In this study, the failure conditions for CUT are assigned to evaluate the performance of diagnostic approach. However, in field applications, the failure conditions for a critical circuit is defined either based on the function of circuit in the whole system or based on the known level of parametric drifts exhibited by circuit components before failing in a catastrophic fashion.

During off-line learning phase, the faults were seeded in the critical components and the severity of the fault was varied to find the threshold at which the circuit failed as per the failure conditions established. The severity of fault in a critical component at which the circuit performance meets failure conditions is denoted as that critical component ‘failure range’. The table accompanying the Figure 7 lists the critical components, their tolerance, and failure threshold (or range).

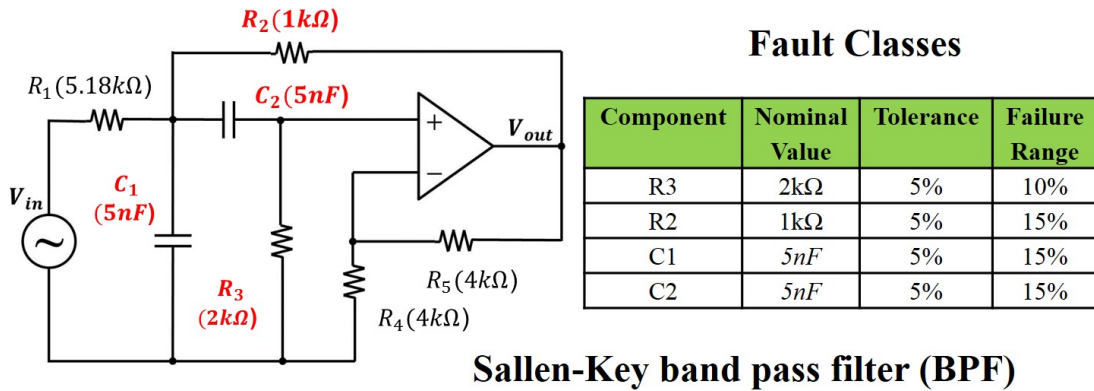


Figure 7. Schematic of a Sallen-Key band pass filter centered at 25 KHz. The table represents the critical components and their failure ranges.

For the Sallen-Key BPF under consideration, the shape of pass-band shifts when any of the critical components degrade. This is illustrated in Figure 8, which shows the magnitude and phase of the Sallen Key BPF's transfer function with no-fault and fault seeded into its critical components.

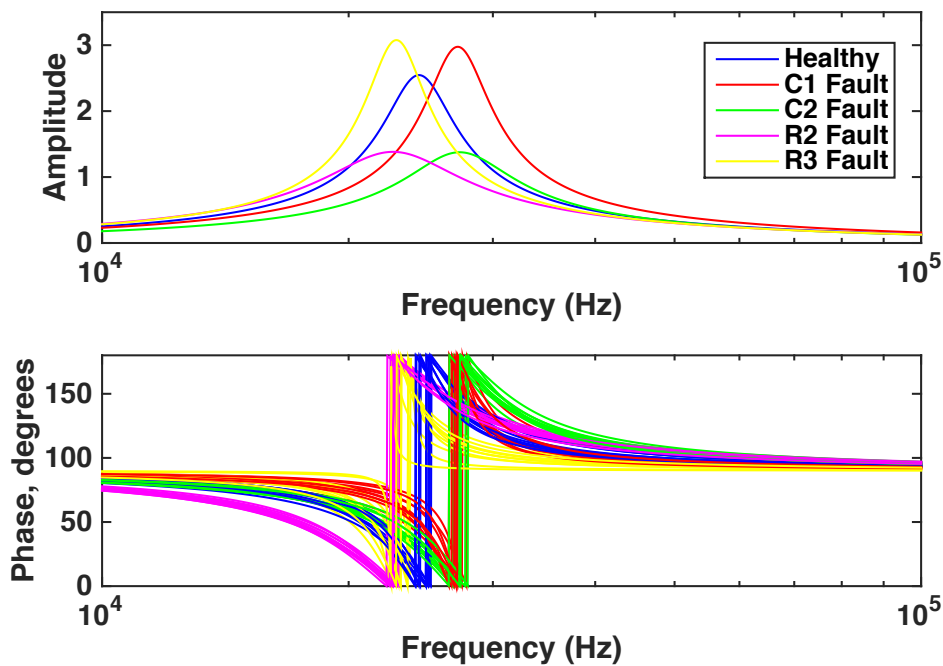


Figure 8. Magnitude and phase of Sallen-Key BPF's transfer function with and without faults.

In order to capture this shift in frequency response, the circuit is stimulated by a sweep signal (shown in Figure 9) containing frequency bandwidth larger than that of the BPF circuit. This study used a sweep signal (5 V) ranging from 100 Hz to 2 MHz with 100msec time window as a test stimulus. This ensured that the BPF circuit was excited by all of the frequency components to which it was sensitive.

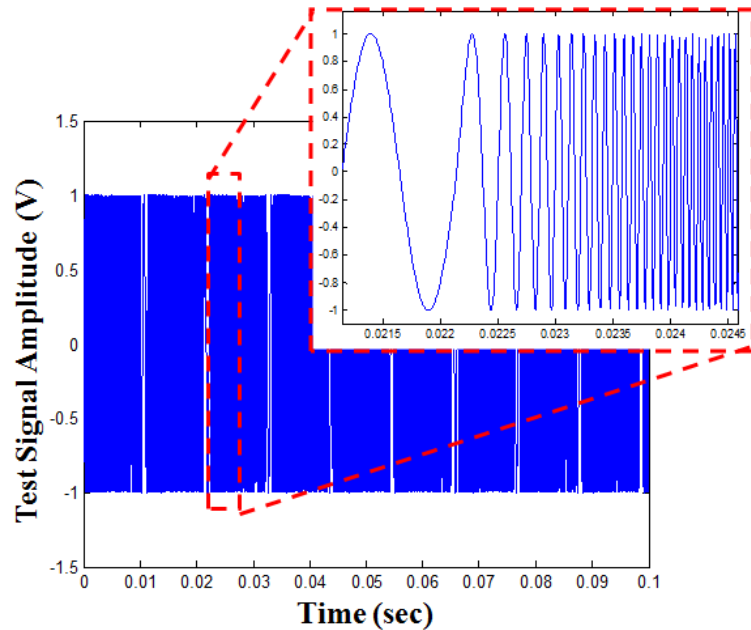


Figure 9. Example of a sweep (test) signal.

Two types of features are extracted from the time domain response of the CUT to sweep test signal, namely the wavelet features and the statistical property features. Fourier analysis is the most commonly used signal analysis method to extract the information embedded in a signal. However, Fourier transformation gives only the global frequency content of a signal and thus is suitable for the analysis of stationary signals only, whose properties do not evolve with time. However, any change in time, in a non-stationary signal, will spread over the entire frequency domain that will not be detected through Fourier analysis [58]. Thus it is impossible to distinguish when

an event took place by using a Fourier transformation which turns out to be a drawback for fault diagnosis as the sort of signals to be analyzed are expected to contain time-varying frequencies. This is where wavelet transformation comes in handy, which is capable of performing local analysis. Wavelet analysis has been proved to reveal signal aspects such as trends, break points and discontinuities. This formed the motivation for choosing wavelet features in the fault diagnosis of filter circuits.

A wavelet representation of a signal automatically tracks back to the concept of multiresolution decomposition, which enables us to have a scale-invariant interpretation of the information content in the signal. In wavelet analysis, the signal's correlation with families of functions that are generated based on the shifted and scaled version of a mother wavelet is calculated, which results in the mapping of the signal of interest to a set of wavelet coefficients that vary continuously over time [59]. The discrete version of the wavelet transform consists of sampling the scaling and shifted parameters but not the signal or the transform. This makes the time resolution good at high frequencies and the frequency resolution becomes good at low frequencies.

In the discrete time version of the wavelet transform [60], the concept of multiresolution is closely related to the concept of multirate filter bank theory. Thus filter banks are used in determining the wavelet coefficients for a discrete signal i.e. the approximation coefficients at a lower resolution level are subjected to high-pass and low-pass filtering (derived from mother wavelet) followed by a downsampling by

two to get the detail and approximation coefficients for a higher resolution level. This is expressed in Figure 10.

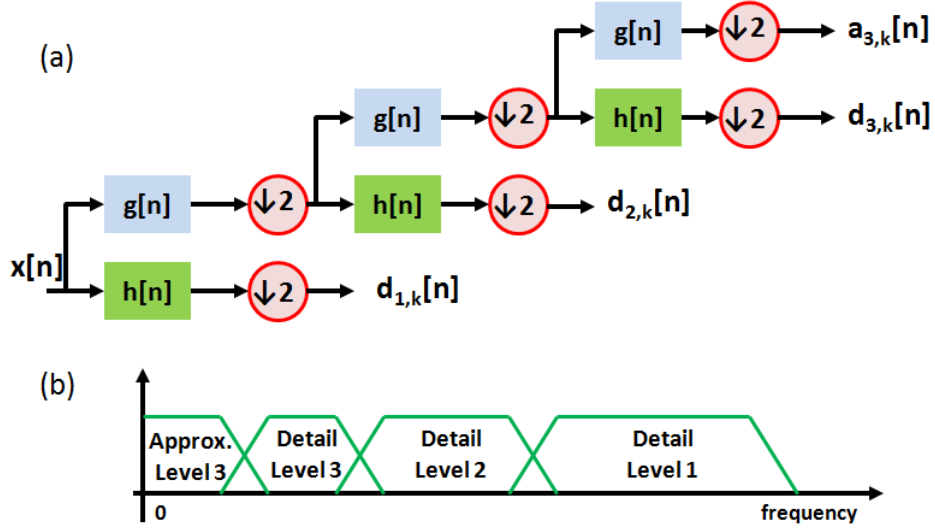


Figure 10. (a) Illustration of wavelet decomposition using filter banks and (b) Frequency range coverings for the details and approximation for three levels of decomposition.

In this work, through discrete wavelet transformation we decompose the time domain response of the CUT to a sweep signal into the approximation and detail signals using multirate filter banks. The information contained in signal is represented using features extracted by computing the energy contained in the detail coefficients at various level of decomposition. This is expressed as follows:

$$E_j = \sum_k |d_{j,k}|^2, \quad j = 1:J \quad (18)$$

where E_j denotes the energy in the detail coefficient d_k at the j th level of decomposition. The second set of features extracted is the kurtosis and entropy of the time-domain response of the CUT to the test signal. Kurtosis is a statistical property that is formally defined as the standardized fourth moment about the mean that represents the movement of probability density function without affecting the variance [61]. Thus, it provides a measure of the heaviness of the tails in the

distribution of the signal, which is related to the abrupt changes in the signal having high values and appearing in the tails of the distribution. Kurtosis is mathematically described as follows:

$$kurt(x) = \frac{E(x-E(x))^4}{(E(x-E(x))^2)^2} \quad (19)$$

On the other hand, entropy provides a measure on the information capacity of the signal, which denotes the uncertainty associated with the selection of an event from a set of possible events whose probabilities of occurrences are known [62]. It is defined for a discrete-time signal as:

$$entropy(x) = -\sum_i P(x = a_i) \log P(x = a_i) \quad (20)$$

where a_i are the possible values of x , and $P(x = a_i)$ is the associated probabilities.

Circuit health estimation was carried out using the extracted features. During the off-line tests, 250 no-fault cases (every component varied within its tolerance range) and 400 fault cases with varying fault levels (at least one of the circuit components varied beyond its failure range) were simulated. During each simulation, the Sallen–Key filter circuit was stimulated with a sweep signal and features were extracted. These features, along with their class labels (healthy or failure), were used to train the kernel-based health estimator. The particle size used for hyperparameter selection was 50. Since the elements of the hyperparameter are known to take values from 10^{-6} to 10^{+6} , the hyperparameter search was conducted in the $\log(h)$ plane from $[-15, +15]$. Figure 11 shows the training error rate, using 5 fold cross validation. It can be seen that, with increase in iteration the training error rate reduces indicating that the proposed hyperparameter optimization approach is moving towards the global

minima. Beyond 15 iterations, the decrease in error rate is reduced as the hyperparameter optimization method gets in the neighborhood of the global minima.

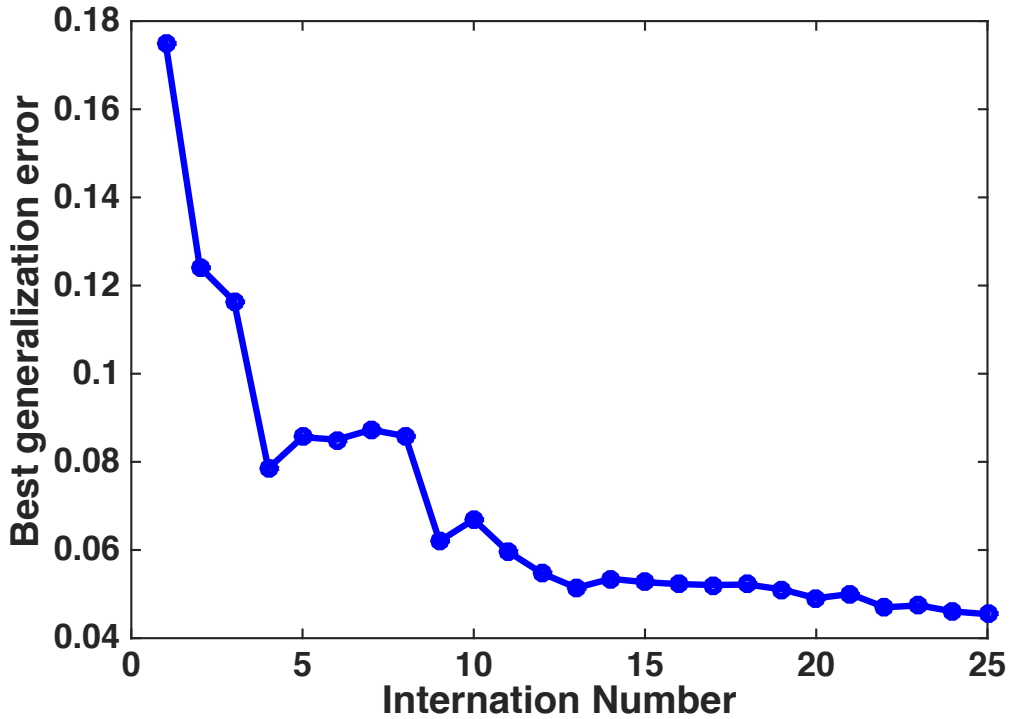


Figure 11. Plot of training error rate with respect to iteration number.

In order to validate the approach, the resistor and capacitor degradation trends from ALT were used to replicate the degradation of components in the BPF circuit. At each level of component degradation, the circuit-level features were extracted and given as input to the trained kernel-based health estimator, which provided an estimate of the circuit health. The results of this validation study are summarized in Table 1 and shown in Figure 12 through Figure 15. For each critical component, two degradation pathways were evaluated and the corresponding circuit health was estimated. The following terminologies are used in Table 1 to evaluate the developed circuit health estimation method:

- T_A : Denotes the actual circuit failure time

- t_F : Denotes the failure time estimated from HI_t (i.e., the time at which HI_t is less than 0.05).
- t_{PF} : Denotes the time at which parametric fault alarm was raised (i.e., time at which HI_t is less than 0.95).
- F_F : Denotes the fault severity at estimated failure time t_F .
- F_{PF} : Denotes the fault severity at time t_{PF} .

Figure 12 through Figure 15 includes the developed kernel-based health estimation results (in blue) along with the results of MD-based health estimation method (in green) described in [25] for comparison. The idealistic health HI_t^I of the circuit is also provided (in red) in the plots to verify the capability of the proposed health estimation methods to reflect the increase in intensity of fault in the component exhibiting parametric fault. Here, the idealistic health HI_t^I of the circuit at time t is defined as follows:

$$HI_t^I = 1 - \left[\frac{X - (1 \pm T)X_n}{X_n[(1 \pm T_f) - (1 \pm T)]} \right] \quad (21)$$

where T_f is the failure threshold for the critical component considered. From Eq. 21 it can be understood that HI_t^I is an ideal case, when all components of the circuit are at their nominal value and there is no variations within their tolerance range. However, this is never the case as circuit component values are not always equal to their nominal value. Thus the expectation is to have the health estimation method generate health estimates as close to HI_t^I as possible.

TABLE 1

PERFORMANCE RESULTS OF DEVELOPED HEALTH ESTIMATION METHOD ON SALLEN-KEY BPF

Component	Tolerance (%)	Failure Range (%)	t_{PF} (hours)	t_F (hours)	F_{PF} (%)	F_F (%)	T_A (hours)
C_1	5	15	214	285	8.6	14.4	298
	5	15	212	280	7.6	13.4	302
C_2	5	15	171	302	6.0	15.0	302
	5	15	209	308	9.4	15.4	298
R_2	5	15	7200	8340	5.83	20.0	8170
	5	15	900	3870	4.46	14.71	3900
R_3	5	10	2970	4120	3.16	13.0	3970
	5	10	2890	3840	4.25	14.4	3810

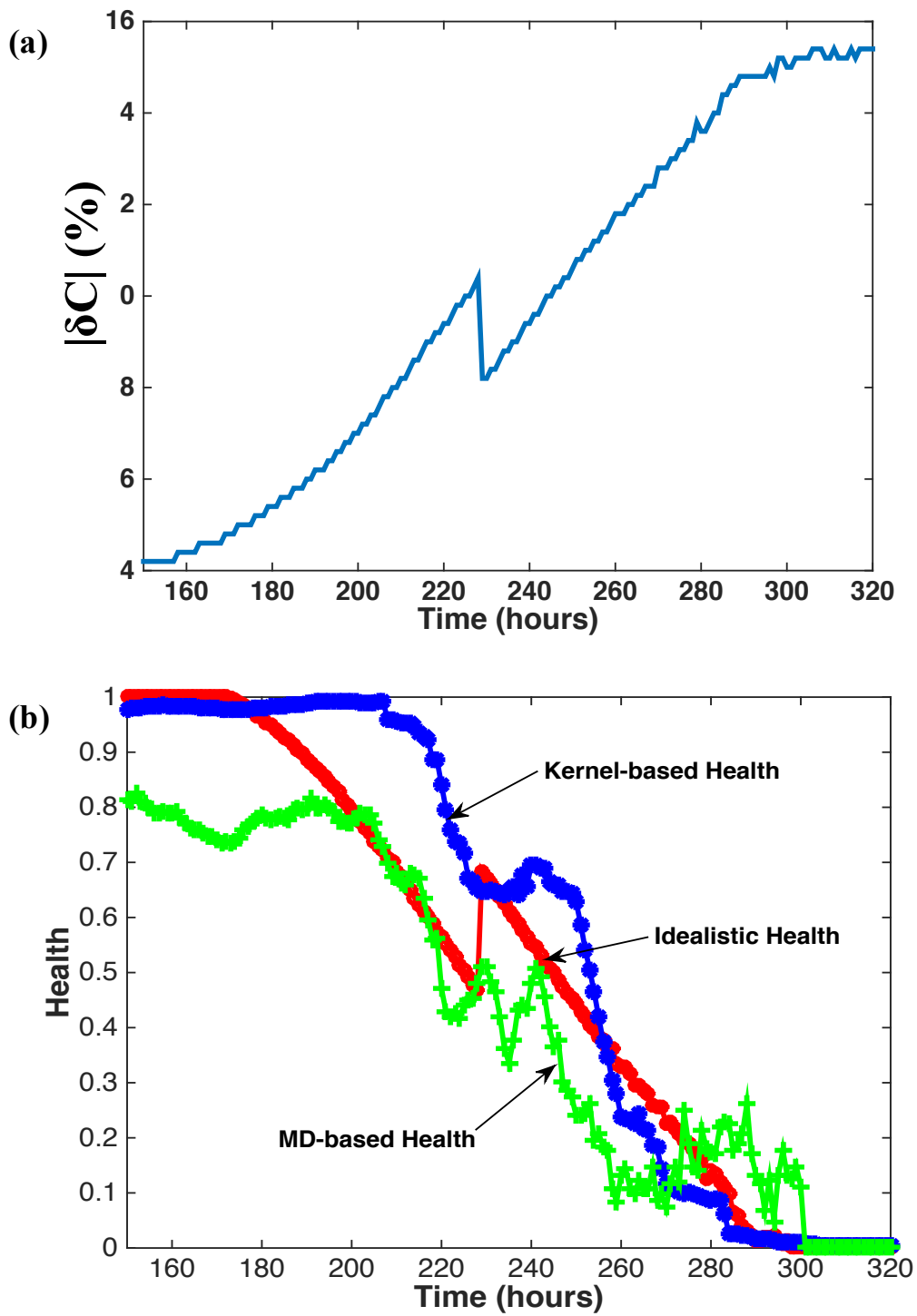


Figure 12. (a) Progression of parametric fault in C_1 of Sallen-Key BPF. (b) Health estimates using the developed kernel (blue) and MD-based (green) method for fault in C_1 .

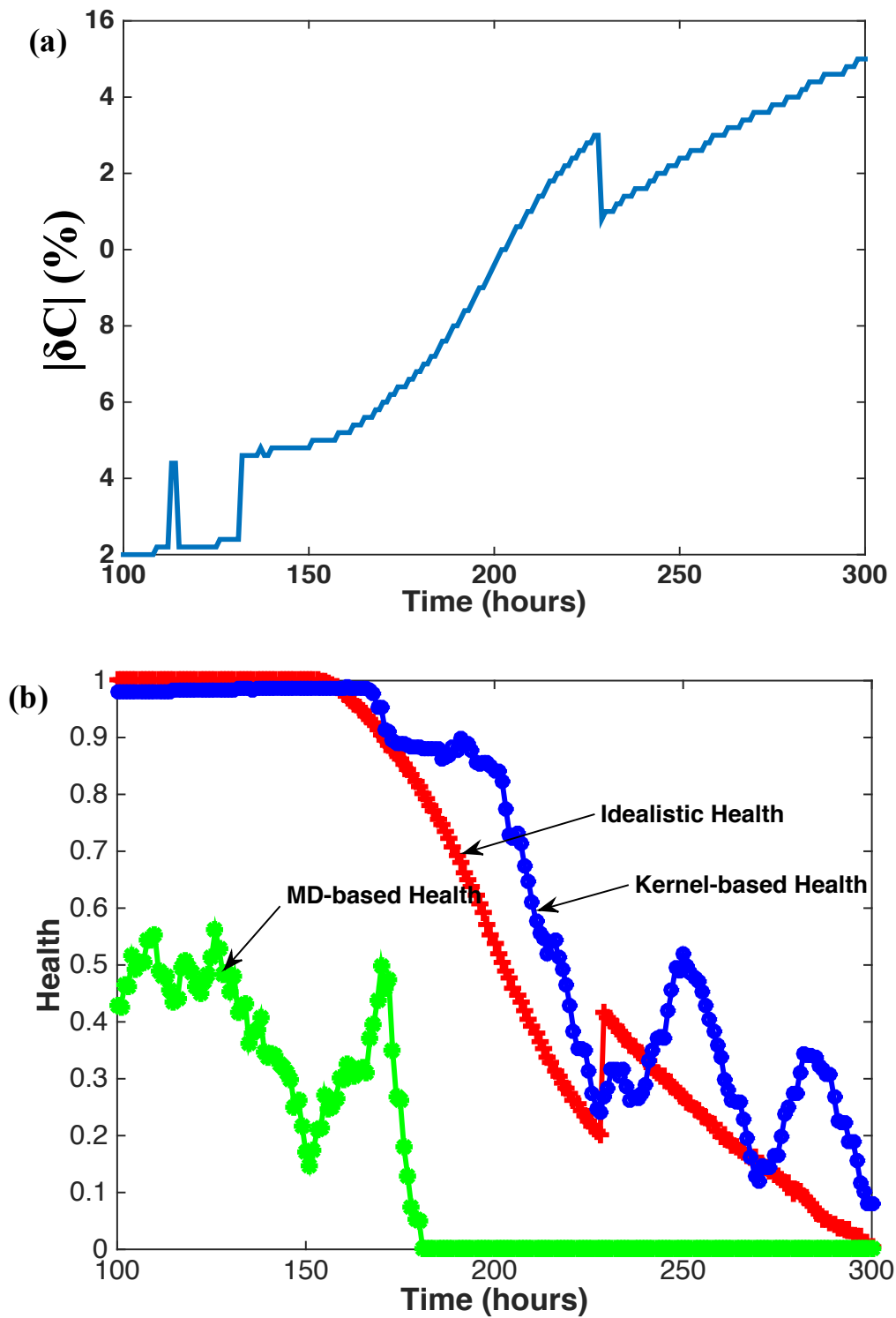


Figure 13. (a) Progression of parametric fault in C_2 of Sallen-Key BPF. (b) Health estimates using the developed kernel (blue) and MD-based (green) method for fault in C_2 .

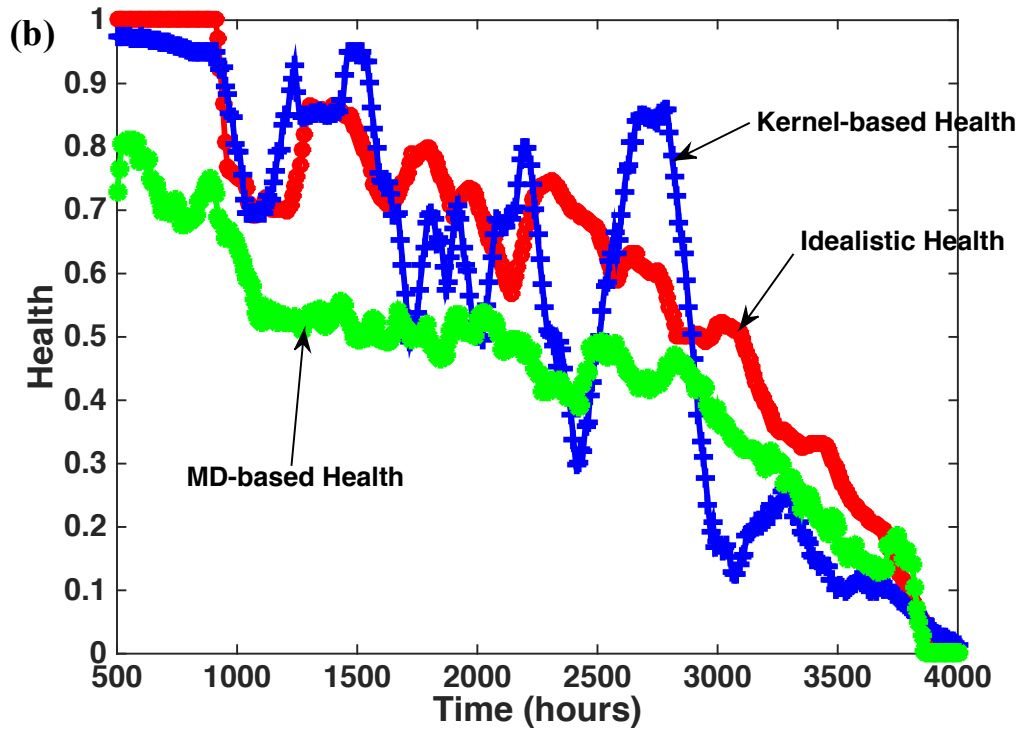
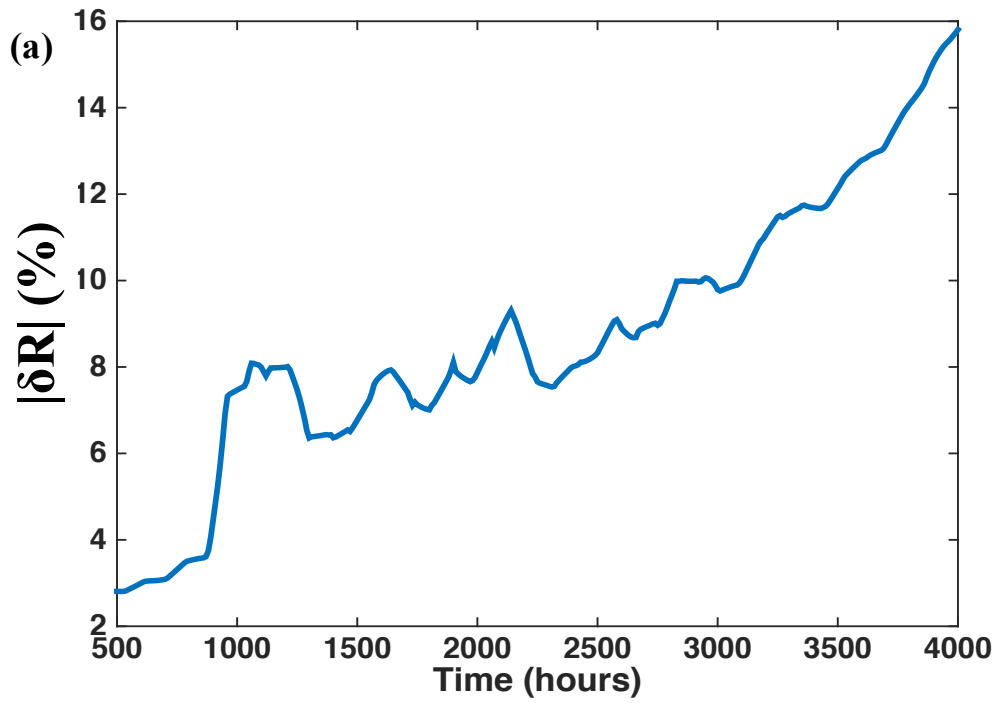


Figure 14. (a) Progression of parametric fault in R_2 of Sallen-Key BPF. (b) Health estimates using the developed kernel (blue) and MD-based (green) method for fault in R_2 .

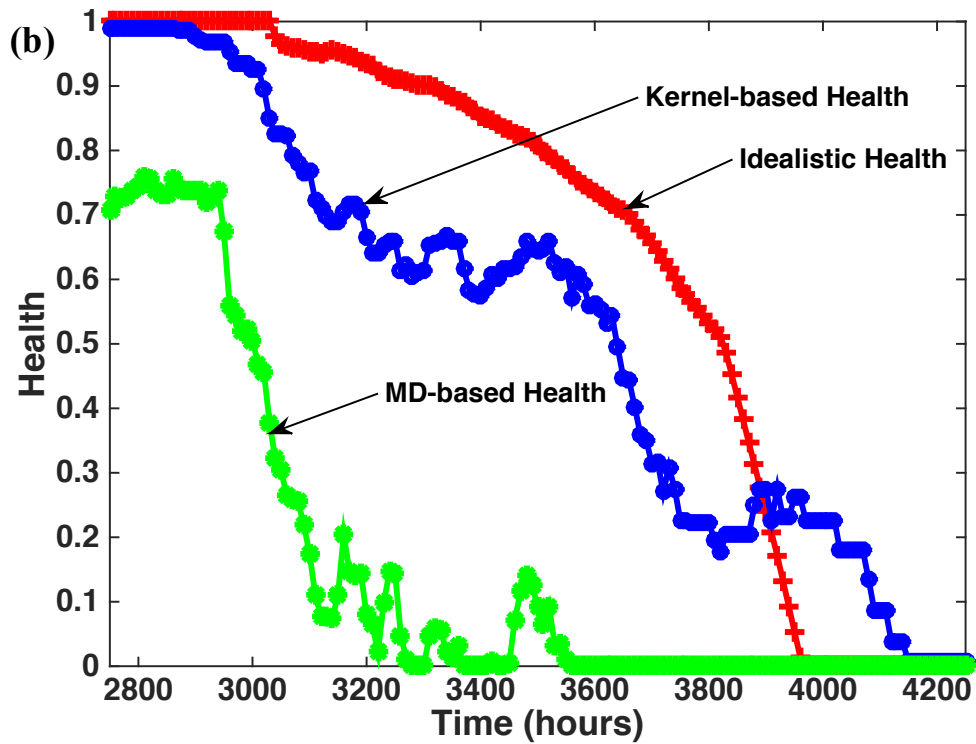
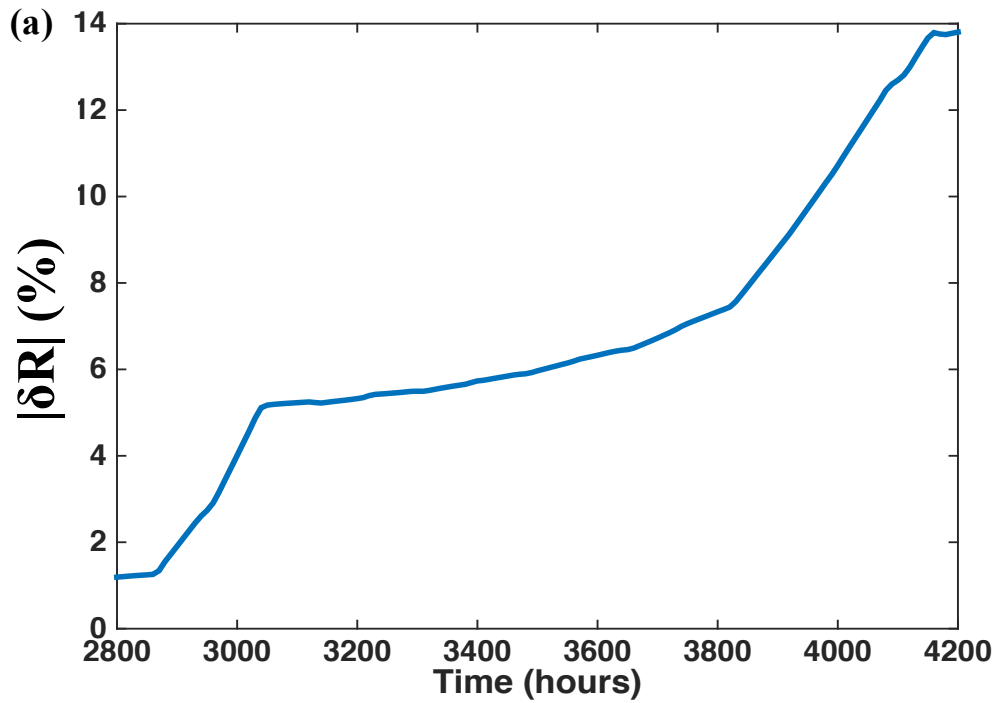


Figure 15. (a) Progression of parametric fault in R_3 of Sallen-Key BPF. (b) Health estimates using the developed kernel (blue) and MD-based (green) method for fault in R_3 .

As can be seen from Table 1 and Figure 12 through Figure 15, the developed approach can identify the circuit health degradation with increase in fault intensity and shows better performance than the MD-based health estimation method. MD-based method can fairly track the circuit health degradation for faults in components C_1 and R_3 . However, for components C_2 and R_2 the health estimates generated by MD-based method does not follow the trend in actual health HI_t^A . This is potentially due to the similarities in amplitude of the BPF's transfer function even when there is a fault in C_2 or R_2 when compared to the healthy circuit. This is where the non-linear kernel-based method stands out, as it can still identify the shifts in frequency and generate health estimates that closely follow HI_t^A .

3.3.2 DC-DC Buck Converter System

A DC–DC buck converter system converts a high-to-low DC voltage level (e.g., 12–5 V) and supports the operation of many low-power consuming electronic products. The three critical circuits within a DC–DC buck converter system are: a low-pass filter, a voltage divider feedback circuit, and a switching circuit. Each of these circuits has discrete circuit elements that have been known to exhibit parametric deviations during field operation (see Figure 16). In this validation study, the health estimation of a low-pass filter and a voltage divider feedback circuit was investigated.

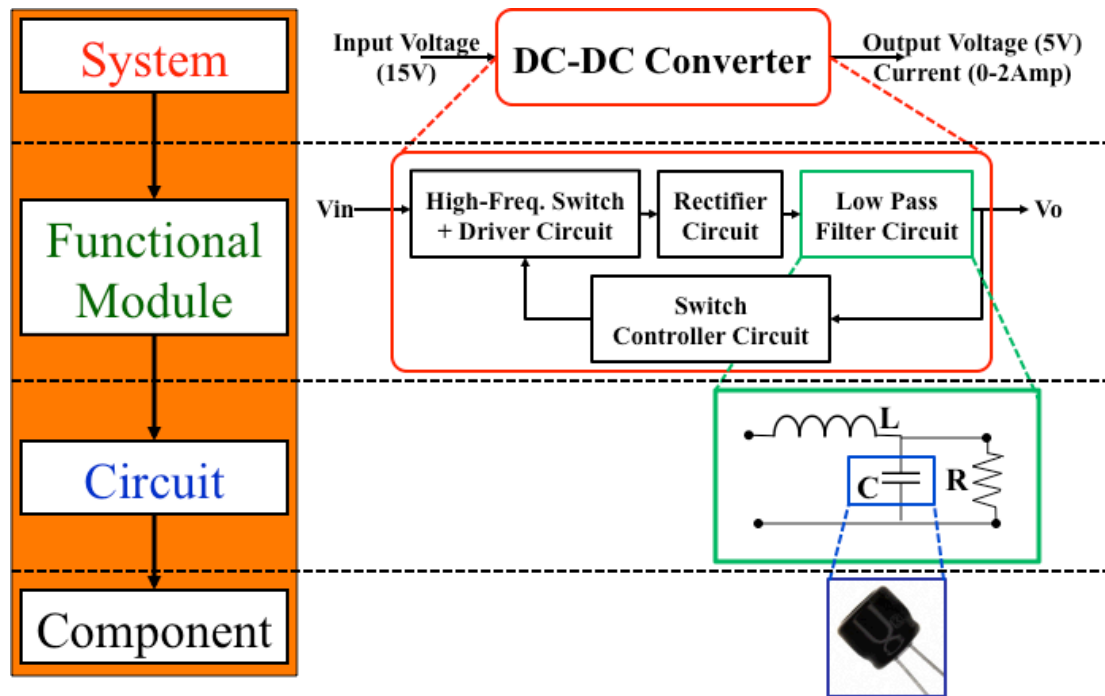


Figure 16. DC-DC buck converter system design abstraction levels.

The low-pass filter circuit, with cut-off frequency of 2 kHz (schematic shown in Figure 17) is used to remove noises from the DC output voltage. Degradation of the electrolytic capacitor increases ripple at the DC output, which damages the electronics powered by the converter. Capacitance value is often used as a precursor parameter to predict electrolytic capacitor failure. However, the capacitance value cannot be extracted once the capacitor is placed in the circuit. Hence, the low-pass filter circuit topology was exploited to capture the parametric degradation of the electrolytic capacitor.

The low-pass circuit was stimulated by a sweep signal with frequency range of 100 Hz to 20 kHz. Frequency and statistical features were extracted from the circuit response using wavelet packet transform. Frequency features included, the energy contained in both approximate and detailed coefficients up to 6-levels of decomposition using discrete wavelet transformation. Haar mother wavelet was used

in wavelet transformation. Statistical features include the kurtosis and entropy of the CUT's response to sweep signal. Thus overall, there were 14 features extracted for low pass filter circuit.

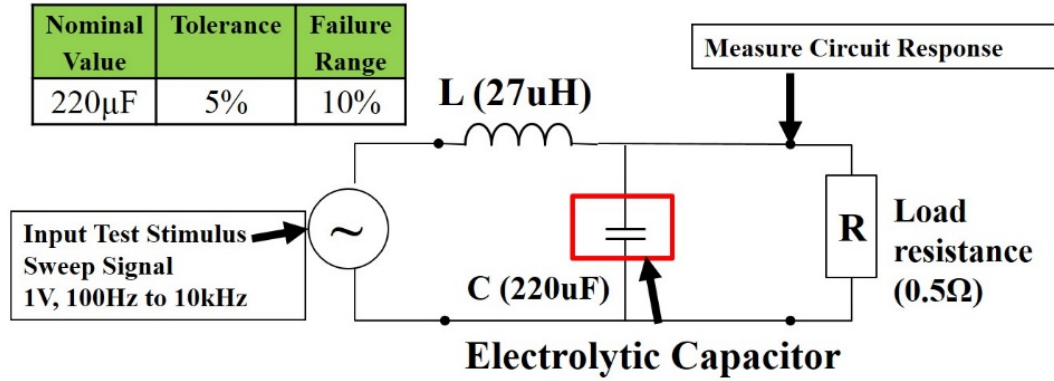


Figure 17. Schematic of a LC low-pass filter circuit in a DC–DC converter system.

Circuit health estimation was carried out using the extracted features. During the off-line tests, 200 no-fault cases (every component varied within its tolerance range) and 200 fault-seeded cases were simulated. Four different degradation trends were obtained from ALT of the electrolytic capacitor and was used to simulate parametric faults in the low-pass filter of the DC–DC converter system. The corresponding circuit health estimated using the kernel method (in blue) is plotted in Figure 18 through Figure 21. The actual health calculated using Eq. 21 is shown in red. It can be seen from the actual health HI_t^A degradation curves that the variation in capacitance with time was gradual and never reached the failure range (10%) over 2,250 h of testing. Still, the kernel-based health estimator provided estimates of the failure time.

Furthermore, the circuit health estimated using the different degradation trends exhibited variations, and the results were not as consistent as HI_t^A degradation trends.

This variation in health estimation performance could result from the contributions of other components in the circuit varying within their tolerance range.

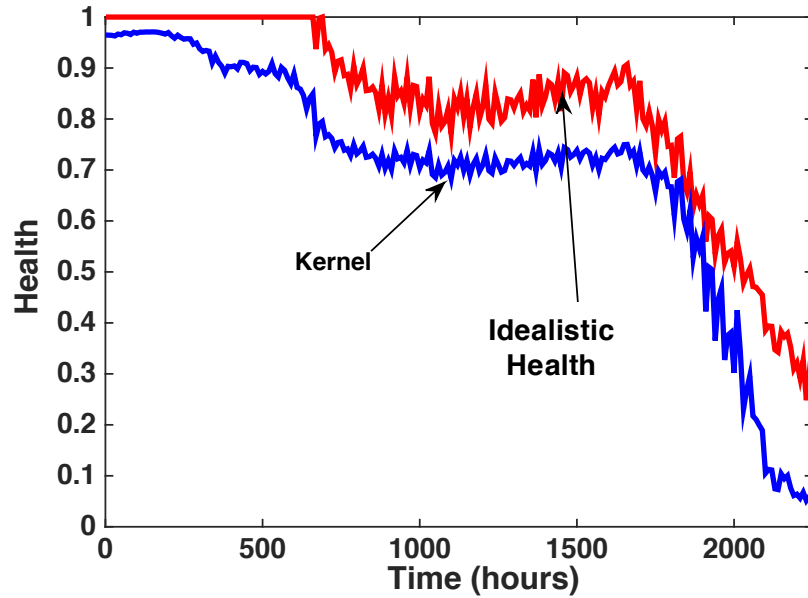


Figure 18. LPF circuit health estimated using the kernel method (blue) in comparison to the actual health HI_t^A for the progression of parametric fault in C – Run 1.

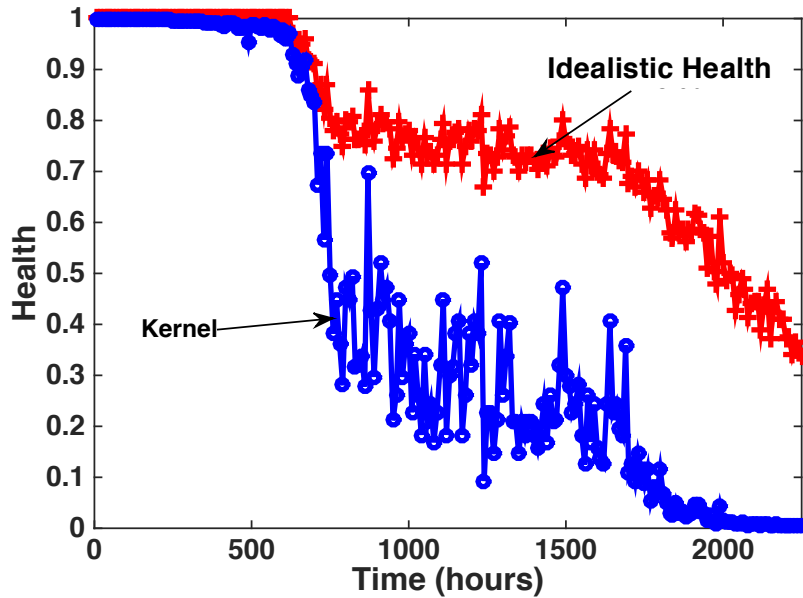


Figure 19. LPF circuit health estimated using the kernel method (blue) in comparison to the actual health HI_t^A for the progression of parametric fault in C – Run 2.

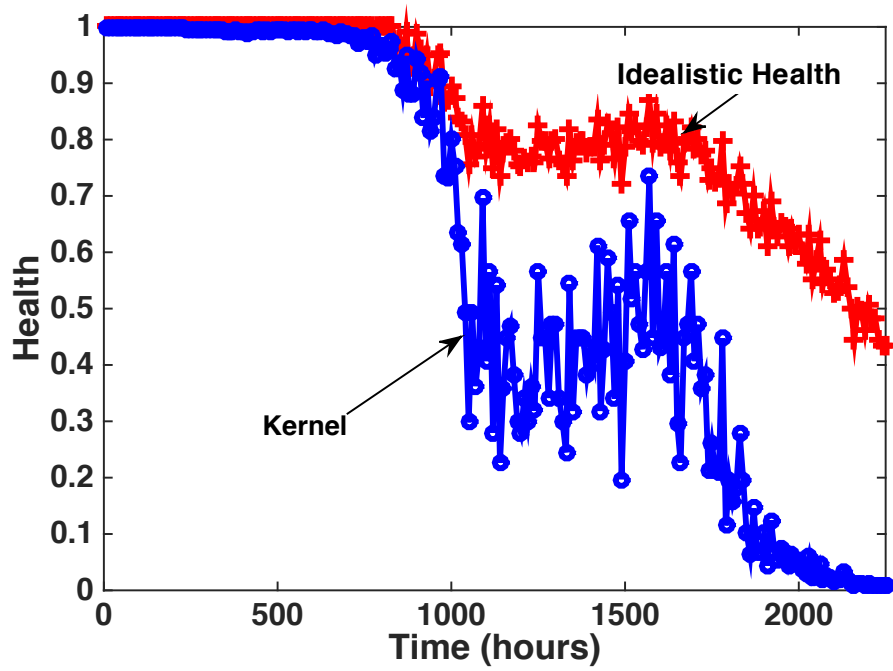


Figure 20. LPF circuit health estimated using the kernel method (blue) in comparison to the actual health HI_t^A for the progression of parametric fault in C – Run 3.

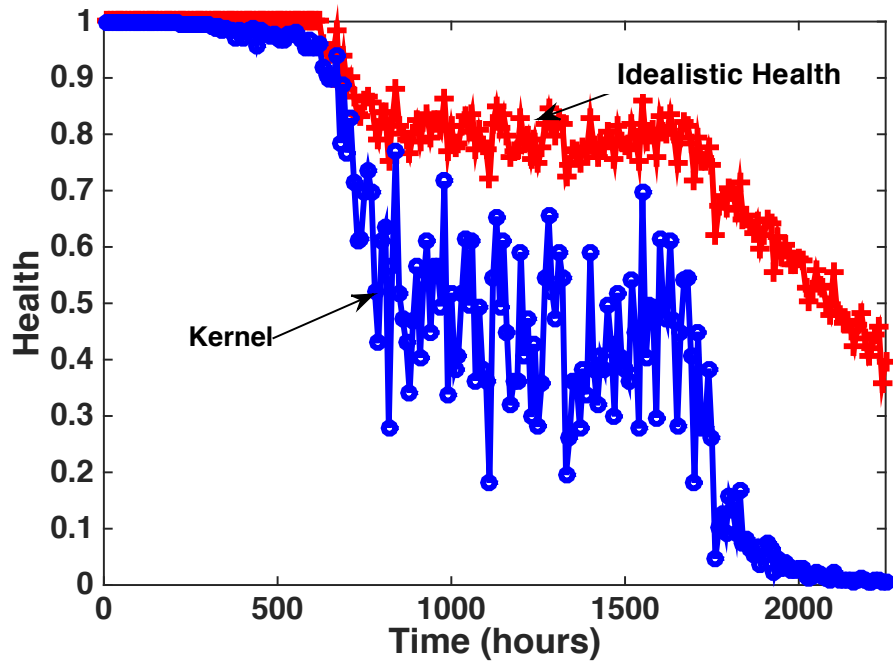


Figure 21. LPF circuit health estimated using the kernel method (blue) in comparison to the actual health HI_t^A for the progression of parametric fault in C – Run 4.

In the DC–DC converter, feedback from output DC voltage is obtained via a voltage divider circuit and fed into the switch controller circuit, in order to regulate the DC voltage. If resistance R_1 and R_3 degrades (see Figure 22), the voltage fed back will be different, resulting in the switch to over-regulate or under-regulate. Resistance value is often used as a precursor parameter to predict resistor failure. Instead of monitoring the two resistors individually, this approach exploited the feedback circuit topology to capture resistor degradation. The feedback circuit was stimulated using a step voltage signal (0–5 V), which steps up by 1 V every 100msec. The voltage response generated by the circuit was directly used as input to the health estimator, and the results are shown in Figure 23 and Figure 24.

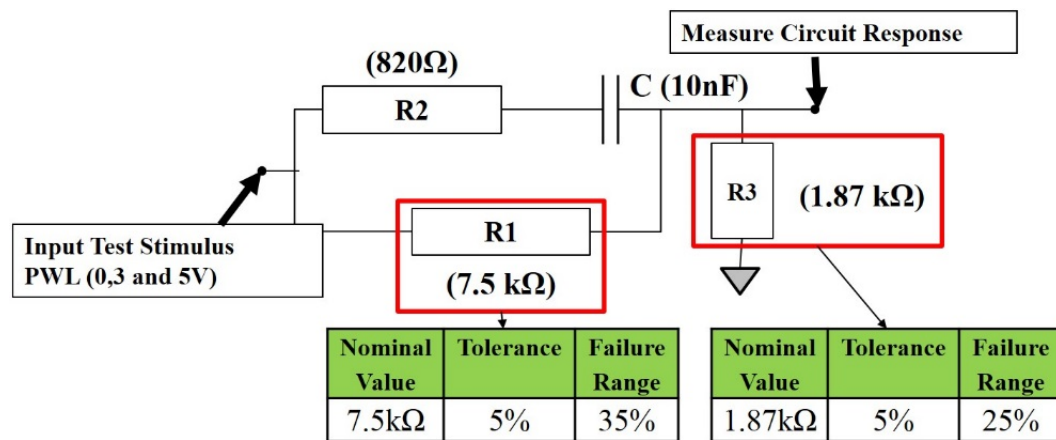


Figure 22. Schematic of voltage divider feedback circuit in a DC–DC converter system.

Table 2 summarizes the performance results of the validation study on the critical circuits of a DC–DC converter. The terminologies used for performance analysis are the same as those described in Table 1.

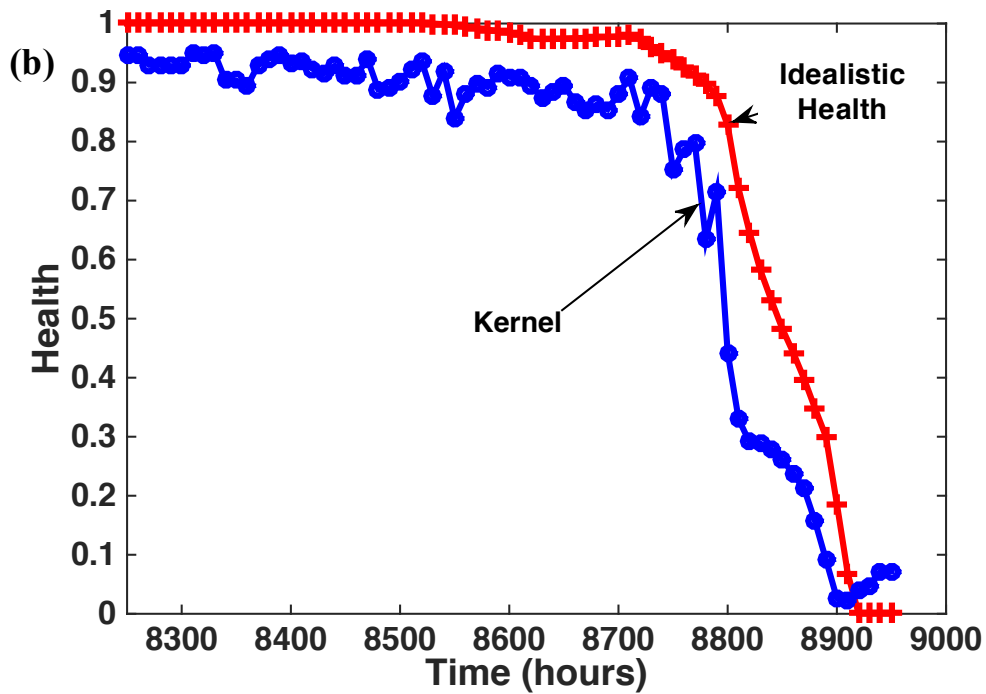
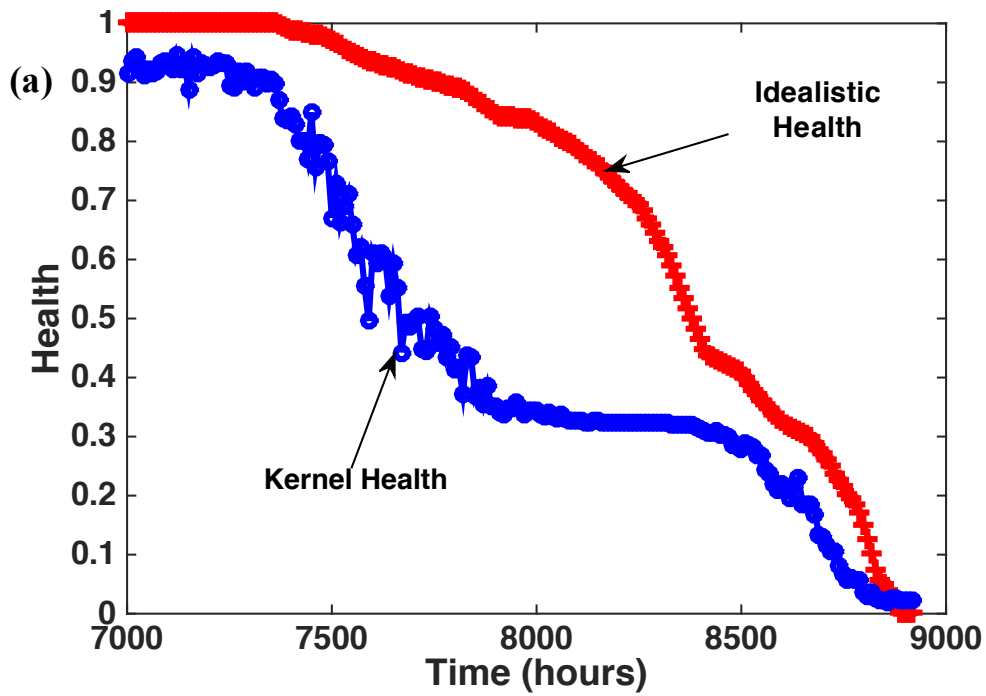


Figure 23. Voltage divider feedback circuit health estimated using the kernel method (blue) in comparison to the actual health HI_t^A for the progression of parametric fault in R_1 . Figure 23(a) and 23(b) represents two different degradation trends.

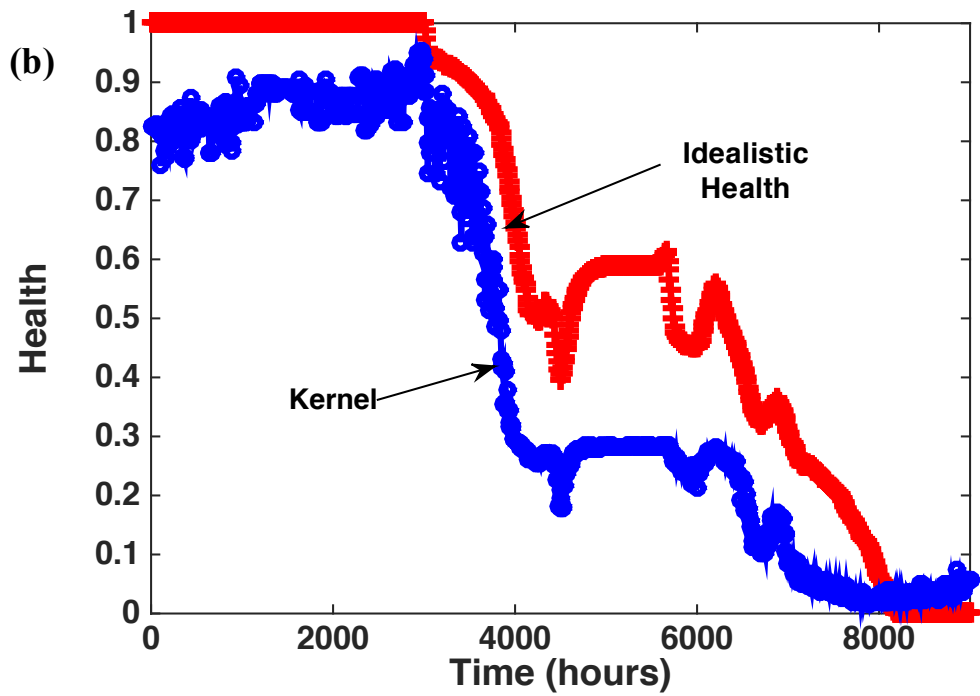
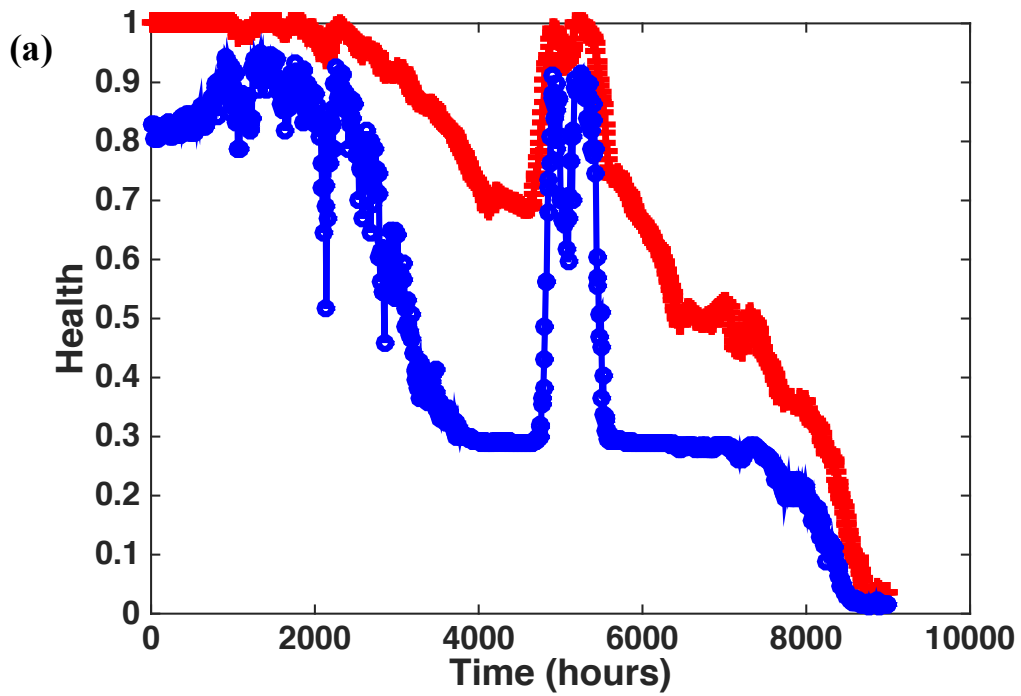


Figure 24. Voltage divider feedback circuit health estimated using the kernel method (blue) in comparison to the actual health HI_t^A for the progression of parametric fault in R_3 . Figure 24(a) and 24(b) represents two different degradation trends.

TABLE 2**PERFORMANCE RESULTS OF DEVELOPED HEALTH ESTIMATION METHOD ON DC-DC CONVERTER SYSTEM**

Component	Tolerance (%)	Failure Range (%)	t_{PF} (hours)	t_F (hours)	F_{PF} (%)	F_F (%)	T_A (hours)
<i>C</i>	5	10	230	2230	3.24	8.56	>2250
	5	10	630	1830	4.01	5.87	>2250
	5	10	810	2010	6.01	7.56	>2250
	5	10	580	1930	3.17	6.39	>2250
<i>R₁</i>	5	35	0	8800	0.15	30.46	8890
	5	35	0	8930	0.09	28.52	8950
<i>R₃</i>	5	25	0	8420	0.25	29.15	8050
	5	25	0	7150	0.24	19.95	8180

As can be seen from Table 2, the health estimator was able to identify the instant at which the parametric fault began to show up in the low-pass filter circuit. However, this was not true with the voltage divider circuit. The estimated health was always less than 0.95 probability even when the resistors R_1 and R_3 were well within their tolerance range. On the other hand, the estimator was able to detect the actual failure time for the voltage divider circuit. However, for the low-pass filter circuit, the health estimator raised early failure warnings i.e., the estimated failure time t_F is less than the actual time-of-failure T_A . This indicates that the developed method raises early failure warning, even before the circuit has actually failed. Although this is desirable feature in any prognostics and health management (PHM) module, the difference ($T_A - t_F$) should not be too large, causing wastage of useful life. It can be deduced from Table 2 that, the difference ($T_A - t_F$) for the electrolytic capacitor in LPF circuit of the DC-DC converter is ~20% of the total lifetime of the capacitors. It is possible that, the features extracted during time t_F was similar to the features extracted while the circuit had failed, and the model adapted kernel method decided that the probability the extracted features belong to the healthy class was less than 0.05.

Thus, although the developed method can capture the trend in health degradation, there is room for improvement and there is a need for consistency in early fault and failure detection.

Chapter 4: RUL Prediction using Model-based Filtering

The prognostics problem involves the prediction of a system or device *end of life* (*EOL*) from which the *remaining useful life* (*RUL*) is estimated, where *RUL* is defined as the duration from the time at which prediction is made to the *EOL*. In the case of circuit functional failures resulting from parametric deviations in electronic components, the degrading component does not necessarily exhibit a hard failure. The degradation is simply accompanied by parametric deviation in component parameters that shifts the circuit characteristics. The component exhibiting parametric fault may still function, but it is just that the circuit in which the component is part of might not operate in permissible predefined range. In this chapter a model-based filtering method is developed for predicting the remaining useful performance (*RUL*) of electronic circuit-comprising components exhibiting parametric faults. The developed prognostics method relies on a first principles-based model that describes the progression of parametric fault in the circuit component and a stochastic filtering technique to first solve a joint ‘circuit health state—parametric fault’ estimation problem, followed by prediction problem in which the estimated ‘circuit health state—parametric fault’ is propagated forward in time to predict *RUL*. The rest of the chapter is organized as follows. Section 4.1 mathematically formulates the prognostics problem. Section 4.2 presents the first principles-based model developed in this dissertation to capture the degradation in circuit performance. The stochastic algorithm used for joint state-parameter estimation and *RUL* prediction is discussed in Section 4.3. Section 4.4 presents the validation results using data obtained from simulation-based experiments on the critical circuits of a DC-DC converter system.

4.1 Prognostics Problem Formulation

In order to realize model-based prognostics a health state vector consisting of one or more metrics that evolve by reflecting the degradation in performance of a system or circuit is required. In most prognostic applications, a measurable parameters exhibiting monotonic trend is chosen as the health state vector. However in some applications such as in circuit prognostics, a health vector has to be constructed from features extracted from circuit responses to test stimulus. Irrespective of whether health state vector is a measured parameter or a variable constructed from measured parameters, the underlying assumption is that the health state vector evolve according to a dynamic state space model as in Eq. 22:

$$\dot{\mathbf{x}}(t) = f(t, \mathbf{x}(t), \boldsymbol{\theta}(t), \mathbf{u}(t)) + \mathbf{v}(t) \quad (22)$$

$$\mathbf{y}(t) = h(t, \mathbf{x}(t), \boldsymbol{\theta}(t), \mathbf{u}(t)) + \mathbf{n}(t) \quad (23)$$

where $\mathbf{x}(t) \in \mathbb{R}^{n_x}$ represents the health vector of length n_x , $\mathbf{y}(t) \in \mathbb{R}^{n_y}$ is the measurement vector of length n_y , $\boldsymbol{\theta}(t) \in \mathbb{R}^{n_\theta}$ is the unknown parameter vector that has to be estimated along with the state $\mathbf{x}(t)$, $\mathbf{u}(t) \in \mathbb{R}^{n_u}$ is the input vector, $\mathbf{v}(t) \in \mathbb{R}^{n_x}$ is the process noise, $\mathbf{n}(t) \in \mathbb{R}^{n_y}$ represents the measurement noise, and finally $f(*)$ and $h(*)$ denotes the state and measurement equations, respectively.

The goal is to predict the time instant at which this health state vector will evolve beyond a certain desired region of acceptable performance. This region represents the condition where the circuit performance no more guarantees reliable system operation and is expressed through a set of requirements $\{r_i\}_{i=1}^{n_r}$. For example, n_r could

represent the number of critical circuits in a system and for each critical circuit, $r_i: \mathbb{R} \rightarrow \mathbb{B}$ denotes a function that maps a subspace in the actual health state space to the Boolean domain, $\mathbb{B} \triangleq \{0,1\}$. For example, assume $x(t) \in [0,1]$ represents the health of a critical circuit, where $x(t) = 1$ represent circuit is healthy and $x(t) = 0$ represent that the circuit has failed. In this case, a requirement could be defined as $r(x(t)) = 1$ if circuit is yet to fail i.e., $1 \geq x(t) > 0.05$, and $r(x(t)) = 0$ once the circuit has failed.

These individual circuit requirements can be combined into a single threshold function for a system $T_{EOL}: \mathbb{R}^{n_x} \rightarrow \mathbb{B}$ that is defined as follows:

$$T_{EOL}(x(t)) = \begin{cases} 1, & 0 \in \{r_i\}_{i=1}^{n_r} \\ 0, & otherwise \end{cases} \quad (24)$$

where $T_{EOL} = 1$ denotes at least one of the system's critical circuit has violated a set requirement. Now, EOL and RUL is defined as

$$EOL(t_p) \triangleq \inf\{t \in \mathbb{R}: (t \geq t_p) \wedge (T_{EOL}(x(t)) = 1)\} \quad (25)$$

$$RUL(t_p) = EOL(t_p) - t_p \quad (26)$$

where EOL represent the earliest time (see Eq. (25)) from the time of prediction t_p at which the system has failed. In practice, uncertainty in modeling, measurement, and choice of initial state for $\mathbf{x}(t_0)$ leads to uncertainty in the estimation of $(\mathbf{x}(t), \boldsymbol{\theta}(t))$. As a result, it is reasonable to compute EOL and RUL as probability distributions, instead of point estimates. Hence, the goal of prognostics is to compute the conditional probability, $p(RUL(t_p)|\mathbf{y}(t_0:t_p))$, at time t_p (see Figure 25). The variables with a cap and without a cap in Figure 25 denote estimates and the ground

truth, respectively. For example, $R\hat{U}L$ and RUL represents the estimated and actual RUL respectively.

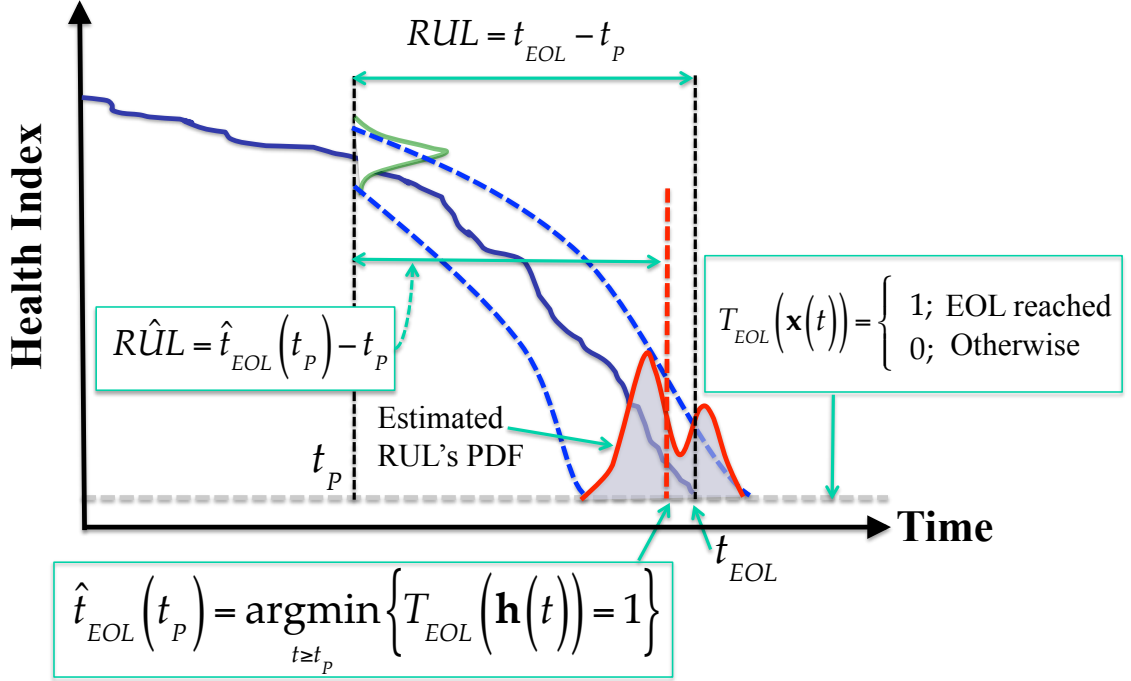


Figure 25. Prognostics illustration.

4.2 Circuit Degradation Modeling

In order to implement model-based prognostics, the first step is to identify or construct a health state vector $\mathbf{x}(t)$. This was carried out in Chapter 3 of this dissertation where $\mathbf{y}(t)$ is equivalent to HI_t produced by the kernel-based health estimator and $\mathbf{x}(t)$ is equivalent to \widehat{HI}_t i.e., the health state estimate from $\mathbf{y}(t)$. The next step is to identify the parameter $\boldsymbol{\theta}(t)$ and input vector $\mathbf{u}(t)$ using which the state $\mathbf{f}(\cdot)$ and observation $\mathbf{h}(\cdot)$ equation is established. This forms the focus of this section.

To model circuit degradation, it is assumed that the degradation in circuit performance (or health) is due to parametric drifts in one or more circuit components. Hence, the circuit health at future time is the sum of current circuit health and the degradation in health resulting from the parametric drifts in circuit components (pictorially illustrated in Figure 26). This can be expressed as:

$$x(t + \Delta t) = x(t) + g\left(\frac{\Delta p_1}{\Delta t}, \frac{\Delta p_2}{\Delta t}, \dots, \frac{\Delta p_N}{\Delta t}\right) \quad (27)$$

where $x(t)$ denotes the health at time t , Δp_i denotes the parametric drift in i^{th} circuit component over Δt , and N denotes the total number of critical components in the circuit. p_i could represent the drift in any component parameter such as C , ESR , R_{CE} and more. Next step is to define the function $g(*)$ in Eq. 27. To define a structure for $g(*)$, assume a simple circuit with one component p_e , a source, and load as shown in Figure 26.

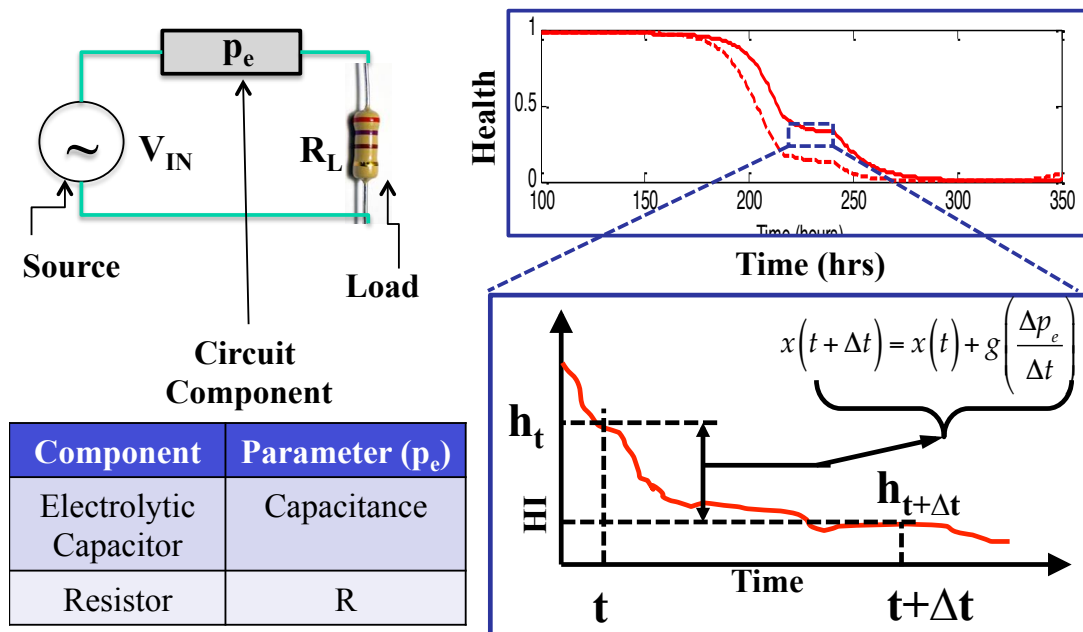


Figure 26. Simple one-component circuit for degradation modeling illustration.

The degradation in performance of this circuit depends only on the parametric deviation in p_e i.e., when $\Delta p_e(t) = 0$ at time t the circuit health $x(t) = 1$. Similarly, when the parametric deviation in p_e has reached the maximum allowable deviation (assume $\Delta p_e(t) = Y_{max}$), the circuit health $x(t) = 0$. Thus the change in health over a short time Δt can be expressed as follows:

$$\frac{x(t+\Delta t)-x(t)}{\Delta t} = \frac{-1}{|Y_{max}|} \Delta p_e(t). \quad (28)$$

The modulus on Y_{max} is because; the deviation in circuit component could either increase or decrease. For example, in the case of embedded capacitor, C is expected to decrease over time. However in electrolytic capacitor, ESR increases with degradation. A modulus accommodates both cases.

From Eq. 28 it can be discerned that the circuit health at a future time instant can be expressed as

$$x(t + \Delta t) = x(t) + \frac{-1}{|Y_{max}|} \frac{dp_e}{dt} \Delta t. \quad (29)$$

The term $-1/|Y_{max}|$ in Eq. 28 can be perceived as the sensitivity of the health metric x to change in the component parameter p_e and thus from now will be replaced with S_e^x , indicating sensitivity of health due to parametric deviations in p_e . S_e^x can be easily determined through fault-seeded simulations.

The second term in Eq. 29 corresponding to component parametric deviation is applicable only if that component is found to have a fault (i.e., parametric deviations are more than the acceptable tolerance range). Thus Eq. 29 can be further refined as follows

$$x(t + \Delta t) = x(t) + \left\{ S_e^x \frac{dp_e}{dt} \Delta t \right\}_{(p_e \in F)}. \quad (30)$$

where $(p_e \in F)$ indicates that this is an indicator function which exists only if the component is faulty. Now, the model for circuit health degradation can be extended for a circuit with multiple components as follows:

$$x(t + \Delta t) = x(t) + \sum_{i=1}^N \left\{ S_{e_i}^x \frac{dp_{e_i}}{dt} \Delta t \right\}_{(e_i \in F)} \quad (31)$$

where N denotes the total number of critical components in the circuit, $S_{e_i}^x$ refers to the sensitivity of circuit health metric x to parametric deviation in circuit component e_i , and dp_{e_i} refers to the parametric deviation in circuit component e_i .

The circuit health degradation model in Eq. 31 can be simplified to a matrix-based state space model with process noise as follows:

$$x(t + \Delta t) = x(t) + \mathbf{P}^T(t) \mathbf{I}(t) \mathbf{S} + v(t) \quad (32)$$

where $\mathbf{P} = \left[\frac{dp_{e_1}}{dt}, \dots, \frac{dp_{e_N}}{dt} \right]$, \mathbf{I} is a diagonal fault matrix with $[\mathbf{I}]_{ii} = \mathbf{1}$ if the i^{th} circuit component is faulty, and $\mathbf{S} = [S_{e_1}^x, \dots, S_{e_N}^x]$ is the deterministic-sensitivity vector. Although the vector \mathbf{P} in Eq. 32 indicates parametric deviations in critical circuit components, the elements of this vector is not known as the components are not measurable in real time. Hence, comparing Eq. 32 with Eq. 22 reveals, \mathbf{P} is equivalent to unknown parameter vector $\boldsymbol{\theta}$ that has to be estimated along with state x , and \mathbf{I} is equivalent to the input vector \mathbf{u} that is obtained from the fault diagnostics module.

4.3 Model-based Prognostic Methodology

Model-based prognostics methodology is realized in two steps. First step is the health state estimation from noisy health state values (estimated by kernel-based learning algorithm) where both state and parameter vectors are estimated i.e., $p(x(t), \theta(t) | \mathbf{y}(t_0:t))$ is computed. Many stochastic filtering algorithms such as unscented Kalman filter or particle filter can be used to jointly estimate state-parameter vectors with nonlinear system models. Particle filter is widely used in the prognostic community for its capability to estimate the state of a nonlinear system with non-Gaussian noise without having to apply a constraint on the state & parameter vector's probability distribution function (PDF). For the same reason sampling importance resampling (SIR) particle filter is used in this study for *RUP* estimation.

In particle filters, the state-parameter PDF is represented using a set of discrete weighted samples, typically referred to as particles

$$\{(x_t^i, \boldsymbol{\theta}_t^i), w_t^i\}_{i=1}^M \quad (33)$$

where M denotes the number of particles, and for each particle i , x_t^i denotes the health state estimate, $\boldsymbol{\theta}_t^i$ represents the parametric deviations estimate, and w_t^i denotes the weight at time t . At each time instant, the particle filter uses the past estimates of state and parameter along with real time measurements to estimate the current state. To realize this multi-step computation, first the parameter vector $\boldsymbol{\theta}_t$ is estimated from the previous time instant parameter estimates using some process that is independent of the state x_t . The typical approach is to use a random walk process, i.e., $\boldsymbol{\theta}_t = \boldsymbol{\theta}_{t-\Delta t} + \boldsymbol{\xi}_{t-\Delta t}$, where $\boldsymbol{\xi}$ is sampled from a distribution such as zero-mean Gaussian

[63]. However, in the circuit prognostic application we have defined θ as parametric deviations in circuit components. For a number of discrete components, first-principles based models exist to describe these parametric deviations. For example, in Kulkarni et al. [15] the deviation in capacitance of an electrolytic capacitor was described using a linear equation as follows:

$$C_t = C_{t-\Delta t} - \Theta v_e \Delta t \quad (34)$$

where C_t denotes the capacitance at time t , Θ is a model-constant that depends on the geometry and materials of the capacitor, and v_e denotes the volume of electrolyte. Similar models have been described by Smet et al. [64], Celaya et al. [14], Patil et al. [5], Alam et al. [6] for IGBT, MOSFET, electrolytic capacitor, and embedded capacitor respectively. These models can be used in-place of random walk process to describe the evolution of the unknown parameter vector θ . Thus, the proposed circuit prognostics approach can make use of existing physics-of-failure (PoF)-based models on circuit components in the overall circuit degradation model and combine it with data-driven circuit health estimates to provide a fusion prognostics outcome.

Once the parameter vector is updated, the circuit health is estimated from the system equation in Eq. 32 after which the associated weights are computed using the principle of importance resampling [65]. The pseudo code for a single iteration of SIR particle filter is given in Algorithm 2 and Figure 27 steps involved in a single iteration of particle filter for state estimation.

Algorithm 2. Pseudo code for a single iteration of particle filtering algorithm for state estimation.

Input: $\{(x_{t-\Delta t}^i, \theta_{t-\Delta t}^i), w_{t-\Delta t}^i\}_{i=1}^M, \mathbf{u}_{t-\Delta t, t}, \mathbf{y}_t$

Output: $\{(x_t^i, \theta_t^i), w_t^i\}_{i=1}^M$

Pseudo Code:

for $i = 1$ to M do

$$\theta_t^i \sim p(\theta_t | \theta_{t-\Delta t}^i)$$

$$x_t^i \sim p(x_t | x_{t-\Delta t}^i, \theta_{t-\Delta t}^i, \mathbf{u}_{t-\Delta t})$$

$$w_t^i \sim p(y_t | x_t^i, \theta_t^i, \mathbf{u}_t)$$

end for

$$W \leftarrow \sum_{i=1}^M w_t^i$$

for $i = 1$ to M do

$$w_t^i \leftarrow w_t^i / W$$

end for

$$\{(x_t^i, \theta_t^i), w_t^i\}_{i=1}^M \leftarrow \text{Resample}(\{(x_t^i, \theta_t^i), w_t^i\}_{i=1}^M)$$

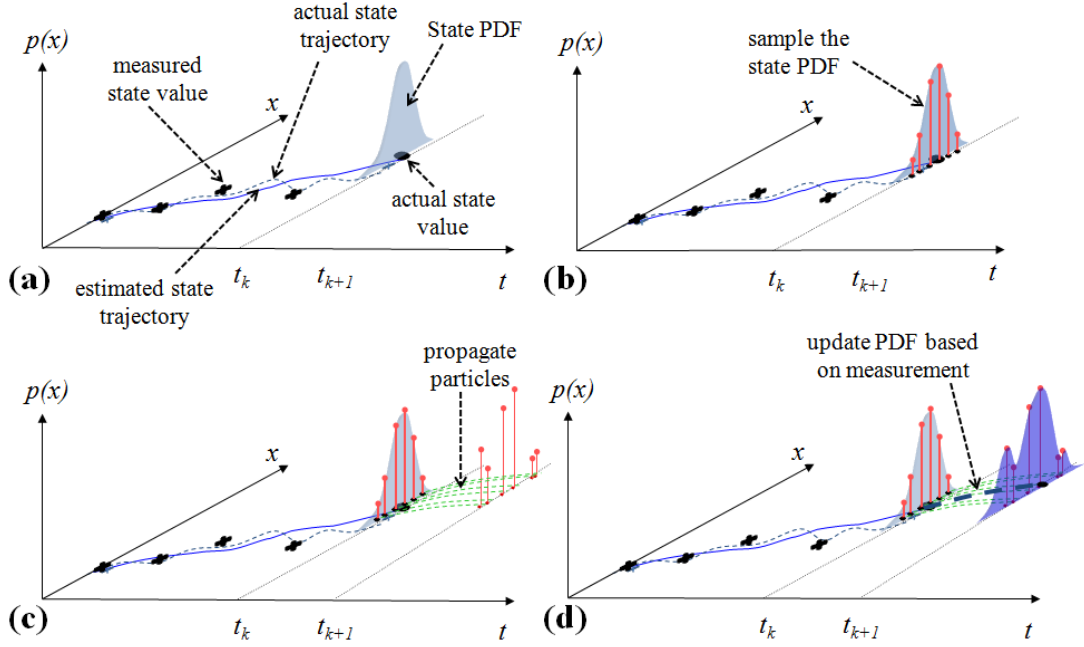


Figure 27. Illustration of the steps involved in simple particle filter.

At the end of iteration the estimated state and parameter vector – particles are investigated for degeneracy and resampled if necessary. During resampling, the particles with least weights are eliminated thereby allowing us to concentrate on the particles with larger weights. Details on degeneracy and resampling can be found in Arulamapalam et al. [65].

The second step in model-based prognostics involve the *RUL* prediction, where the goal is to compute $p(RUL(t_p)|\mathbf{y}(t_0:t_p))$ at time t_p using the joint state-parameter estimates $(x(t_p), \boldsymbol{\theta}(t_p)|\mathbf{y}(t_0:t_p))$. The idea to solve the *RUL* prediction problem is to simply let the state and parameter vector – particles to evolve without Bayesian updating, until the threshold function evaluates to $T_{EOL}(x_t^i) = 1$ for each particle. The predicted time $t: t \geq t_p$ at which $T_{EOL}(x_t^i) = 1$ provides the $EOL_{t_p}^i$, from which

$RUL_{t_p}^i$ is estimated using Eq. 26. The pseudo code for the *RUL* prediction method is given in Algorithm 3.

Algorithm 3. Pseudo code for *RUL* prediction using particle filtering algorithm.

Input: $\{(x_{t_p}^i, \theta_{t_p}^i), w_{t_p}^i\}_{i=1}^M$

Output: $\{(x_t^i, \theta_t^i), w_t^i\}_{i=1}^M$

Pseudo Code:

for $i = 1$ to M do

$t \leftarrow t_p$

$\theta_t^i \leftarrow \theta_{t_p}^i$

$x_t^i \leftarrow x_{t_p}^i$

while $T_{EOL}(x_t^i) = \mathbf{0}$ do

$\theta_{t+\Delta t}^i \sim p(\theta_{t+\Delta t}^i | \theta_t^i)$

$x_{t+\Delta t}^i \sim p(x_{t+\Delta t}^i | x_t^i, \theta_t^i, u_t)$

$t \leftarrow t + \Delta t$

$x_t^i \leftarrow x_{t+\Delta t}^i$

$\theta_t^i \leftarrow \theta_{t+\Delta t}^i$

end while

$EOL_{t_p}^i \leftarrow t$

$RUL_{t_p}^i \leftarrow EOL_{t_p}^i - t_p$

end for

4.4 Implementation Results

In this section, simulation-based experimental results are presented demonstrating the model-based fusion prognostics methodology on the two critical circuits of a DC–DC converter system i.e., low pass filter (Figure 17) and voltage divider feedback circuit (See Figure 22). This demonstration focuses on circuit failure prediction due to the presence of a single-fault condition wherein one critical component is degrading. Situations where two or more components are exhibiting parametric drifts will be considered in future work.

Although the prognostic results are obtained from simulation-based experiments, the component degradation trends are extracted from accelerated life tests (ALTs) conducted in previous CALCE studies [4][7]. Resistor degradation trends were obtained from the temperature cycling test (–15 to 125 °C with 10-min dwell) on 2512 ceramic chip resistors (300 Ω) [7]. On the other hand, capacitor degradation trends were obtained from concurrent ripple current (at 1.63A) and isothermal aging tests at 105 °C on 680 μ F 35V liquid electrolytic capacitor [4].

The circuit topology, component tolerance and failure range, features extracted and failure conditions for both low pass filter (Figure 17) and voltage divider feedback circuit (See Figure 22) remains the same as the description provided in Section 3.3.2.

4.4.1 Low-Pass Filter Circuit

Low-pass filter circuit health was estimated from the extracted features using the approach summarized in Section 3.1 and was used as input to the prognostics module. Figure 28 shows the degradation in health of the low-pass filter circuit with progression of parametric fault in electrolytic capacitor i.e., it plots the variation of

$E(x(t)|y(t_0:t))$ with respect to time. The solid blue curve that is referred to as ‘Observed Health’ represents the noisy health computed using the method described in Chapter 3. The dashed red line represents the health estimated using the model in Section 4.2, Eq. 32. Figure 29 shows the estimated parametric deviation in circuit component beyond tolerance (i.e., 5%) in comparison to the ground truth (solid blue line). The difference in the estimated parametric deviation in electrolytic capacitor with respect to the ground truth is attributed to the difference between HI_t^A the circuit and the circuit health estimate generated by the kernel-method, see Figure 19.

The red dashed lines in Figure 28 and Figure 29 together represents the joint state-parameter estimates. It can be seen from Figure 29 that the developed model in Eq. 31 is capable of capturing the degradation trend in the actual deviation of the component parameter without having to monitor the component individually. This capability has never been demonstrated before with any of the previous circuit diagnostic or prognostic studies.

In order to realize prognostics, a failure threshold function has to be defined with respect to the health state. Based on the discussion in Section 3, the ideal failure threshold should be $x(t) = 0$. In order to generate conservative *RUL* estimates, a health value of 0.05 as the failure threshold in this study. Based on this failure threshold, the low-pass filter circuit was found to fail at 183 hours. Failure prediction of low-pass filter circuit was realized by using the following model for dynamic evolution of unknown parameter vector:

$$\theta_t = \theta_{t-\Delta t} + m_1 \Delta t \quad (35)$$

where m_1 is a model constant that is estimated at each iteration by curve fit. However, in practice it is better to evaluate m_1 using for a given capacitor material and geometry. The Eq. (35) is similar to the PoF-based model described by Kulkarni *et al.* [15] for liquid electrolytic capacitor.

Figure 30 shows the prediction result for the low-pass filter circuit as a $\alpha - \lambda$ plot, which requires that at a given prediction point λ , β of the predicted RUL distribution must fall within α of the true RUP. In this case study, $\alpha = 0.30$ and $\beta = 0.5$ for all λ was used, indicating that at each prediction time at least 50% of the RUL distribution lie within 30% error with respect to the ground truth [66]. It can be seen from Figure 30 that an acceptable RUL estimate can be obtained as early as 149 hours, indicating that a prognostic distance of 34 hours. The fluctuation in RUL estimate (Figure 30) can result from the fluctuations in health estimate or due to uncertainty in modeling.

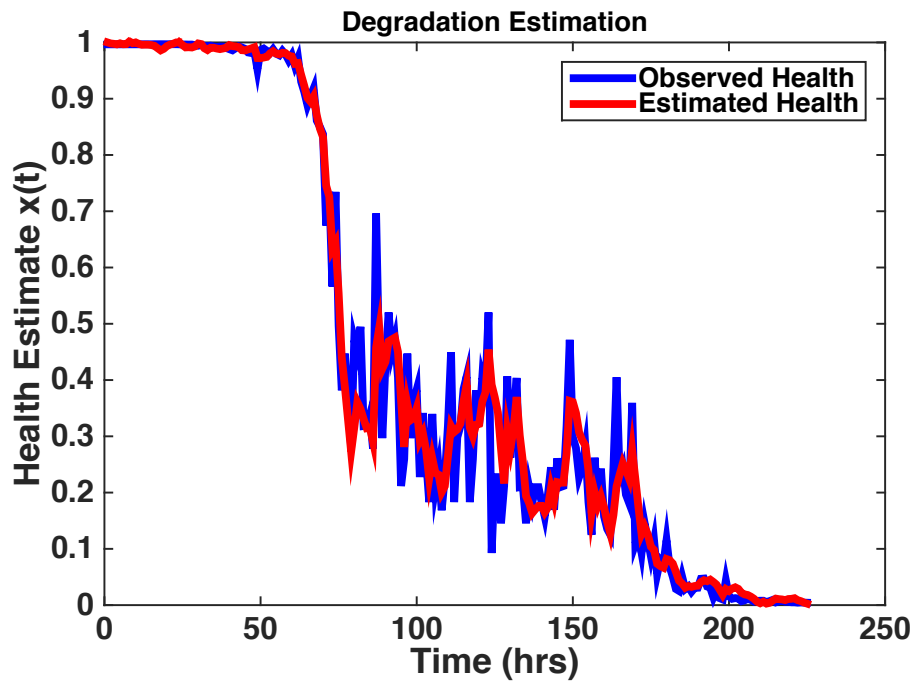


Figure 28. Observed and estimated degradation in health of low pass filter circuit due to progression of fault in electrolytic capacitor.

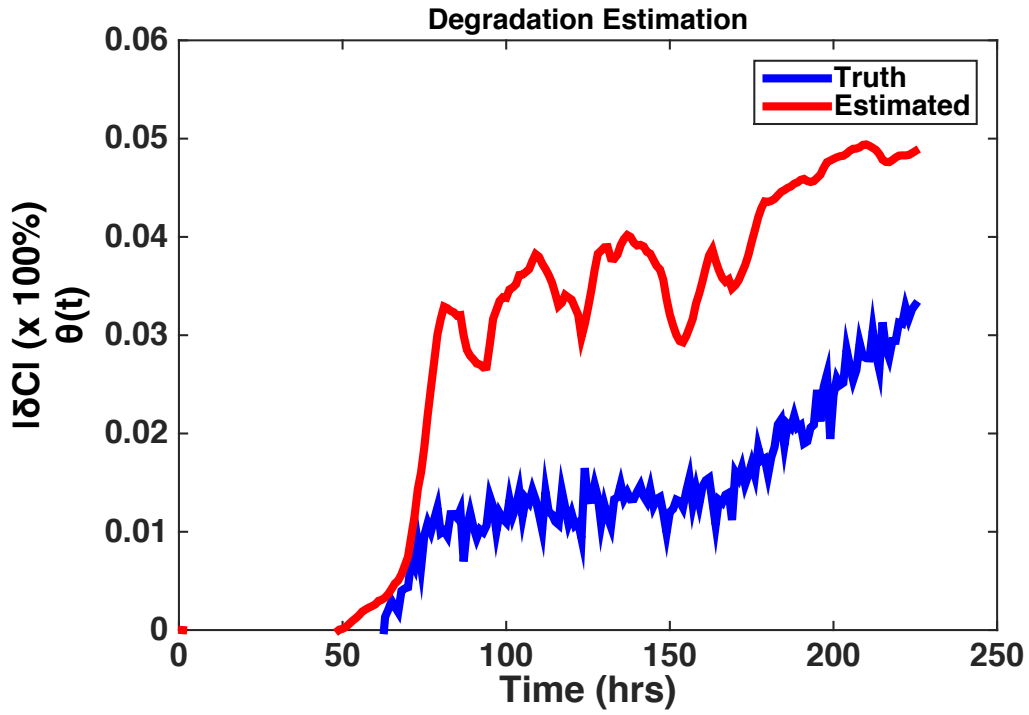


Figure 29. Estimated deviation in capacitance of liquid electrolytic capacitor.

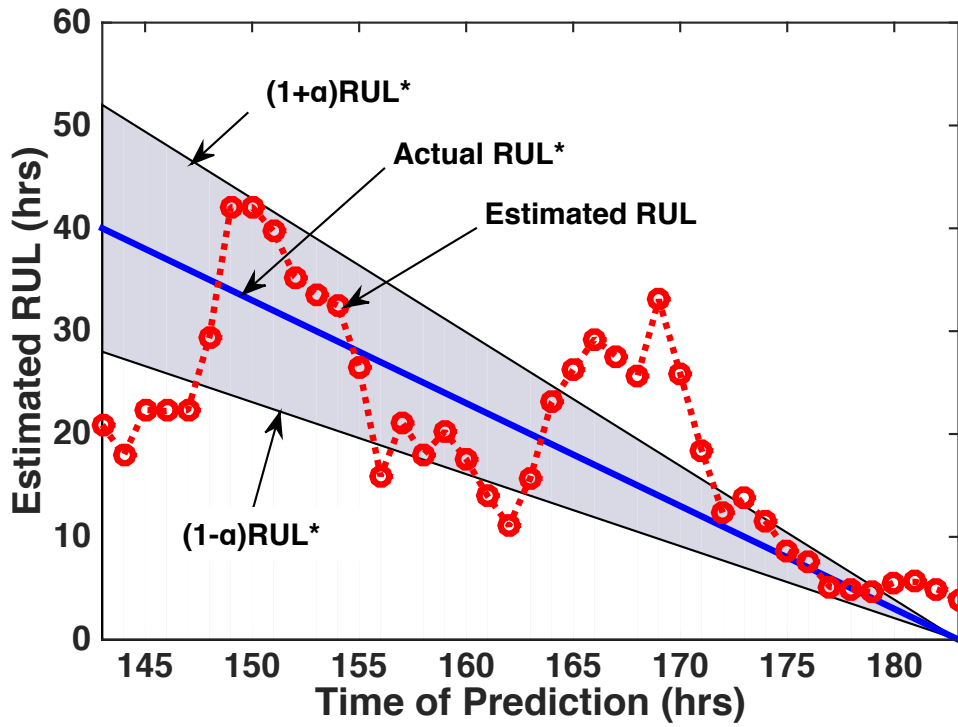


Figure 30. RUL estimation result for low pass filter circuit using model-based filtering method.

4.4.2 Voltage Feedback Circuit

The voltage feedback circuit was stimulated using a step voltage signal (0–5 V), which steps up by 1 V every 100ms. The voltage response generated by the circuit was directly used as input to the health estimator in Chapter 3. The following resistor degradation model was used to evolve the unknown parameter vector for voltage feedback circuit prognostics:

$$\theta_t = \theta_{t-\Delta t} + m_2 e^{m_3 t} [e^{m_3 \Delta t} - 1] \quad (36)$$

where m_2 and m_3 are model constants that are estimated at each prediction iteration by curve fit. The model in Eq. 36 is similar to the solution of the quadratic differential equation proposed by Lall et al [67] for increase in resistance due to degradation of solder joints.

Figure 31 shows the degradation in health of the voltage divider feedback circuit due to progression of fault in R_1 . Figure 32 shows the estimated increase in resistance of R_1 beyond its tolerance. Similar to the electrolytic capacitor in low pass filter, the developed degradation model in Eq. 32 does a reasonable job in capturing the parametric deviation trend without having to monitor the resistance value. Finally, the prognostic result for voltage feedback circuit due to fault in R_1 is shown in Figure 33. The actual circuit performance failure occurred at 2310 hours. And the model-based filtering prognostics method can provide reliable predictions as early as 2000 hours. The details for the $\alpha - \lambda$ plot and failure threshold are same as in low pass filter topology [66]. Similar results are presented in Figure 34 through Figure 36 for progression of fault in R_3 , where the actual failure occurred at 8950 hours and reliable *RUL* estimates were generated as early as 6000 hours.

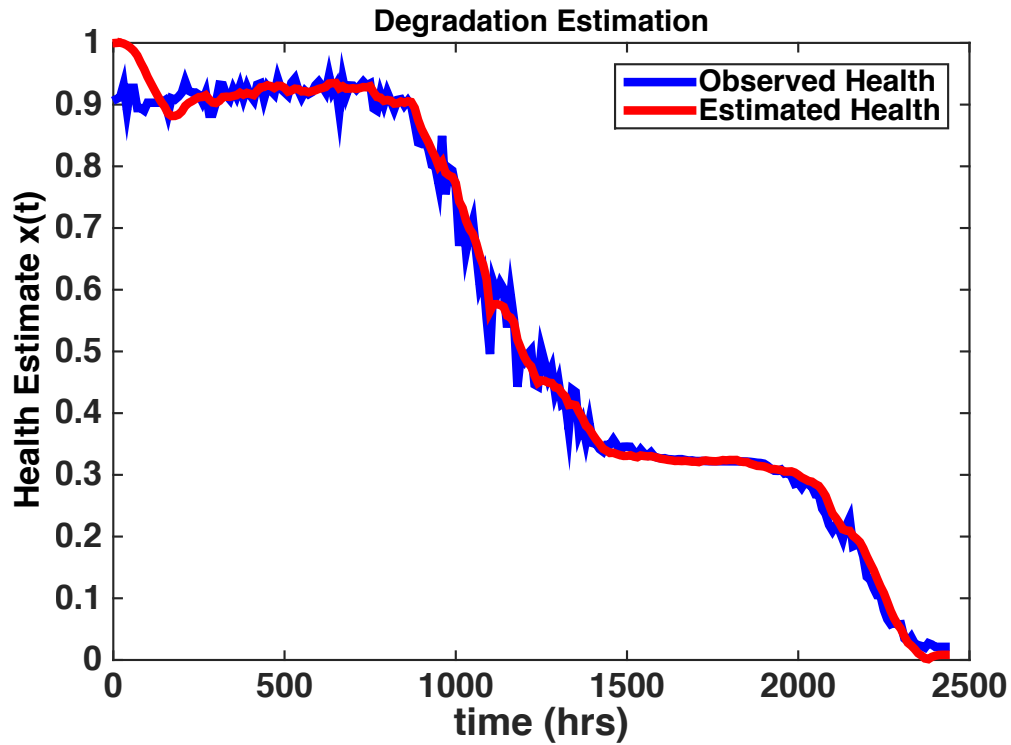


Figure 31. Observed and estimated degradation in voltage feedback circuit health due to progression of fault in R_1 .

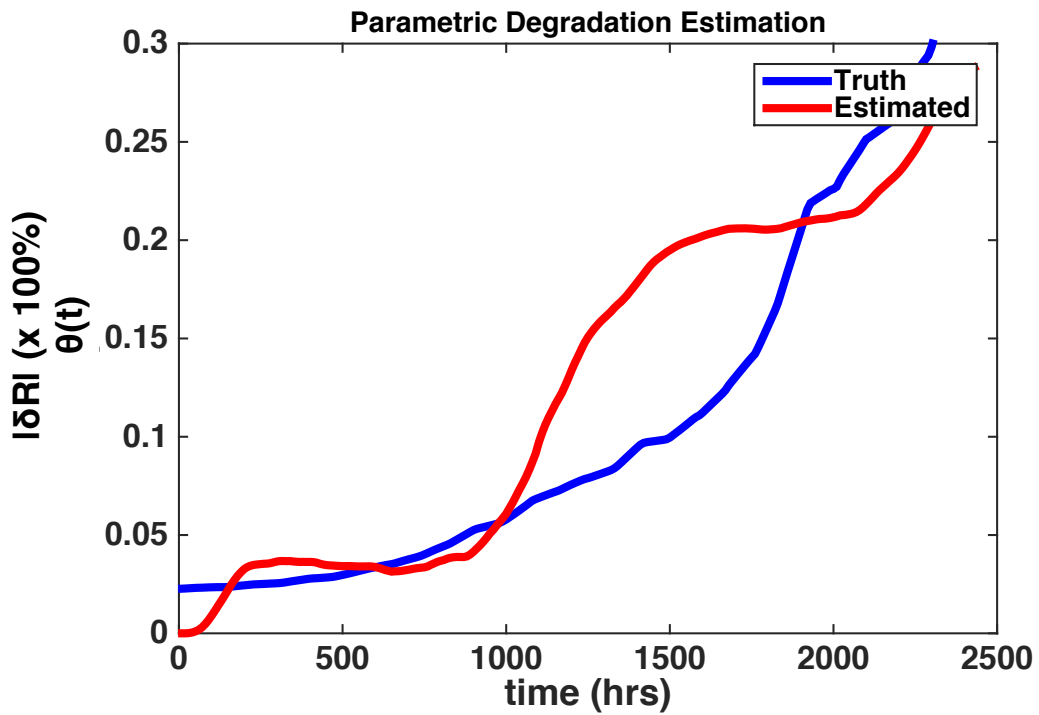


Figure 32. Estimated deviation in resistance R_1 of voltage feedback circuit.

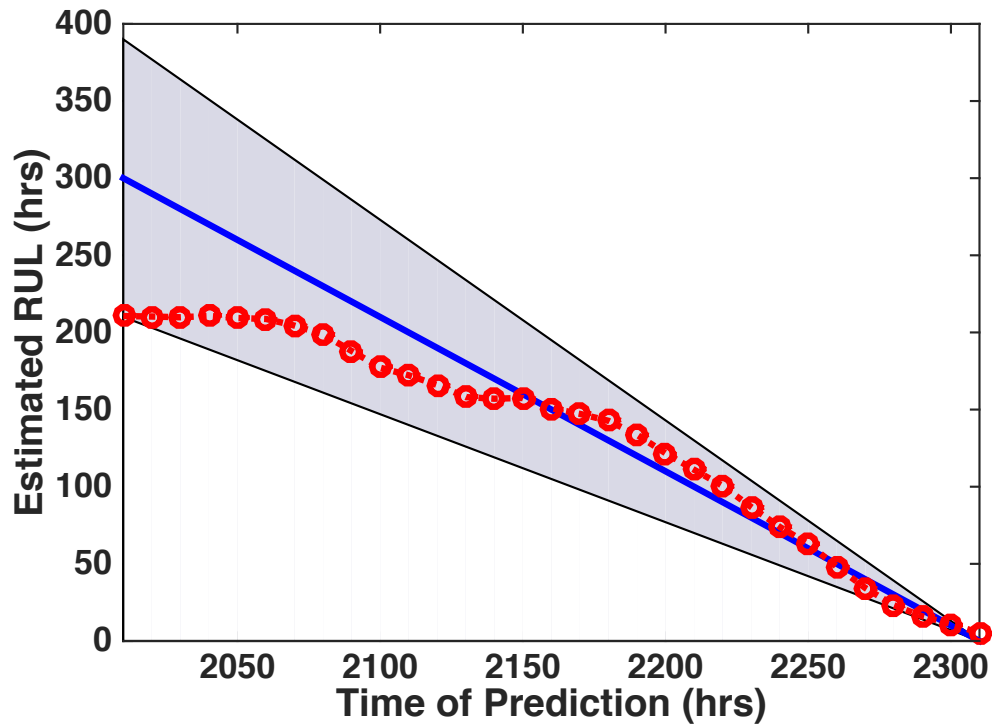


Figure 33. *RUL* estimation result in voltage feedback circuit due to progression of fault in R_1 using model-based filtering method.

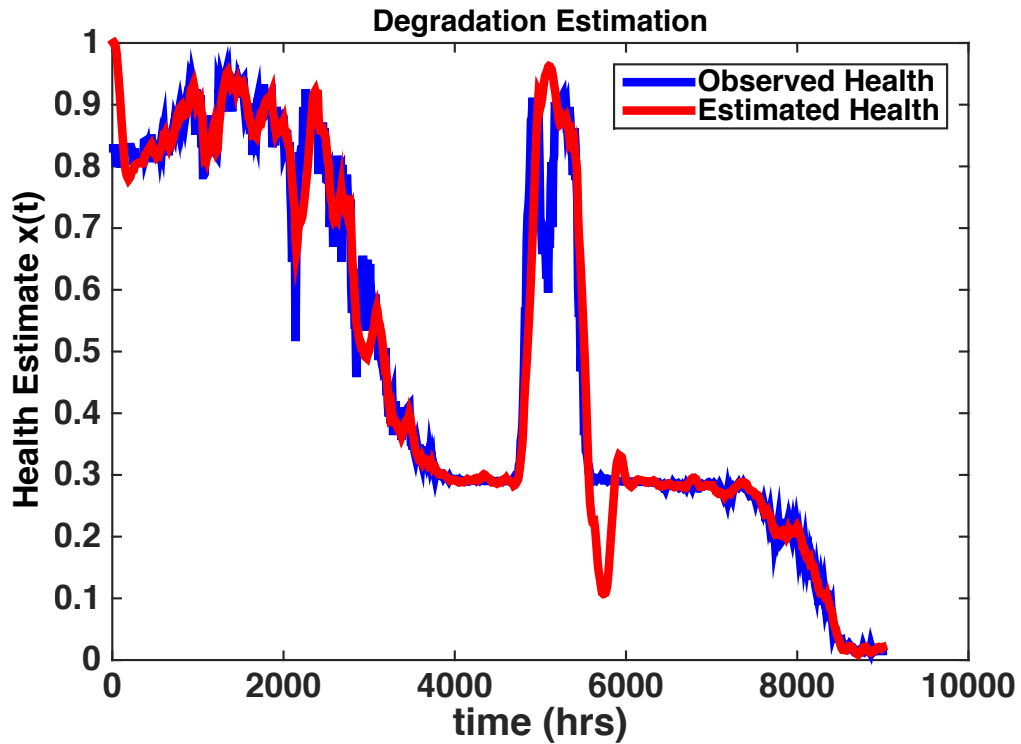


Figure 34. Observed and estimated degradation in voltage feedback circuit health due to progression of fault in R_3 .

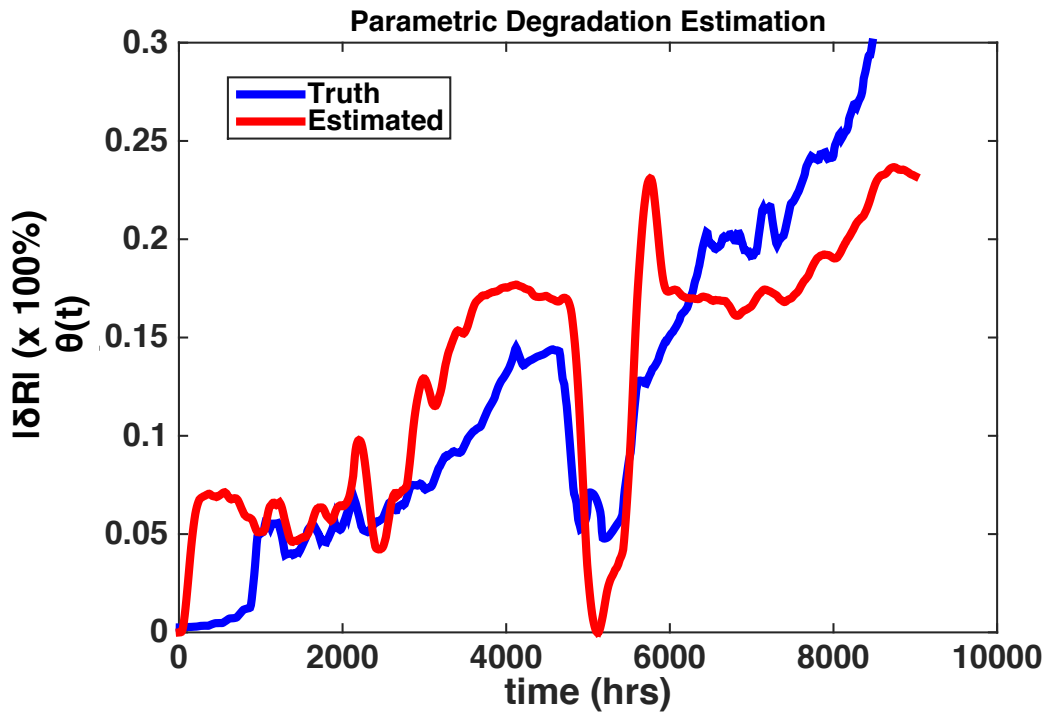


Figure 35. Estimated deviation in resistance R_3 of voltage feedback circuit.

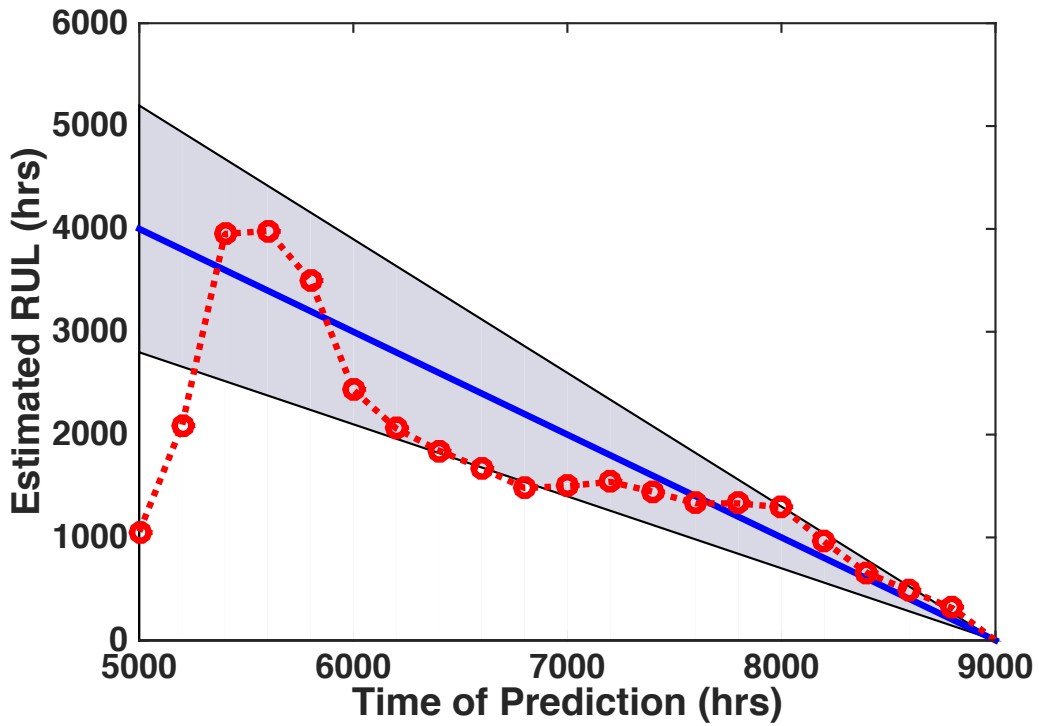


Figure 36. RUL estimation result in voltage feedback circuit due to progression of fault in R_3 using model-based filtering method.

4.4.3 Source of RUL Prediction Error

In Figure 30 and 36, the RUL prediction trend did not linearly correlate with the expected RUL trend. The source of RUL prediction error can be the fluctuations in estimated circuit health (i.e., input to degradation model) or the uncertainty in degradation modeling. In order to identify the source of RUL prediction error, simulated degradation experiments were carried out instead of using degradation trends from actual ALT. In this experiment, component R_3 of the voltage divider feedback circuit was set to gradually degrade and all other components were fixed to their nominal values. The corresponding circuit health estimate for this scenario is shown in Figure 37.

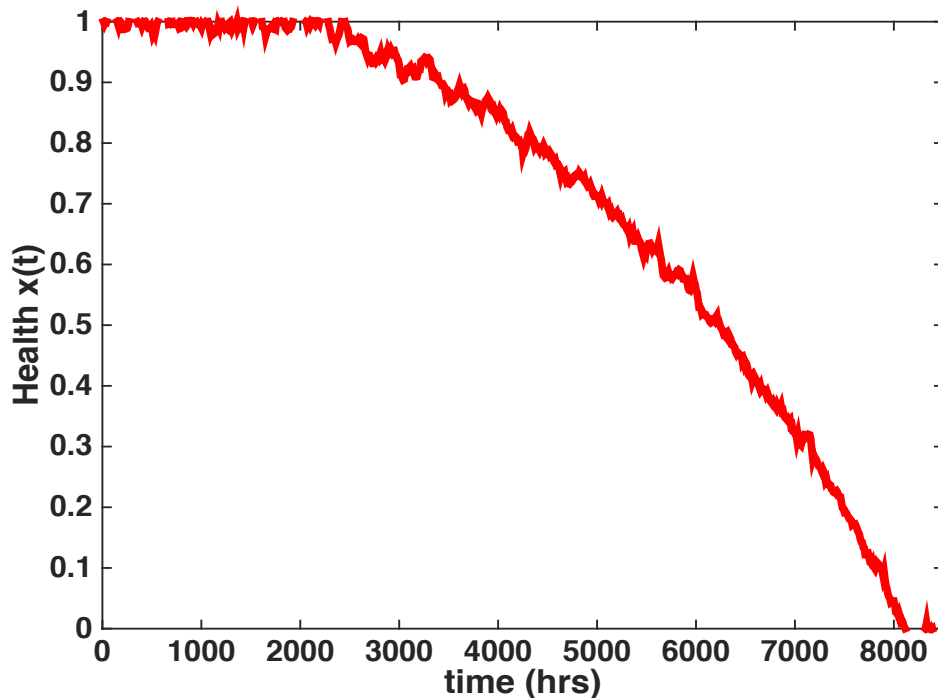


Figure 37. Estimated voltage feedback circuit health due to simulated progression of fault in component R_3 .

Figure 38 shows the estimated increase in resistance of R_3 beyond its tolerance using degradation model in Eq. 36. As seen from Figure 38, the error in parameter estimation has significantly reduced with simulated degradation. Finally, the prognostic result for voltage feedback circuit due to fault in R_3 is shown in Figure 39. The actual circuit performance failure occurred at 8050 hours. And the model-based filtering prognostics method can provide reliable predictions as early as 7000 hours. Additionally, the RUL prediction trend falls in-line with the expected RUL trend. This result proves that the major source of RUL prediction error is the fluctuations in the health values given as input to degradation model and not the model itself.

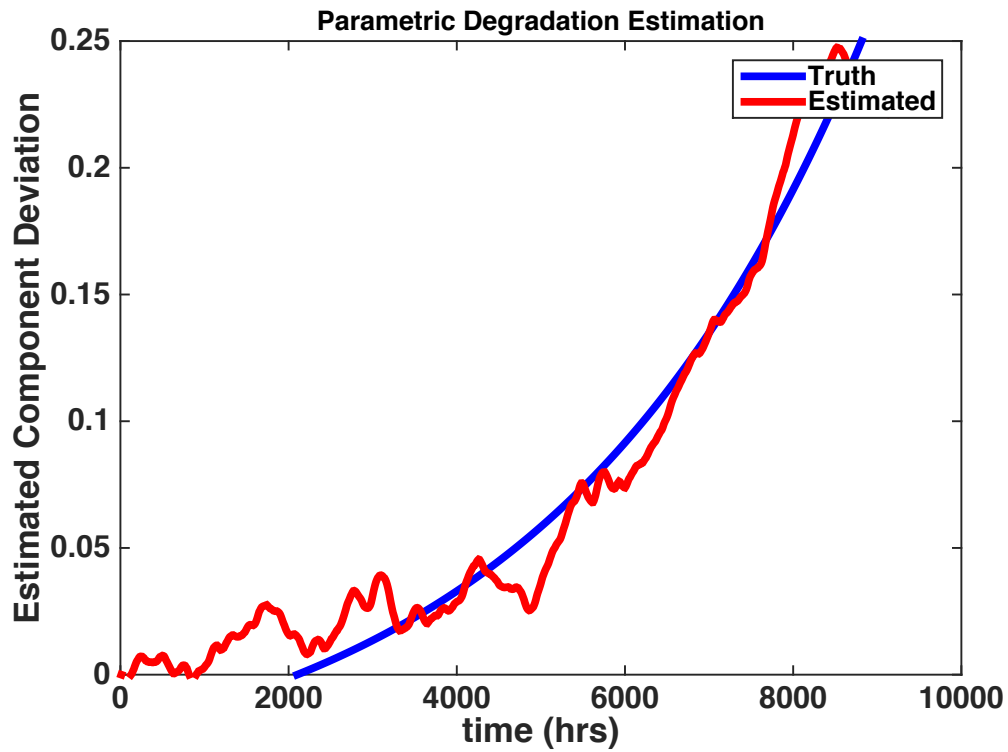


Figure 38. Estimated deviation in resistance R_3 of voltage feedback circuit with simulated component degradation.

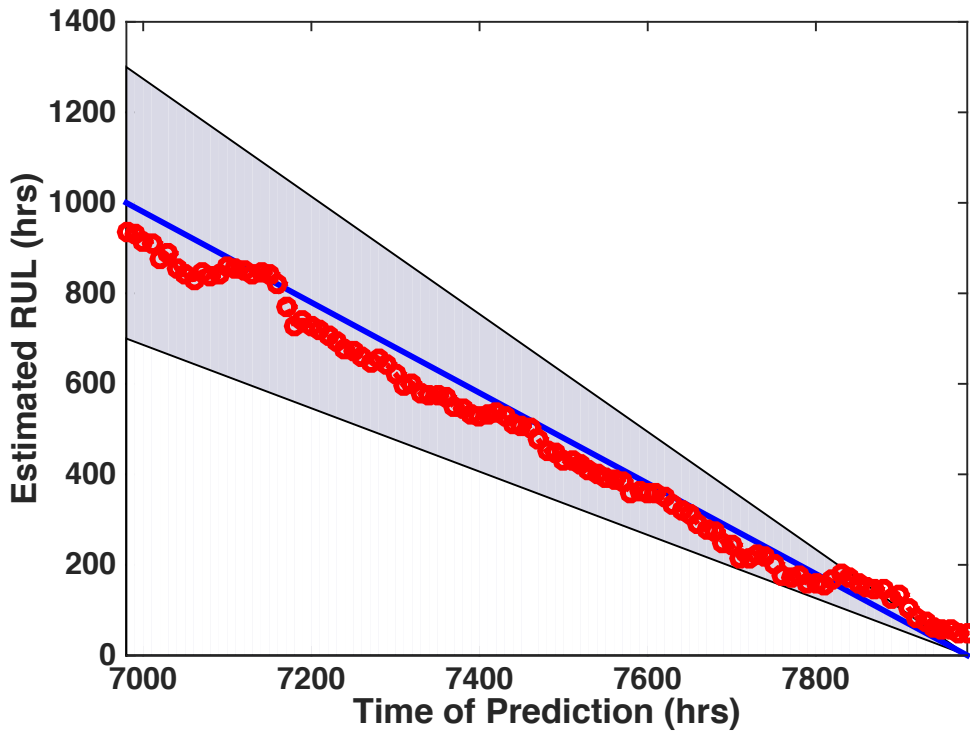


Figure 39. RUL estimation result in voltage feedback circuit due to simulated progression of fault in R_3 using model-based filtering method.

4.4.4 Effect of first principles-based modeling of θ_t

Experiment was performed with and without random walk model (or without and with first principles-based model respectively) to determine the improvement in RUL prediction using first principles-based model for θ_t . Figure 40(a) and (b) presents the prediction result with random walk for θ_t and with first principles-based model for θ_t , respectively, for the voltage divider feedback circuit as a $\alpha - \lambda$ plot. Clearly, the RUL prediction with first principles-based model is reliable and robust when compared to the RUL prediction with random walk for this CUT. Furthermore, the variance in RUL prediction 100hours and 50hours before failure show that the

confidence in RUL prediction with first principles-based model is better than that with simple random walk (see Figure 41).

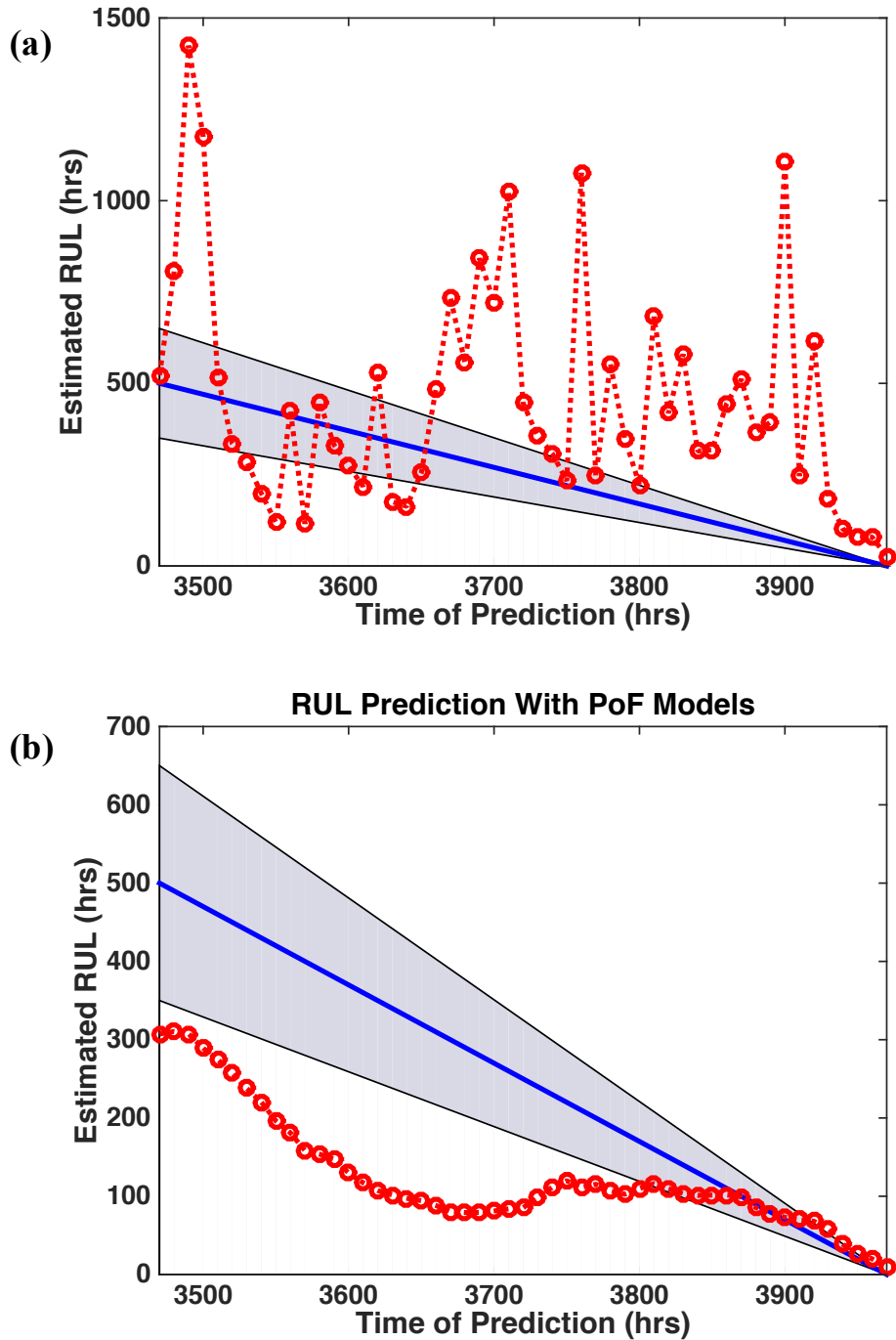


Figure 40. *RUL* prediction results for voltage divider feedback circuit with (a) random walk model for θ_t and (b) first principles-based model for θ_t .

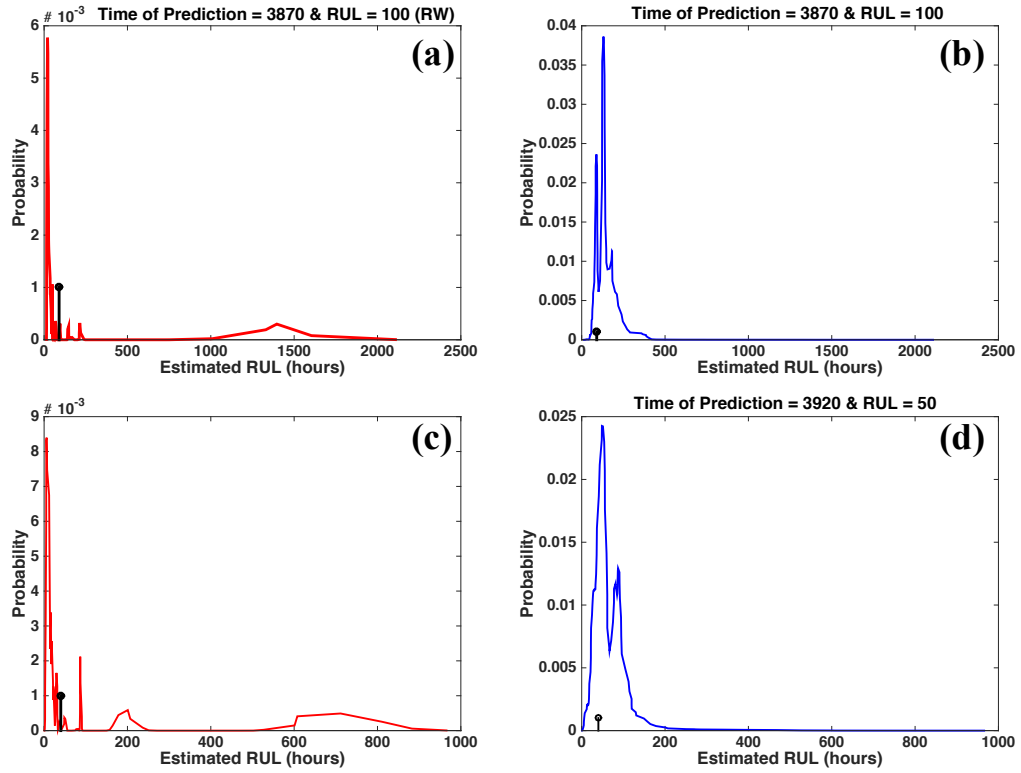


Figure 41. Predicted *RUL* distribution for voltage divider feedback circuit with random walk model (red) and first principles-based model (blue) for θ_t at (a)-(c) 100hours and (b)-(d) 50hours before failure.

Chapter 5: Conclusions and Future Work

Electronic circuit and system failures due to parametric faults in circuit components regularly occur in fielded applications requiring longer service life. A good example includes solar industry, where inverter and optimizer failures contribute the largest to balance-of-system downtime. Methods that can predict circuit failures resulting from parametric faults will aid in improving the reliability of fielded systems.

Most of the existing prognostics research focuses on exploiting component-level features to predict component failures. However, these approaches become impractical when cost and complexity are taken into consideration. Furthermore, most of the component-level parameters cannot be measured once the component is part of a circuit. To address this problem, a circuit prognostics methodology is developed in this dissertation to predict circuit performance-related failures resulting from progression of parametric faults in discrete electronic components.

First, to facilitate prognostics, a circuit health estimation method using a kernel-based learning technique was developed and demonstrated on a benchmark circuit and DC–DC buck converter system. Second, a model-based filtering method with first principles-based degradation model was developed for *RUL* prediction.

The developed circuit health estimation method exploits features that are extracted from circuit responses, instead of component parameters. In the process of establishing the circuit health estimation method, an approach was also developed to solve the model selection problem in kernel-based health estimation. The *RUL* prediction method on the other hand, allows the estimation of parametric deviation in faulty circuit component (i.e., parametric fault severity) along with the degradation in

circuit health, while taking into consideration unit-to-unit variations. This is meaningful from a health management perspective, where a maintenance personnel is given not only *RUL* information but also fault severity information. Additionally, the developed model-based filtering method is capable of generating fusion-prognostics outcome provided, physics of failure based knowledge and model exists for the critical components. This is beneficial from performance standpoint, as it has been proved in the past that fusion-prognostic outcome is reliable and desirable over a data driven or physics-of-failure approach.

Implementation results indicate that the developed circuit health estimation approach is able to capture the actual degradation trends of the faulty component. In most of the cases, the estimated failure time, t_F , was less than the actual failure time, T_A , indicating that the developed health estimation method raised early failure warning prior to the actual circuit failure. Although this attribute is desirable in any diagnostic method, it is actually beneficial only if the difference between T_A and t_F is kept minimal, else there will be wastage of useful life. This problem of early failure detection was experienced with the estimation of healthy of low pass circuit due to parametric fault in electrolytic capacitor. Recollecting the definition of *HI* as a posterior class probability representing the conditional probability of a healthy class for the extracted feature set, the wastage of useful life could result (i.e., rapid drop in *HI* towards zero) due to two reasons. First reason being, the size of the failure class features in the kernel Hilbert space is much bigger than the size of the healthy class features thereby biasing the conditional probability value towards fault class. Second reason, is that the healthy and failure classes are well spaced apart in the kernel

Hilbert space, and thus are easily classifiable. The second reason could be easily tackled by relaxing the failure threshold i.e., choose a value much closer to 0, the theoretical failure limit. However, to tackle first reason, further studies need to be conducted in order to investigate the potential impact of having tighter control on the distribution of faulty features in kernel Hilbert space.

Another observation from the conducted health estimation study is that the health estimate is dependent on the contributions from component tolerances. Component tolerance effects on the extracted features control the distribution of features in the kernel Hilbert space. In spite of the inclusion of regularization parameters to address the contributions from component tolerances, there were fluctuations in the circuit health estimate as seen with the low-pass filter example in the DC–DC converter system. Further investigation needs to be conducted in order to account for application-specific constraints in the hyperparameter optimization framework to control the spread of healthy class features in the kernel Hilbert space in order to achieve a more robust circuit health estimate.

A limitation of the developed model-based filtering method for *RUL* prediction is that the degradation model is developed with a single fault condition in mind. If two or more components exhibit parametric fault, the model will capture the effect of individual component fault in a linear fashion, which may not be the case. As a result the developed model will most likely generate early failure warnings, resulting in wastage of useful life. Future work is required to address the nonlinear relation between circuit health and the effect of more than one component being faulty.

Chapter 6: Dissertation Contributions

The contributions of this dissertation are as follows:

- A circuit health estimation method based on kernel-learning that takes into account the effect of component tolerances and allows for health estimation:
 - Irrespective of whether healthy and failure classes are linearly separable or not.
 - Without having to monitor the parameters of the individual circuit components.
- A stochastic filtering approach for the automatic selection of optimal hyperparameter values in kernel methods
- A degradation model for RUL prediction, that is capable of estimating the intensity of parametric faults and generating fusion prognostic outcome.

Appendix A: Comparison of Particle Filter with Other Global Optimization Methods

Zhou et al [48][49] developed a global optimization method using particle filter, which falls under the category of model reference adaptive search. Zhou compared her approach with well-known cross entropy (CE) methods with varying smoothing factor v . Figure 37 shows the comparison of optimization with particle filter (referred to as CEA in Figure 37) and CE for 20-dimension Powell singular function that has multiple local minima and one global minima of $H(x^*) = 0$ at $x^* = [0 \ 0 \ \dots \ 0 \ 0]_{20 \times 1}^T$, where:

$$H(x) = \sum_{i=1}^{n-2} [(x_{i-1} + 10x_i)^2 + 5(x_{i+1} - x_{i+2})^2 + (x_i - 2x_{i+1})^4 + 10(x_{i-1} - x_{i+2})^4]. \quad (37)$$

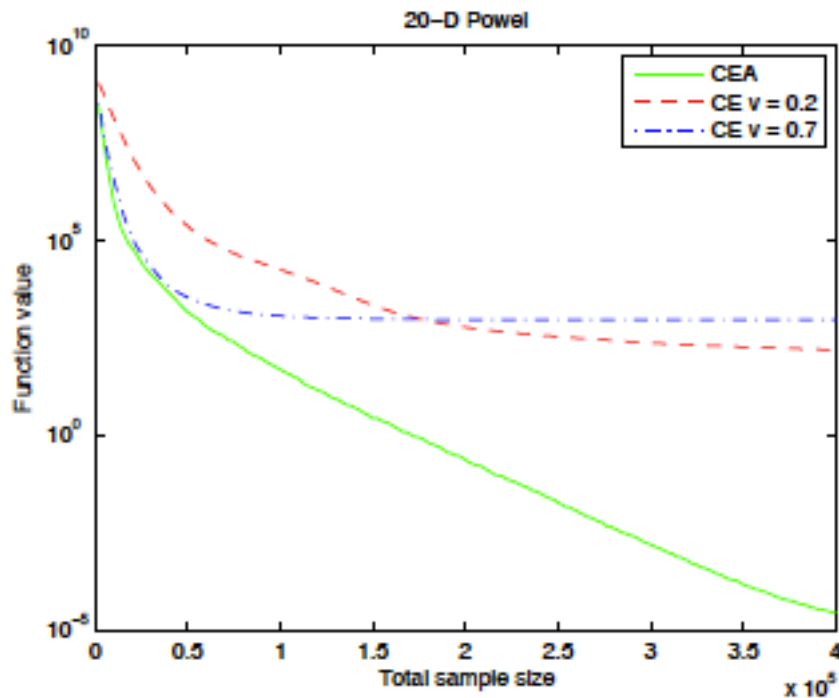


Figure 42. Average performance of particle filter and CE optimization methods on 20-D Powell singular function [49].

Figure 37 clearly shows that particle filter outperforms CE method for a complex objective function with multiple local minima and single global minima. For the same objective function, Hu et al [68] used a model reference adaptive search (MRAS) similar to Zhou [49] (with the only difference being the assumption on the distribution being Gaussian) and compared with Simulated Annealing (SA). The result of Hu et al [68] is shown in Figure 38 where it can be seen that a MRAS method will outperform CE and SA method. This lies in agreement with results from Zhou [49].

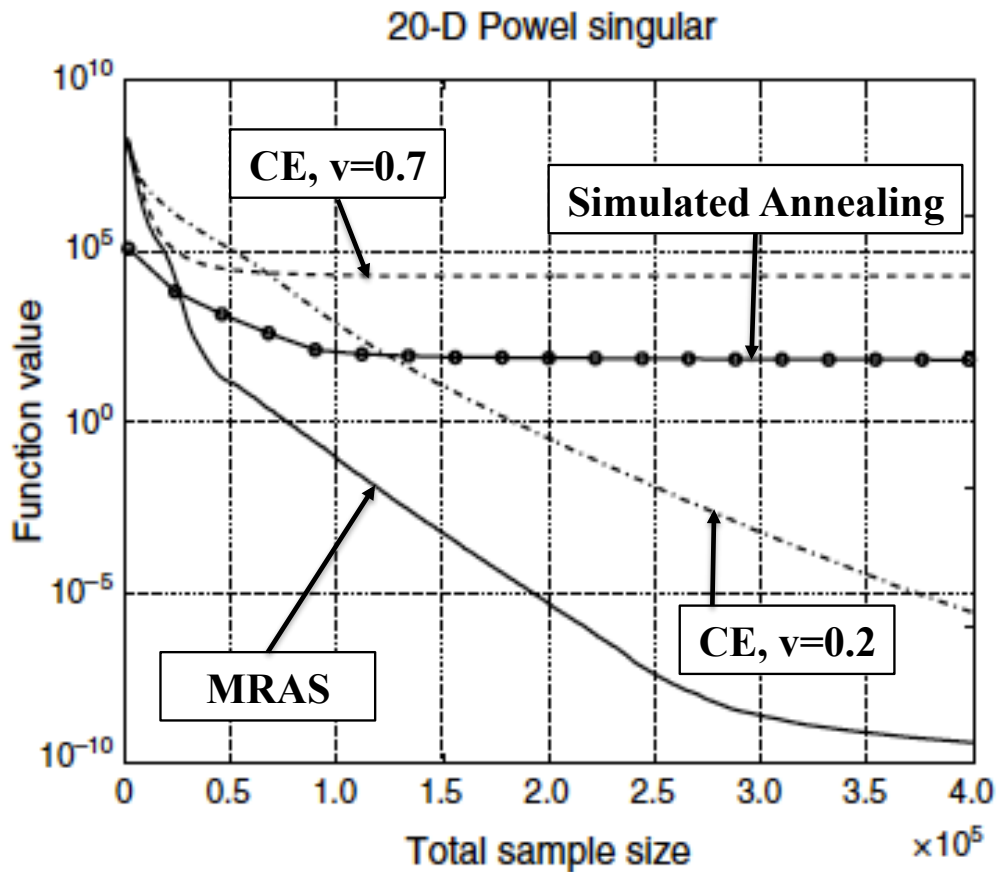


Figure 43. Average performance of MRAS, CE, and SA optimization methods on 20-D Powell singular function [68].

Furthermore, Boubezoul and Paris [50] compared the use of CE search method with particle swarm optimization and grid search methods to automatically select the

hyperparameters of a support vector machine for classification. Boubezoul and Paris [50] demonstrated that the classification accuracy using CE search method outperformed both particle swarm optimization (PSO) and grid search method for selecting the hyperparameters of support vector machine classifier (see Table 3). Thus a stochastic filtering-based global optimization approach that falls under the category of MRAS is expected to provide the best solution among global optimization methods to solve the model selection problem.

TABLE 3
Comparison of CE, PSO, and Grid search methods for optimal selection of hyperparameters in SVM on various benchmark classification datasets [50]. The format of the numbers in the table is $R \pm std$, where R is the average classification accuracy and std is the standard deviation in classification accuracy.

Datasets	CEMSVM	PSOSVM	Grid Search
Iris	(95.11) ± (2.73)	(93.33) ± (3.47)	(92.88) ± (3.74)
Thyroid	(94.84) ± (2.85)	(94.68) ± (2.35)	(94.68) ± (2.57)
Liver	(70.38) ± (2.20)	(65.82) ± (3.90)	(65.04) ± (4.16)
Diabetes	(76.00) ± (2.67)	(70.78) ± (4.96)	(64.69) ± (1.47)
Glass	(69.38) ± (7.15)	(67.23) ± (5.18)	(62.30) ± (3.98)
Vowel	(98.18) ± (0.91)	(97.67) ± (1.03)	(91.14) ± (2.05)
WBC	(72.53) ± (3.72)	(68.35) ± (4.77)	(65.18) ± (1.81)
Wine	(98.11) ± (1.98)	(97.73) ± (2.63)	(40.00) ± (0.79)
Heart	(81.35) ± (4.13)	(75.67) ± (3.63)	(57.65) ± (1.54)
Image	(97.72) ± (0.52)	(97.45) (± 0.42)	(94.88) (± 0.66)
Segment	(97.44) ± (0.62)	(97.08) (± 0.54)	(92.19) (± 0.81)
Twonorm	(97.70) ± (0.21)	(95.93) (± 0.85)	(50.14) (± 0.04)

Additional simulation studies (see Figure 39) were carried out comparing Zhou's [49][50] stochastic filtering-based global optimization method with PSO on benchmark optimization problems such as trigonometric function (20-D), Powel's singular function (20-D), and Rosenbrock function (20-D). In each of these cases, filtering-based optimization exhibited faster convergence when compared to PSO.

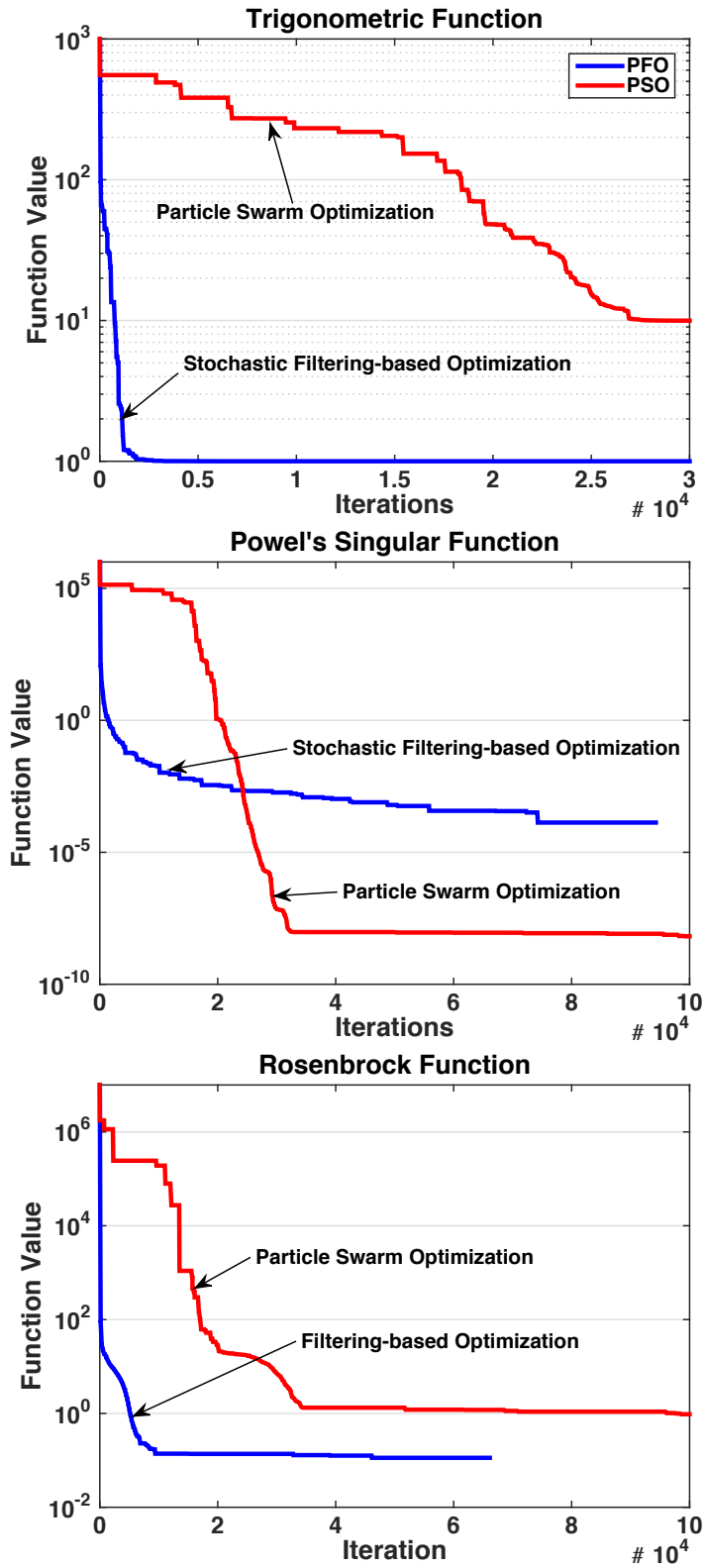


Figure 44. Comparison of filtering-based optimization with PSO on benchmark problems: (a) Trigonometric, (b) Powell's Singular, and (c) Rosenbrock functions.

Figure 40 compares the performance of filtering-based optimization method with and without gradient information on Trigonometric optimization problem. Clearly, the inclusion of gradient information increases the convergence rate, although it doesn't change the identified optimum location.

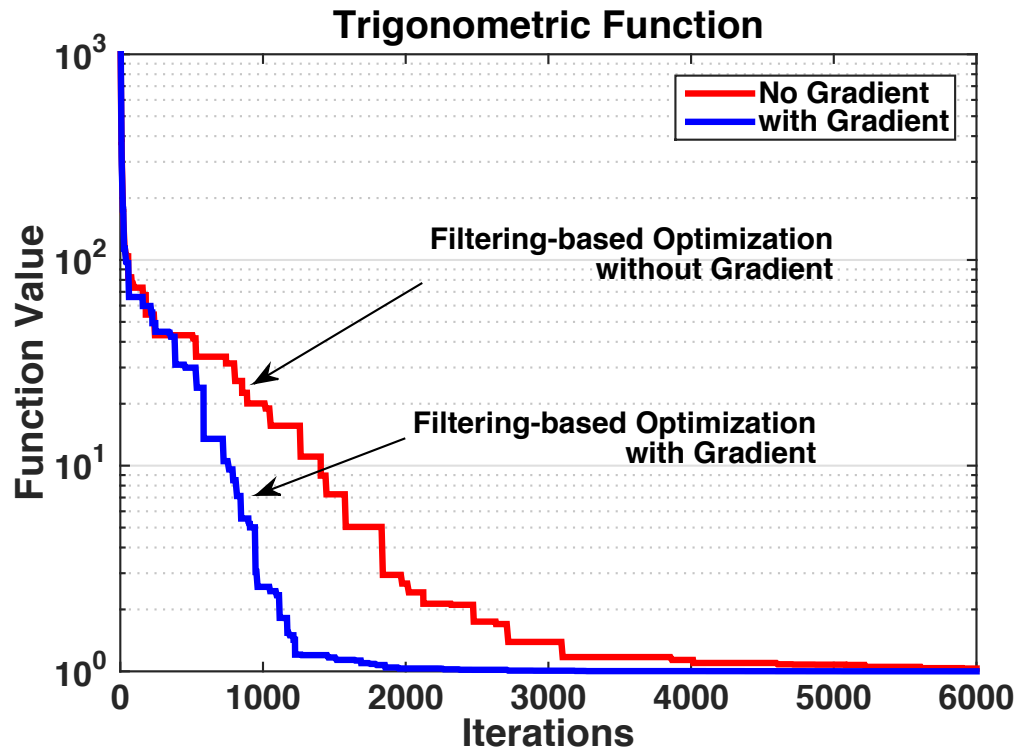


Figure 45. Comparison of filtering-based optimization with and without gradient information on Trigonometric function.

Bibliography

- [1] M. Pecht and R. Jaai, "A prognostics and health management roadmap for information and electronics rich systems," *Microelectronics Reliability*, vol. 50, pp. 317–323, 2010.
- [2] N. Vichare and M. Pecht, "Prognostics and health management of electronics," *IEEE Transactions on Components Packaging Technology*, vol. 29, pp. 291–296, 2006.
- [3] J. Bandler, "Fault diagnosis of analog circuits," *Proceedings of the IEEE*, vol. 73, no. 8, pp. 1279-1325, 1985.
- [4] A. Shrivastava, "Reliability evaluation of liquid and polymer aluminum electrolytic capacitors," Ph.D. Thesis, University of Maryland, 2014.
- [5] N. Patil, D. Das, and M. Pecht, "A prognostic approach for non-punch through and field stop IGBTs," *Microelectronics Reliability*, vol. 52, no. 3, pp. 482-488, 2012.
- [6] M. Alam, M. Azarian, M. Osterman, and M. Pecht, "Prognostics of failures in embedded planar capacitors using model-based and data-driven approaches," *Journal of Intelligent Material Systems and Structures*, vol. 22, no. 12, pp. 1293-1304, 2011.
- [7] E. George, M. Osterman, M. Pecht, and R. Coyle, "Effects of extended dwell time on thermal fatigue life of ceramic chip resistors," *45th International Symposium on Microelectronics*, San Diego, September, 2012.

- [8] S. Harb and R. S. Balog, "Reliability of candidate photovoltaic module-integrated-inverter (PV-MII) topologies-a usage model approach," *IEEE Transactions on Power Electronics*, vol. 28, no. 6, pp. 3019-3027, 2013.
- [9] A. Ristow, M. Begovic, A. Pregelj, and A. Rohatgi, "Development of a methodology for improving photovoltaic inverter reliability," *IEEE Transactions on Industrial Electronics*, vol. 55, no. 7, pp. 2581-2592, 2008.
- [10] L. Oukhellou, A. Debiolles, T. Denceux, and P. Aknin, "Fault diagnosis in railway track circuits using Dempster-Shafer classifier fusion," *Engineering Applications of Artificial Intelligence*, vol. 23, no. 1, pp. 117-128, 2010.
- [11] B. Zhang, C. Sconyers, C. Byington, R. Patrick, M. Orchard, and G. Vachtsevanos, "A probabilistic fault detection approach: application to bearing fault detection," *IEEE Transactions on Industrial Electronics*, vol. 58, no. 5, pp. 2011-2018, 2011.
- [12] L. Liao, "Discovering prognostic features using genetic programming in remaining useful life prediction," *IEEE Transactions on Industrial Electronics*, vol. 61, no. 5, pp. 2464-2472, 2014.
- [13] C. Chen, B. Zhang, G. Vachtsevanos, and M. Orchard, "Machine condition prediction based on adaptive neuro-fuzzy and high-order particle filtering," *IEEE Transactions on Industrial Electronics*, vol. 58, no. 9, pp. 4353-4364, 2014.
- [14] J. Celaya, C. Kulkarni, G. Biswas, S. Saha, and K. Goebel, "A model-based prognostics methodology for electrolytic capacitors based on electrical

- overstress accelerated aging,” in *Proceedings of the Annual Conference of the PHM Society*, 2011.
- [15] C. Kulkarni, J. Celaya, K. Goebel, and G. Biswas, “Bayesian framework approach for prognostic studies in electrolytic capacitor under thermal overstress conditions,” in *Proceedings of the Annual Conference of the PHM Society*, 2011.
- [16] J. Celaya, A. Saxena, S. Saha, and K. Goebel, “Prognostics of power MOSFETs under thermal stress accelerated aging using data-driven and model-based methodologies,” in *Proceedings of the Annual Conference of the PHM Society*, 2011.
- [17] D. Kwon, and J. Yoon, “A model-based prognostic approach to predict interconnect failure using impedance analysis,” accepted to *Journal of Mechanical Science and Technology*.
- [18] D. Kwon, M. H. Azarian, and M. Pecht, “Remaining life prediction of solder joints using RF impedance analysis and Gaussian process regression,” *IEEE Transactions on Components, Packaging, and Manufacturing Technology*, vol. 5, no. 11, pp. 1602-1609, 2015.
- [19] R. Spina and S. Upadhyaya, “Linear circuit fault diagnosis using neuromorphic analyzers,” *IEEE Transactions on Circuits and Systems II, Express Briefs*, vol. 44, no. 3, pp. 188–196, 1997.
- [20] M. Aminian and F. Aminian, “A modular fault-diagnostic system for analog electronic circuits using neural networks with wavelet transform as a

- preprocessor,” *IEEE Transactions on Instrumentation and Measurement*, vol. 56, no. 5, pp. 1546–1554, 2007.
- [21] Y. Xiao and Y. He, “A novel approach for analog fault diagnosis based on neural networks and improved kernel PCA,” *Neurocomputing*, vol. 74, pp. 1102–1115, 2011.
- [22] B. Long, S. Tian, and H. Wang, “Diagnostics of filter analog circuits with tolerance based on LS-SVM using frequency features,” *Journal of Electronic Testing*, vol. 28, pp. 291–300, 2012.
- [23] J. Cui and Y. Wang, “A novel approach of analog circuit fault diagnosis using support vector machines classifier,” *Measurement*, vol. 44, pp. 281–291, 2011.
- [24] Z. Zhang, Z. Duan, Y. Long, and L. Yuan, “A new swarm-SVM-based fault diagnosis approach for switched current circuit by using kurtosis and entropy as a preprocessor,” *Analog Integrated Circuits and Signal Processing*, vol. 81, no. 1, pp. 289–297, 2014.
- [25] A. Vasan, B. Long, and M. Pecht, “Diagnostics and prognostics method for analog electronic circuits,” *IEEE Transactions on Industrial Electronics*, vol. 60, no. 11, pp. 5277–5291, 2013.
- [26] M. Li, W. Xian, B. Long, and H. Wang, “Prognostics of analog filters based on particle filters using frequency features,” *Journal of Electronic Testing*, vol. 29, pp. 567–584, 2013.

- [27] C. Zhang, Y. He, L. Yuan, and F. Deng, "A novel approach for analog circuit fault prognostics based on improved RVM," *Journal of Electronic Testing*, vol. 30, pp. 343–356, 2014.
- [28] J. Zhou, S. Tian, and C. Yang, "A novel prediction method about single components of analog circuits based on complex field modeling," *The Scientific World Journal*, vol. 2014, article ID 530942, pp. 14, 2014.
- [29] S. Kumar, N. Vichare, E. Dolev, and M. Pecht, "A health indicator method for degradation detection of electronic products," *Microelectronics Reliability*, vo. 52, pp. 439–445, 2012.
- [30] E. Sutrisno, "Fault detection and prognostics of IGBT using k-Nearest Neighbor classification algorithm," *Master's Thesis*, University of Maryland, 2013.
- [31] S. Menon, X. Jin, T. Chow, and M. Pecht, "Evaluating covariance in prognostic and system health management applications," *Mechanical Systems and Signal Processing*, vol. 58-59, pp. 206-217, 2015.
- [32] B. Saha, K. Goebel, and J. Christophersen, "Comparison of prognostic algorithms for estimating remaining useful life of batteries," *Transactions of the Institute of Measurement and Control*, vol. 31, no. 3-4, pp. 293-308, 2009.
- [33] G. Wahba, "Soft and hard classification by reproducing kernel Hilbert space methods," *Proceedings of the National Academy of Science*, vol. 99, no. 26, pp. 16524–16530, 2002.
- [34] T. Hofmann, B. Scholkopf, and A. J. Smola, "Kernel methods in machine learning," *Annals of Statistics*, vol. 36, no. 3, pp. 1171–1220, 2008.

- [35] J. Pillai, M. Puertas, and R. Chellappa, “Cross-sensor iris recognition through kernel-learning,” *IEEE Transactions on Pattern Analysis and Machine Intelligence*, vol. 36, no. 1, pp. 73–85, 2014.
- [36] J. Mercer, “Functions of positive and negative type, and their connection with the theory of integral equations,” *Philosophical Transactions of the Royal Society of London, Series A*, vol. 209, pp. 415-446, 1909.
- [37] V. Vapnik, “An overview of statistical learning theory,” *IEEE Transactions on Neural Networks*, vol. 10, no. 5, pp. 988–999, 1999.
- [38] J. Suykens and J. Vandewalle, “Least squares support vector machines classifiers,” *Neural Processing Letters*, vol. 9, no. 3, pp. 293–300, 2000.
- [39] T. Poggio and S. Smale, “The mathematics of learning: dealing with data,” *Notices of the AMS*, vol. 50, no. 5, pp. 537–544, 2003.
- [40] O. Chapelle and V. Vapnik, “Model selection for support vector machines,” In *Advances in Neural Information Processing Systems*, 1999.
- [41] T. Glasmachers and C. Igel, “Maximum likelihood model selection for 1-norm soft margin SVMs with multiple parameters,” *IEEE Transactions on Pattern Analysis and Machine Intelligence*, vol. 32, no. 8, pp. 1522–1528, 2010.
- [42] M. Adankon and M. Chriet, “Model selection for the LS-SVM. Application to handwriting recognition,” *Pattern Recognition*, vol. 42, pp. 3264–3270, 2009.
- [43] S. Keerthi, “Efficient tuning of hyperparameters using radius/margin bound and iterative algorithms,” *IEEE Transactions on Neural Networks*, vol. 13, no. 5, pp. 1225–1229, 2002.

- [44] F. Friedrichs and C. Igel, "Evolutionary tuning of multiple SVM parameters," *Neurocomputing*, vol. 64, pp. 107–117, 2005.
- [45] S. Li and M. Tan, "Tuning SVM parameters by using a hybrid CLPSO-BFGS algorithm," *Neurocomputing*, vol. 73, pp. 2089–2096, 2010.
- [46] L. Diosan, A. Rogozan, and J.-P. Pecuchet, "Improving classification performance of support vector machine by genetically optimizing kernel shape and hyper-parameters," *Applied Intelligence*, vol. 36, pp. 280–294, 2012.
- [47] G. S. dos Santos, L. G. J. Luvizotto, V. C. Mariani, and L. Coelho, "Least squares support vector machines with tuning based on chaotic differential evolution approach applied to the identification of a thermal process," *Expert System with Applications*, vol. 39, pp. 4805–4812, 2012.
- [48] E. Zhou, M. C. Fu, and S. Marcus, "Particle filtering framework for a class of randomized optimization algorithms," *IEEE Transactions on Automatic Control*, vol. 59, no. 4, pp. 1025–1030, 2014.
- [49] E. Zhou, "Particle filter for stochastic control and global optimization," Ph.D. Thesis, University of Maryland, 2009.
- [50] A. Boubezoul and S. Paris, "Application of global optimization methods to model and feature selection," *Pattern Recognition*, vol. 45, pp. 3676–3686, 2012.
- [51] S. Mathew, A. Alam, and M. Pecht, "Identification of failure mechanisms to enhance prognostic outcomes," *Journal of Failure Analysis and Prevention*, vol. 12, no. 1, pp. 66–73, 2012.

- [52] L. Yuan, Y. He, J. Huang, and Y. Sun, "A new neural network based fault diagnosis approach for analog circuits by using kurtosis and entropy as preprocessor," *IEEE Transactions on Instrumentation and Measurement*, vol. 59, no. 3, pp. 586–595, 2010.
- [53] Y. Wang and J. Cui, "A SVDD approach of fuzzy classification for analog circuit fault diagnosis with FWT as preprocessor," *Expert Systems with Applications*, vol. 38, no. 8, pp. 10554–10561, 2011.
- [54] B. Long, M. Li, H. Wang, and S. Tian, "Diagnostics of analog circuits based on LS-SVM using time domain features," *Circuit Systems and Signal Processing*, vol. 32, no. 6, pp. 2683–2706, 2013.
- [55] Y. Tan, Y. Sun, and X. Yin, "Analog fault diagnosis using S-transform preprocessor and a QNN classifier," *Measurement*, vol. 46, no. 7, pp. 2174–2183, 2013.
- [56] J. Platt, "Probabilistic outputs for support vector machines and comparisons to regularized likelihood methods," in *Advances in Large Margin Classifiers*, pp. 61–74, MIT Press, 1999.
- [57] H.-T. Lin, C.-J. Lin, and R. Weng, "Platt's probabilistic outputs for support vector machines," *Machine Learning*, vol. 68, pp. 267–276, 2007.
- [58] O. Rioul and M. Vetterli, "Wavelets and signal processing," *IEEE Signal Processing Magazine*, vol. 8, no. 4, pp. 14–38, 1991.
- [59] O. Rioul, "A discrete-time multiresolution theory," *IEEE Transactions on Signal Processing*, vol. 41, no. 8, pp. 2591–2606, 1993.

- [60] S. Mallat, "A theory for multiresolution signal decomposition: the wavelet representation," *IEEE Transactions on Pattern Analysis and Machine Intelligence*, vol. 11, no. 7, pp. 674-693, 1989.
- [61] L. DeCarlo, "On the meaning and use of kurtosis," *Psychological Methods*, vol. 2, no. 3, pp. 292-307, 1997.
- [62] J-F. Bercher and C. Vignat, "Estimating the entropy of a signal with applications," *IEEE Transactions on Signal Processing*, vol. 48, no. 6, pp. 1687-1694, 2000.
- [63] M. Daigle and K. Goebel, "Model-based prognostics with concurrent damage progression process," *IEEE Transactions on Systems, Man, and Cybernetics: Systems*, vol. 43, no. 3, pp. 535-546, 2013.
- [64] V. Smet, F. Forest, J-J. Huselstein, F. Richardeau, Z. Khatir, S. Lefebvre, and M. Berkani, "Ageing and failure modes of IGBT modules in high-temperature power cycling," *IEEE Transactions on Industrial Electronics*, vol. 58, no. 10, pp. 4931-4941, 2011.
- [65] M. Arulampalam, S. Maskell, N. Gordon, and T. Clapp, "A tutorial on particle filters for online/non-Gaussian Bayesian tracking," *IEEE Transactions on Signal Processing*, vol. 50, no. 2, pp. 174-188, 2002.
- [66] A. Saxena, J. Celaya, B. Saha, S. Saha, and K. Goebel, "Metrics for offline evaluation of prognostic performance," *International Journal of Prognostics and Health Management*, vol. 1, no. 001, 2010.
- [67] P. Lall, R. Lowe, and K. Goebel, "Prognostics and health management of electronic systems under mechanical shock and vibration using Kalman filter

models and metrics,” *IEEE Transactions on Industrial Electronics*, vol. 59, no. 11, pp. 4301-4314, 2012.

- [68] J. Hu, M. Fu, and S. Marcus, “A model reference adaptive search method for global optimization,” *Operations Research*, vol. 55, no. 3, pp. 549-568, 2007.